Analysis of TCSC Controllers

Projects:
RP 8030-02
RP 8050-03
RP 8050-04

Draft January 1996

Prepared by
University of Wisconsin-Madison
Electrical and Computer Engineering Department
1415 Engineering Drive
Madison WI 53706 USA

Principal Investigators
Robert Lasseter
Ian Dobson
William Sethares

Authors
Sasan Jalali
Rajesh Rajaraman
Jim Gronquist
Robert Lasseter
Ian Dobson
William Sethares

Prepared for
Electric Power Research Institute
3412 Hillview Avenue
Palo Alto, California 94304

EPRI Project Managers
A-A. Edris
T. Schneider
D.Sobajic

DISCLAIMER OF WARRANTIES AND LIMITATION OF LIABILITIES

THIS REPORT WAS PREPARED BY THE ORGANIZATION(S) NAMED BELOW AS AN ACCOUNT OF WORK SPONSORED OR COSPONSORED BY THE ELECTRIC POWER RESEARCH INSTITUTE, INC. (EPRI). NEITHER EPRI, ANY MEMBER OF EPRI, ANY COSPONSOR, THE ORGANIZATION(S) BELOW, NOR ANY PERSON ACTING ON BEHALF OF ANY OF THEM:

(A) MAKES ANY WARRANTY OR REPRESENTATION WHATSOEVER, EXPRESS OR IMPLIED, (I) WITH RESPECT TO THE USE OF ANY INFORMATION, APPARATUS, METHOD, PROCESS, OR SIMILAR ITEM DISCLOSED IN THIS REPORT, INCLUDING MERCHANTABILITY AND FITNESS FOR A PARTICULAR PURPOSE, OR (II) THAT SUCH USE DOES NOT INFRINGE ON OR INTERFERE WITH PRIVATELY OWNED RIGHTS, INCLUDING ANY PARTY'S INTELLECTUAL PROPERTY, OR (III) THAT THIS REPORT IS SUITABLE TO ANY PARTICULAR USER'S CIRCUMSTANCE; OR

(B) ASSUMES RESPONSIBILITY FOR ANY DAMAGES OR OTHER LIABILITY WHATSOEVER (INCLUDING ANY CONSEQUENTIAL DAMAGES, EVEN IF EPRI OR ANY EPRI REPRESENTATIVE HAS BEEN ADVISED OF THE POSSIBILITY OF SUCH DAMAGES) RESULTING FROM YOUR SELECTION OR USE OF THIS REPORT OR ANY INFORMATION, APPARATUS, METHOD, PROCESS, OR SIMILAR ITEM DISCLOSED IN THIS REPORT.

UNIVERSITY OF WISCONSIN-MADISON

ORDERING INFORMATION

Price: ($Report Price)

Requests for copies of this report should be directed to the EPRI Distribution Center, 207 Coggins Drive, P.O. Box 23205, Pleasant Hill, CA 94523, (510) 934-4212. There is no charge for reports requested by EPRI member utilities.

ABSTRACT

Begin typing abstract text here.

CONTENTS

1

INTRODUCTION

Includes need for SSR analysis in presence of TCSC

2

BASIC OPERATION OF TCSC

2.1 Basic Characteristics

A Thyristor Controlled Series Capacitor (TCSC) is the merging of a conventional series capacitor with power electronic technology. The power electronic components are placed in parallel with a conventional capacitor allowing variable series compensation. Current projects in operation are the Kayenta Substation [Juette 1992] and the Slatt Substation [Urbanek 1992] in the USA. The technical benefits derived from these projects include:

- Flexible control of power flow within the network.
- Damping of local and inter-area oscillations.
- Subsynchronous resonance (SSR) mitigation.
- Improved protection of the series capacitor.

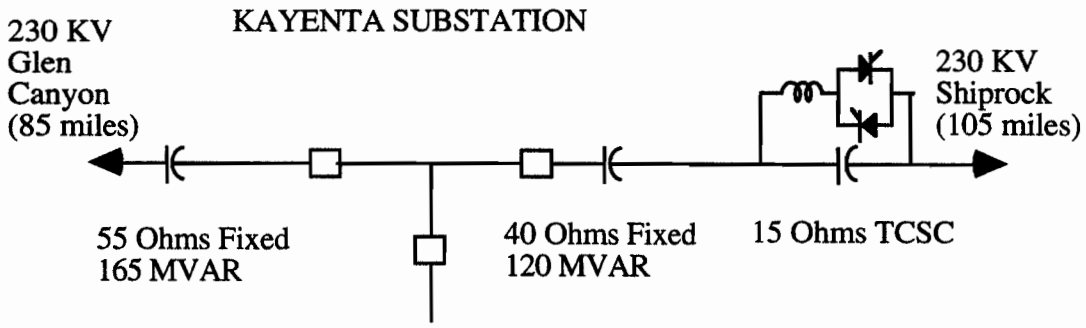

Figure 2.1 Example of a Thyristor Controlled Series Capacitor

The example shown in Figure 2.1 is the Kayenta Substation. This TCSC is placed on the 190 mile, 230 kV transmission line between Glen Canyon and Shiprock. This transmission line was constructed as part of the original Federal 230/345 kV Colorado River Storage Project. With completion in 1964, this line integrated the Colorado River Storage Project loads with new

generation at Glen Canyon and Flaming Gorge. The scheduling capability of the Glen Canyon-Shiprock line was approximately 300 MW. In 1968, the four Corners Cholla 345 kV line was completed followed by a 500kV line. The addition of these and other transmission lines out of Four Corners diminished the ability of the Glen Canyon-Shiprock line to carry scheduled power. This ability was regained by the addition of a phase shifter to the line in 1977.

Load growth on the interconnected system and restriction on building new lines opened the possibility of operation of the Glen Canyon-Shiprock line closer to its thermal capacity. This resulted in a decision to add 330 Mvar of series capacitor with a 15 Ohm section being controlled using a TCSC. This was placed at the Kayenta Substation as shown in Figure 2.1.

2.1.1 Basic Operation

One phase of a TCSC system consists of a Thyristor Controlled Reactor (TCR) and a fixed parallel capacitor. The switching element of the TCR consists of two oppositely poled thyristors which conduct on alternate half cycles of the supply frequency. The operation of the circuit depends on the switch on and off times of the thyristors and the rest of the system. The operation is different than that of a Static VAR Compensator (SVC) due to the small size of the reactor. Unlike a SVC there is a fundamental resonance between the capacitor and the inductor.

Basic modes

TCSC modules have three basic modes of operation; thyristor blocked (Figure 2.2), thyristor bypassed (Figure 2.3) and operating in vernier mode with phase control of the TCR (Figure 2.4). Figure 2.2 shows the module with the thyristors blocked. This results in no current in the inductor and thyristors. The module's impedance is the capacitor reactance. Figure 2.3 shows a module operating in the thyristor bypassed mode. The thyristor are fully conducting in this mode. The resulting module impedance is inductive and close to the value of the inductor. Figure 2.4 illustrates vernier operation. In this mode the thyristors conduct for part of a cycle. This allows for continuous control between the blocked and bypassed modes. For small conduction time the circulating current results in a capacitive impedance greater than the nominal capacitor reactance. When the thyristor conduction time become larger the module passes through a fundamental resonance. The circulating current becomes reversed which results in a net inductive impedance.

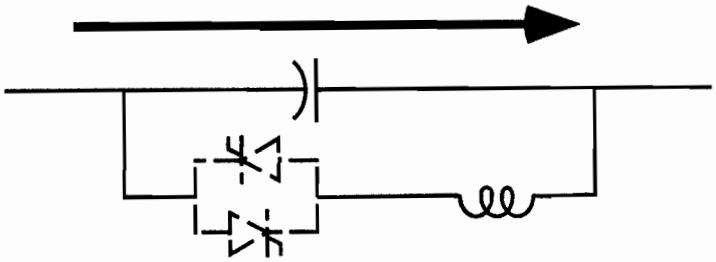

Figure 2.2 Thyristor blocked mode

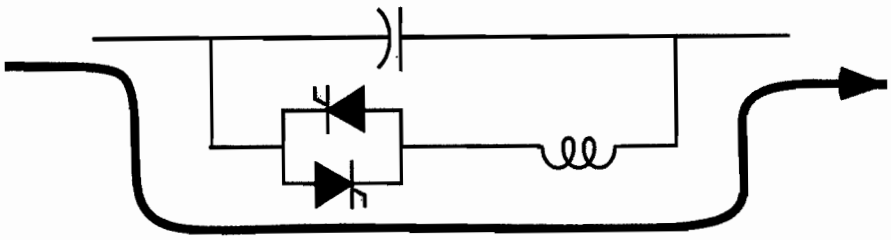

Figure 2.3 Thyristor bypassed mode

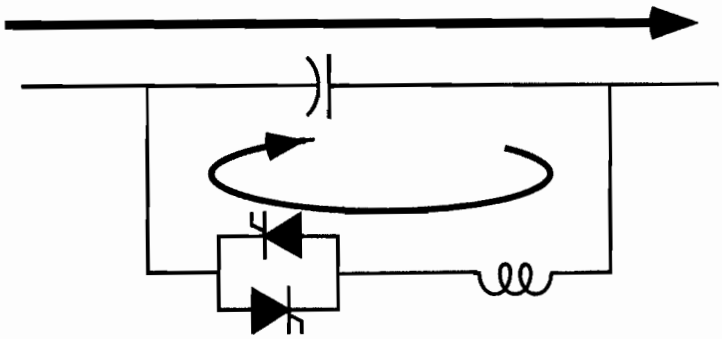

Figure 2.4 Vernier mode

2.1.2 Basic Operation of the Switching Circuit

The basic power electronic element is the Thyristor Controlled Reactor shown in Figure 2.5. The switching element of the TCR consists of two oppositely poled thyristors which conduct on alternate half cycles of the supply frequency. The operation of the circuit depends on the switch on and off times of the thyristors. In this simple case the voltage is assumed to be sinusoidal. When the thyristors are both open or non-conducting the voltage is across the thyristors. Firing the thyristor when the voltage is positive allows current I_+ to flow. The current shown in Figure 2.5 is the result of the voltage imposed across the reactor. When the current is forced to zero by the reversed voltage the thyristor will turn off. This is followed by the conduction of the other thyristor with current I_-. This results in two conductions per cycle. The conduction time, σ, can be controlled between zero

and half of a cycle. It is important to know where the voltage is zero to allow precise operation of the TCR. For example, the conduction or firing point for I_- is measured from the zero voltage point as the voltage becomes negative (see the circle in Figure 2.5). This ensures that the firing is synchronized to the ac voltage. How the system is synchronized has a major impact on the operation of a TCR in a power system.

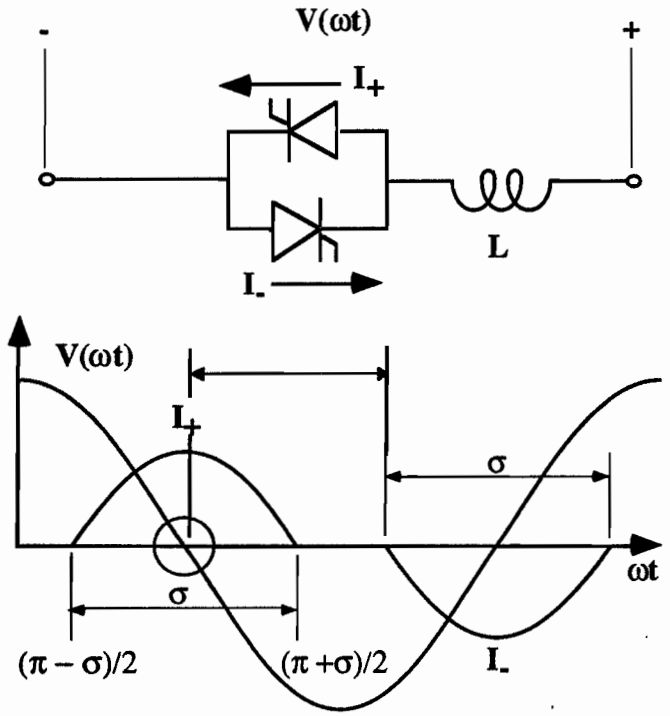

Figure 2.5 Thyristor Controlled Reactor (TCR)

When a TCR is placed across a capacitor we have a TCSC. The wave forms are not the same as the TCR since the voltage is not sinusoidal. Figures 2.6-2.7 show the operation in both the capacitive and inductive vernier regions. Figure 2.6 shows the capacitor voltage and thyristor current for small conduction times. In this case the fundamental impedance is capacitive at a value greater than the fixed capacitor due to the boost in the capacitor voltage. The resulting capacitive reactance is controllable between 1.0 and up to 3.0 pu. These wave forms assumes that the line current is very stiff and sinusoidal. Constant current is an excellent approximation when the TCSC is applied to a long transmission line. Figure 2.7 shows the same wave forms when the TCSC has large conduction times. The fundamental impedance is now inductive.

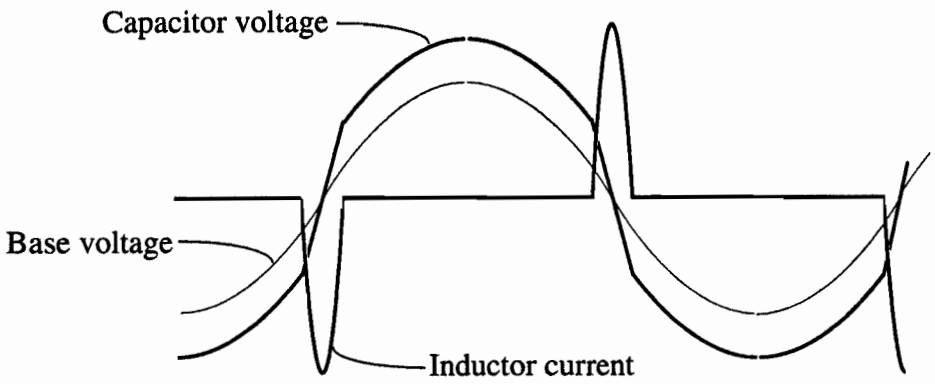

Figure 2.6 TCSC operation in the capacitive region

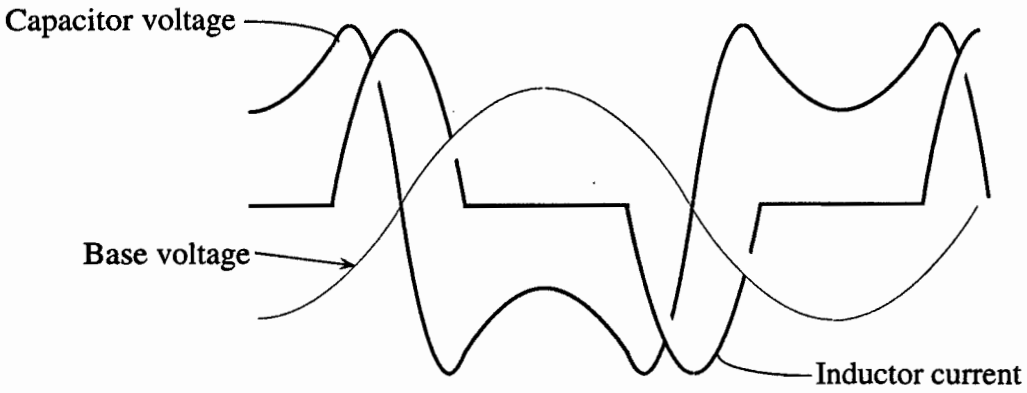

Figure 2.7 TCSC operation in the inductive region

The fundamental impedance as a function of conduction time, σ, is shown in Figure 2.8. The capacitive region is to the left of the singular point shown by the dotted line. In this region the capacitive reactance increases as the conduction time is increased. It is possible to have five or ten times the pu capacitance by operating near the resonance point. The dominant factor is the insulation level of the equipment. This imposes a maximum operating voltage across the series capacitor which usually restricts the reactance to levels of three pu or less. An important aspect of this voltage constraint is its duration; short-time operation above the continuous rating of the system is allowed.

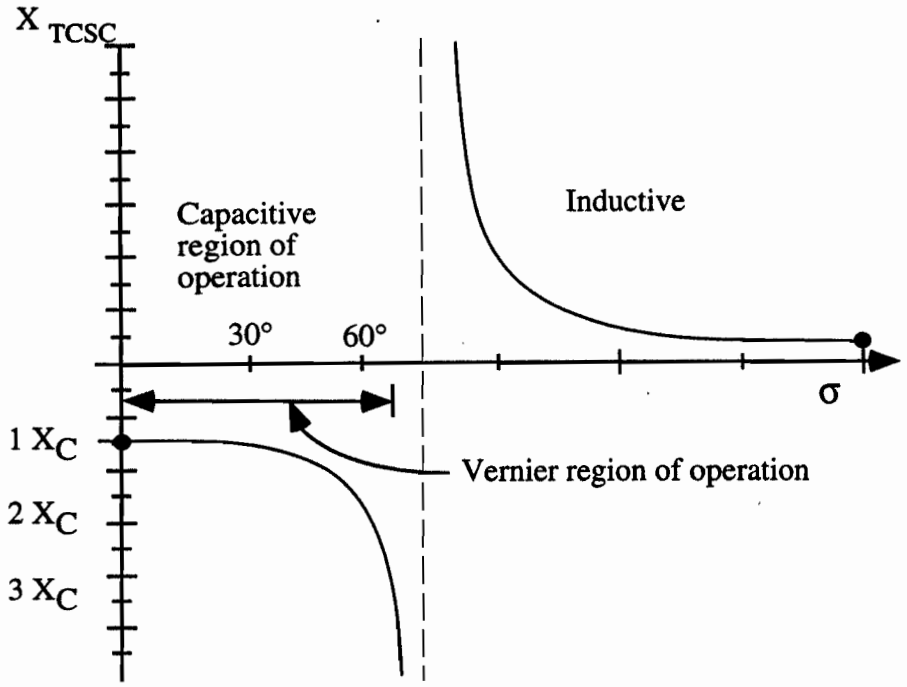

Figure 2.8 Fundamental impedance as a function of conduction time, σ.

2.2 Applications

Competitive pressures and open access policies are changing the nature of power systems. With greater competition the Nation's transmission system will become the new market place for selling and purchasing electrical power. Transmission line are currently unevenly loaded and will have difficulty in handling these changing patterns of power flow. The transmission system also has little flexibility for accommodating dispersed, small power plants. These pressures can result in reduced reliability for the system, increased voltage variation, more power loop flows, and less efficient transmission of electrical power.

An ideal power system of the future must find ways to utilize the lowest cost power generation and provide a high level of reliability. It needs to provide efficient transmission services to non-utility generation and have power export/import flexibility to accommodate this emerging reality. There needs to be a dramatic increase in the utilization of existing transmission systems with improvements in stability, fast control of power flow patterns and a more efficient operation. These requirements are some of the forces behind the growing use of power electronics such as TCSC in transmission systems.

Series compensation is a well established technology for increasing the power transfer capability of transmission lines and for controlling power flows on parallel transmission corridors. This enables utilities to economically increase the power transfer capability and thus increase the utilization of transmission-limited power plants. In spite of the economic incentives, the level of installed series capacitors has been limited due to concerns of subsynchrous resonance (SSR) interactions and lack of flexibility to accommodate the emerging reality of open transmission

Thyristor controlled series capacitors (TCSC) offer benefits to the power system which exceed the benefits of fixed series capacitor. Some of the TCSC benefits are:

- Provides flexibility in operation of a power system through control of power flow.
- Control of a TCSC can damp low-frequency power system oscillations in the range of 0.2-2.0 Hz.
- Vernier operation of a TCSC can eliminate the risk of SSR even at high levels of compensation. Care must be taken to insure that power swing modes do not become unstable.
- During line faults the thyristors can bypass the series capacitor, thus reducing the fault currents ratings of the capacitors.

Thyristor controlled series capacitors (TCSC) have three basic modes of operation: insert, bypass, and vernier. In the capacitive vernier mode, a TCSC effectively boosts the voltage of the capacitor segment making the capacitor segment appear as a larger capacitor . TCSC can be used for power flow control, damping power oscillations and mitigating SSR.

2.2.1 Power flow control

Plow flow control between regions can take two forms. In radial power transfer only one transmission corridor exists for the transfer of power between two areas. The other situation is meshed power transfer. In this case there is more than one transmission corridor for the transfer of power . There can also be more than two areas.

For radial power transfers, the principal issue is the capability of the transmission line(s) interconnecting the two regions. Figure 2.9 shows a conceptual diagram of high voltage line interconnection of two areas using a TCSC. The power flow equation indicates that as X_C increases

the power flow increases. For example in the case of 50% compensation the power flow will double assuming the voltage and power angle at both buses stay fixed.

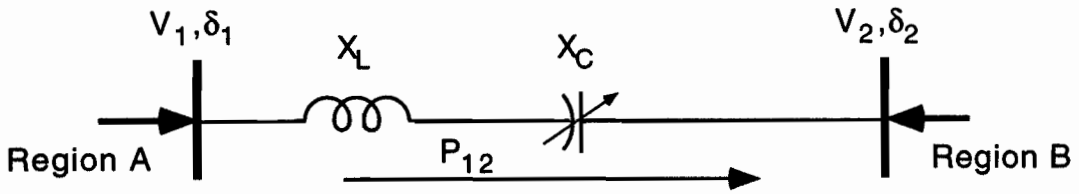

$$P_{21} = \frac{V_1 V_2}{X_L - X_C} \sin(\delta_2 - \delta_1)$$

Figure 2.9 Power flow between two regions

For meshed power transfer, several issues should be considered. TCSC offers the flexibility of varying the level of inserted series compensation in order to increase the power flow over the compensated lines. This allows the operator to off load an overloaded line and/or shift the power flow to higher-voltage transmission circuits which could lower electrical losses. TCSC can also be used to minimize the loop flow in the meshed system.

In an interconnected power system, the transfer of power from one region to another may take unscheduled routes. Figure 2.10 shows a conceptual diagram using a TCSC to control power flow in which the inter region power exchange is 3000 MW. For the case of no TCSC the export of Region A takes two routes. Line AC provides 1400 MW directly to Region C with the additional 600 MW flowing through region B. This extra power flow along with 1000 MW from region B overloads the line B C.

Solutions to this overloading are to back off the export power, build another line, add series capacitors to line A-B, use a phase shifting transformer, or add series inductance to the overloaded line. The major problem is that different export patterns require different compensation solutions.

Three possible FACTS controllers can be used in this case.

- A thyristor controlled series capacitor (TCSC) of a rating 0-5 ohms would increase the power flow up to 350 MW. Ratings larger than 5 ohms will increase the power flow further.
- A thyristor controlled phase angle controlled transformer in line AC with a range between 0° and -4.3° has the same effect as the TCSC.

- A TCSC in line B-C operating in the reactor region.

For each case Figure 2.10 shows the new power flow values for each line in parentheses.

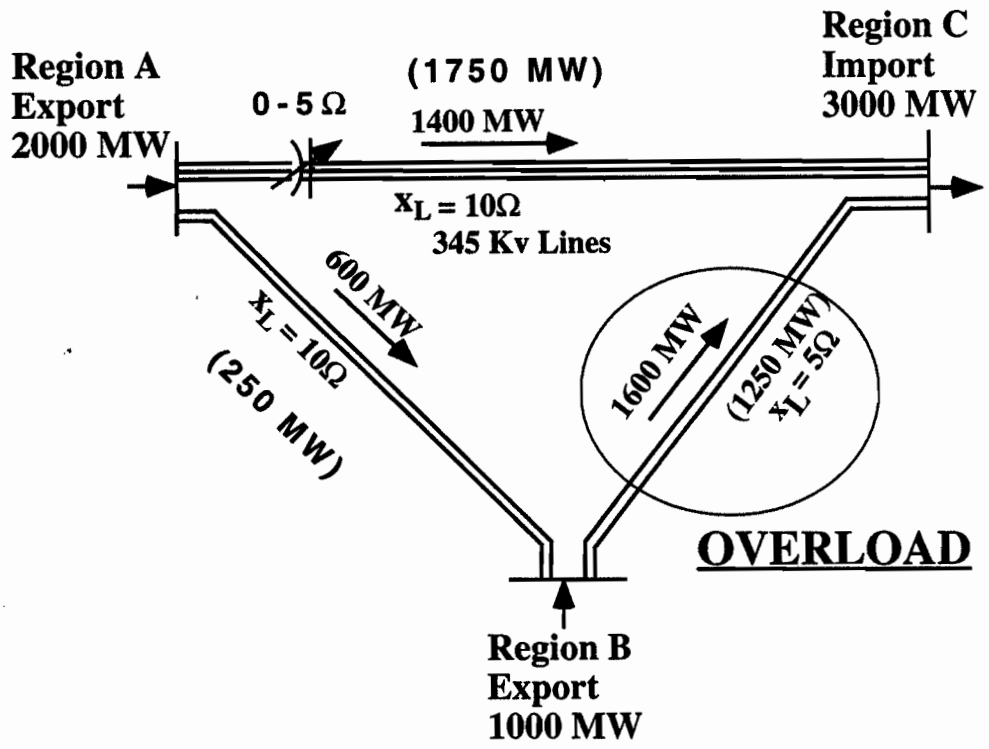

Figure 2.10 Mesh power flow control

In some applications, a phase shifting transformer could be more cost effective than a TCSC in controlling the flow on a transmission circuit. Other meshed networks need bus voltage support through an SVC to provide greater power transfer. In all cases a careful analysis of the power system is need in order to determine the most cost-effective control mechanism.

2.2.2 Damping of power swings

TCSC can effectively damp power swings resulting from major faults and undamped oscillations between regions. TCSC can improve the damping of power oscillations and increase levels of stable power transfer between two regions. Issues related to utilization of TCSC in damping power oscillations involve the size of the module and choice of controlling signals. In most cases a small segment of the series capacitor(e.g. ±10%) is sufficient for power oscillation damping. Local feedback measurements involving line current and its rate of change are effective for detecting oscillations and controlling the TCSC to enhance the damping [Gronquist 1995].

2.2.3 Subsynchronous Resonance (SSR)

Interactions between an electrical network and mechanical shafts of generator-turbine sets has been studied for many years. The components of such interactions are network switching, faults and series capacitors. Thyristor controlled series capacitors (TCSC) can help to minimize undesirable subsynchronous oscillations. This opens the possibility of increasing the level of installed series compensation with little risk of SSR problems.

Two approaches to SSR mitigation are possible. The first is to design an active controller which monitors SSR oscillations and controls the TCSC to introduce a damping torque. The requires estimates of remote measurements and a well designed controller. The major draw back to this approach is the risk of its ineffectiveness when the system conditions change from the design conditions. The estimation of the subsynchronous shaft oscillations from local measurements is not a trivial task and its robustness is questionable. Such controllers become more questionable when system conditions vary frequently. However, this approach has the potential to counteract harmful SSR interactions when some of the series compensation is a combination of a TCSC and conventional series compensation.

The second approach is to exploit the inherent SSR damping provided by TCSC when operating in the vernier mode. When a TCSC is operating above 1.05-1.15 pu compensation there is reduced risk of SSR. This approach offers more security in the face of varying conditions than the active controller required in the first approach.

It has been shown [Rajaraman 1995b] that operating a TCSC at a constant firing point or firing delay can mitigate SSR interactions when operating above a minimum level. In some cases TCSC operating at constant firing angle also can cause instabilities in the basic power swing mode. Care needs to be taken to identify the per unit operating range of the TCSC where SSR and power swing modes are not excited. Use of additional control features over the fixed firing point can remove the power swing mode problem without limiting the operational region [Angquist 1994].

Inherent SSR mitigation is discussed in detailed in Chapter 6. The philosophy is to make the TCSC benign to SSR. The main drawback of the inherent SSR mitigation approach is the need to install thyristor valves across the level of series compensation which causes SSR. For example, a system which is acceptable from an SSR point-of-view at a fixed compensation of 50%, but unacceptable at 70% requires TCSC control on the extra 20%.

The inherent SSR mitigation capability requires that the capacitor has a voltage boost above the 1 pu level. In most cases this is a level above 1.05 or larger. For retro-fit situations this can be a problem since the time-overvoltage characteristics of the existing capacitors seldom exceeds the 10% level. In general, for a TCSC to be useful in power flow control, system damping, and SSR mitigation the range of vernier control will exceed this 10% level.

2.3 Basic Control and Synchronization

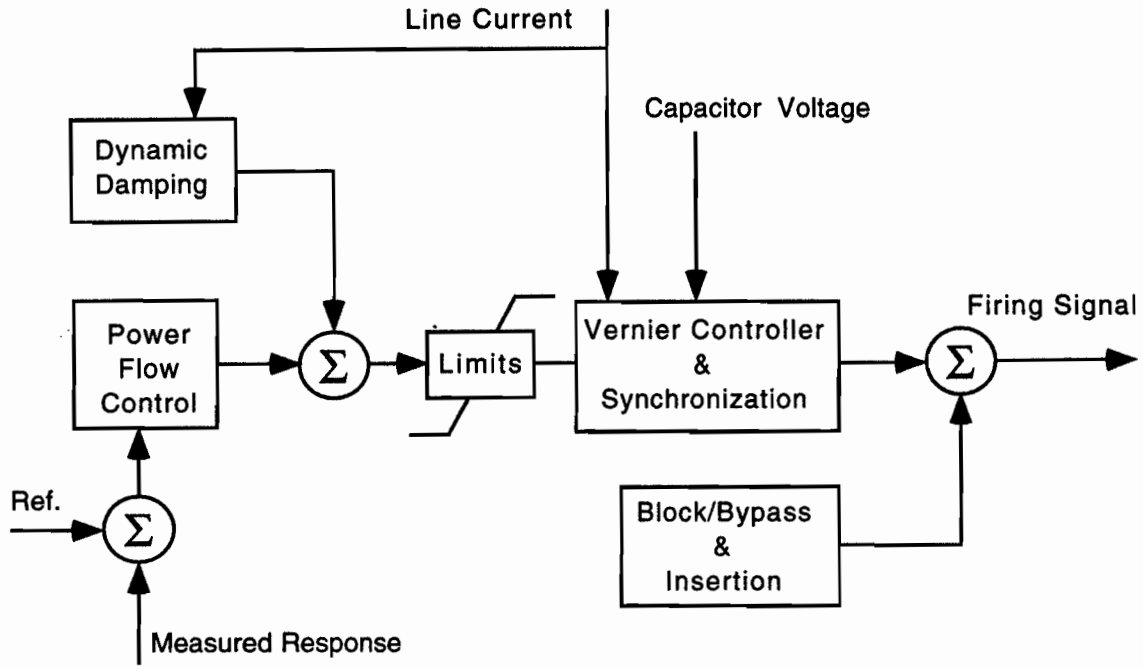

Figure 2.11 Thyristor Controlled Series Capacitor Controller

A general TCSC controller is shown in Figure 2.11. The central element is the vernier controller block with synchronization. This element must generate a firing pulse synchronized to the system's current. This element's external signals are line current, capacitor voltage and in some cases thyristor charge. Its control input is a signal proportional to requested reactance or capacitor voltage boost. This input is limited to ensure that the system operates in its rated region. The block and bypass function is to allow operation in the other modes discussed in section 2.1.1. It also provides firing signals for capacitor insertion without dc voltage components.

The power flow control relates to the steady state characteristics of the TCSC device. It normally use an error function based on a requested and measured operating point. Different modes may be used: power, current, and reactance control. In the first case, the power flow control algorithm has to modify the TCSC reactance to achieve a specified active power flow through the line. Current

control mode is used for maintaining a constant current magnitude through the line. Reactance is the most common mode of operation, and is used for inserting a constant reactance into the line. All of these modes need to be limited. The reactance limits can be fixed, or made variable depending on the level of the line current and capacitor voltage. There are basic problems with the power and current modes when there are other FACTS controllers in parallel line. In such cases the two systems will work against each other. The resulting steady state operating point for each FACTS controller will be at one of its reactance limit points.

The dynamic damping block provides a very useful function which is discussed in great detail in Chapter 7. Damping can be accomplished using a control loop based on the local measurement of the line current and is rate of change. Using this information it is possible to modulate the reactance of the TCSC to damp oscillations. This modulated signal is imposed on the power flow signal as shown in figure 2.11

2.3.1 Synchronization and Dynamics

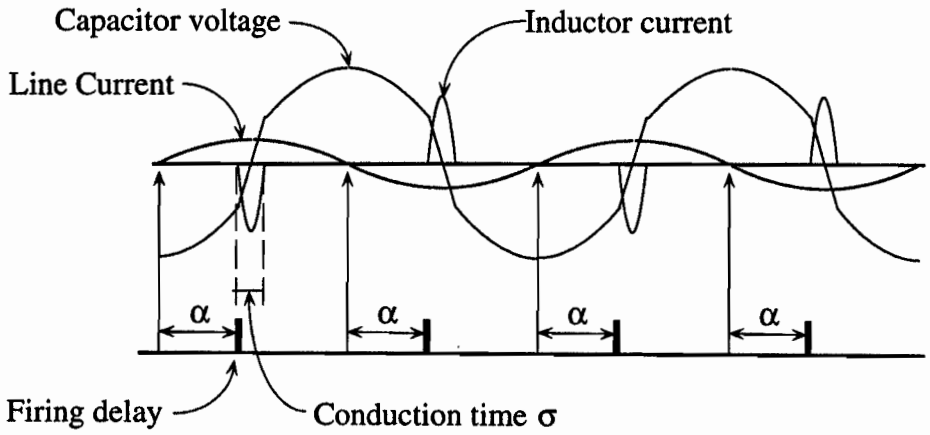

Figure 2.12 TCSC current synchronizing

The most basic need for any power electronic system is to ensure that the devices receive a firing signal at the correct point in time. If this is not done correctly the devices will not operate as expected and in some cases will fail. The firing of the power electronic devices must be synchronized to the system's voltage or current. Dynamic studies of a TCSC show [Jalali 1994a] that the stability of the circuit is improved by using line current as the synchronizing reference. In most TCSC applications line current is a very stiff due to the inductance of the transmission lines.

Figure 2.12 shows capacitor voltage, thyristor current, and line current for a TCSC in steady state. There is a delay, α, from the current zero which determines the point of thyristor firing. During conduction the current in the thyristor increases until the voltage across the thyristor is reversed. At this point the thyristor current is driven to zero and turns off. In steady state there is a relationship between the firing delay, α, and the conduction time, σ, namely: $\alpha+\frac{\sigma}{2}=\frac{\pi}{2}$. During dynamics this relationship will not hold.

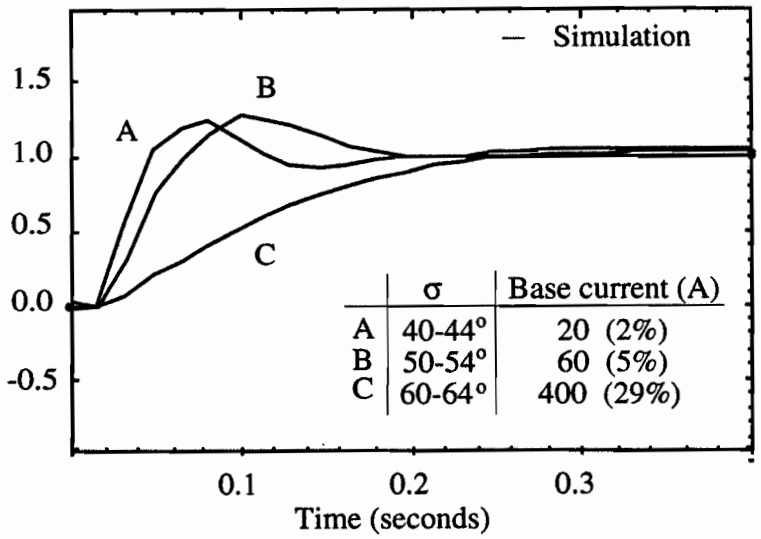

Figure 2.13 Current response to a step change in a TCSC operating point.

The most basic controller is one with an input of requested reactance which is converted to a fixed firing delay, α. The first task is to look at the response of line current for this basic controller including synchronization to line current. The dynamics shown in figure 2.13 are for the Kayenta system. More details are found in Chapter 5. The solid lines are the envelope of line current using a detailed EMTP model. This response shows the dependence of the dynamics on the operating point, σ, and the level of the line current. Operating region A is underdamped while region C is highly overdamped.

Insight into the dynamics can be gained from figure 2.14. In this case there is a step change in the firing delay. The capacitor voltage increases towards the new steady state point. In this example the line current was assumed to be constant. The conduction times are not constant and the capacitor voltage is not symmetric. The firing delay is fixed but the conduction time is a function of the magnitude of the capacitor voltage.

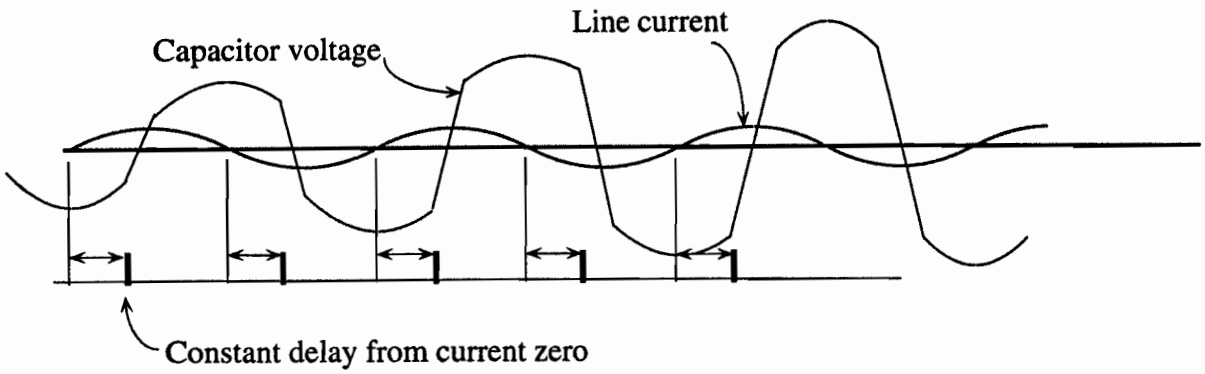

Figure 2.14 TCSC capacitor voltage during a change in operating point.

To understand why conduction times are not constant and the capacitor voltage is not symmetric let us look at the TCSC waveforms in detail. Figure 2.15(a) shows the steady state wave forms for two different operating points. The solid curves show the capacitor voltage, the thyristor current, and the line current for a fixed firing delay. The dotted curves show the same voltage and current waveforms for a smaller firing delay. This earlier firing results in a longer conduction time, larger thyristor currents and a greater capacitor voltage. Each steady state point has a unique firing point. The results are dependent on the line current, the firing delay and the value of the capacitor voltage at firing. Also note the symmetry of the thyristor current and capacitor voltage and the 90° phase shift between line current and capacitor voltage.

Figure 2.15(b) shows what happens when the firing delay is reduced. This new firing delay is correct for the new operating point, but the capacitor voltage is lower than the value required for steady state. This is indicated in figure 2.15(b) by the labels "actual voltage" and "required voltage". The solid curve in figure 2.15(b) shows the transients wave forms for this the first firing. The thyristor current starts at the required point in time, but the conduction time is much smaller than expected for the new steady state. The capacitor voltage reversal is also phase advanced relative to its steady-state positions. The voltage phase error is shown by the hatched area. The line current between voltage reversals is not symmetric and the sum of the positive and negative charge provided by the current is not zero. The extra positive charge results in a net increase in the capacitor voltage. This increase in voltage is proportional to the line current and the phase deviation of voltage reversal point from the steady state point. Much of the complexity of the vernier controllers comes from addressing this unbalance in the waveforms during transients.

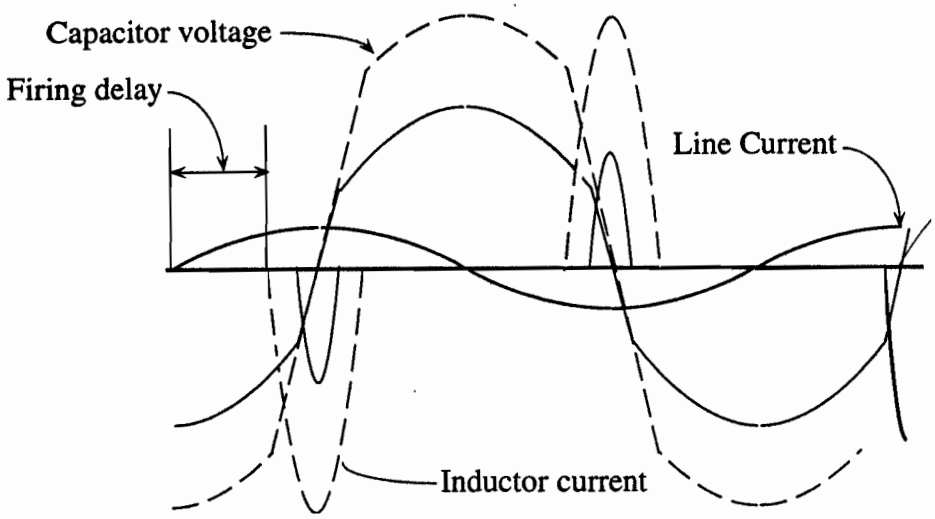

Figure 2.15(a) Steady State Wave Forms for Two Operating Points

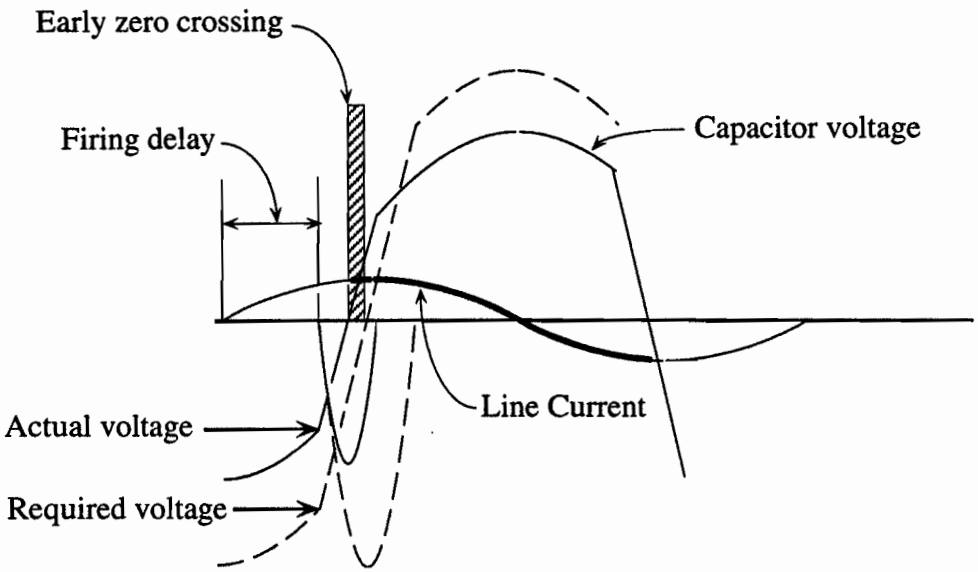

Figure 2..15(b) First Voltage Reversal after a Change in Firing Point.

2.3.2Vernier Controller

The design of the TCSC vernier controller affects the speed of response, its ability to mitigate SSR, and stability of power swing modes. In cases where these issues are important the vernier controller needs to be modeled in detail. Chapters 3, 5 and 6 provide methods for studying these issues without detailed electromagnetic transient simulations.

Three different vernier designs have been discussed in the literature [Jalali 1994a, Larsen 1993, Angquist 1994]. Each of these designs relies on controlling the firing point to effect the transient response discussed in the last section.

The first controller [Jalali 1994a] improves the dynamic response using the error in conduction time, σ, during the transition between operating points. To reduce the variance in dynamic response shown in figure 2.13, a feed back control on σ is used. In this controller the error function is the difference between a requested σ_r and a measured value, $<\sigma>$.The measured value $<\sigma>$ is updated twice per cycle while the requested value can change continuously depending on the action of higher level controllers. This results in a feedback control on σ, which provides a faster and more uniform response to step changes.

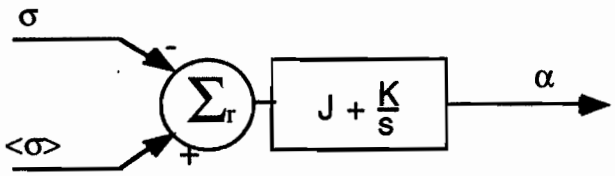

Figure 2.16 Nonlinear Sigma Controller

The controller used is a simple PI controller with a nonlinear gain. The nonlinear gain is defined as $J = A(1 + e^S)$. For example in the case illustrated in figure 2.15(b) the measured σ, $<\sigma>$, is smaller than the requested σ resulting in a reduction in α. The phase deviation of voltage reversal point from the steady state increasing provides more charge to the capacitor. The nonlinear gain ensures constant response over the full operation range. For more details see Chapter 5.

The second controller [Larsen 1993] is extremely fast. It relies on the measurement of the capacitor voltage, the thyristor charge and the line current for its operation. It utilizes a two-dimensional look-up table using line current and capacitor voltage at the last conduction point. The speed of response to higher level commands is on the order of 1/2 cycle. For SSR mitigation this speed of response is reduced by a higher level controller.

The third controller [Angquist 1994] focuses on the voltage reversal error, figure 2.15(b). This controller estimates firing delay from measurements to ensure a constant voltage reversal point. The location of this point determines the phase deviation of the voltage reversal and hence the rate of voltage increase. This increase in voltage is proportional to the line current and the phase deviation of voltage reversal point. This circuit measures the capacitor voltage and the line current to estimate

the current voltage reversal point assuming that the thyristor would be triggered immediately. The trigger pulse is released when the estimated reversal point coincides with the requested point. This results in linear response depending on the size and polarity of the requested reversal point.

3

ANALYTIC TOOLS (BASIC CONCEPTS)

3.1 Modeling of switching circuits and thyristors

For systems studies of high power circuits, it is appropriate to use an ideal thyristor model. This ideal thyristor model conducts current only in the forward direction, can block voltage in both directions, turns on when a firing signal is provided and turns off after a current zero. The ideal thyristor is a short circuit when on and an open circuit when off. Thus the circuit changes as the thyristors switch on and off. Even if the circuits are linear between switchings, the thyristor switch off times are determined by the instant at which thyristor currents become zero and the overall system is nonlinear. Nonlinearity can also be introduced by the thyristor switch on time depending on the system state via the firing control. Our methods take full account of these nonlinearities.

The following sections explain methods of analyzing both the steady state [Jalali1991, Jalali1992a, Jalali1993, Jalali1994b] and small signal dynamics [Jalali1994a, Dobson1995a, Dobson1995b, Jalali1996] of thyristor switching circuits; it is important to distinguish the steady state and dynamic analyses. Analysis of the periodic steady state addresses the harmonic distortion present. Analysis of small signal dynamics assumes a particular steady state and studies the behavior of the transients which occur when the system is slightly perturbed from the steady state. Since thyristor switching circuits are nonlinear, there is little connection between the steady state harmonic distortion and the behaviour of transients and their analyses are quite distinct.

3.2 Modeling variable structure circuits

Figure 3.1 shows a single phase TCSC system consisting of a TCR and a fixed parallel capacitor. The ac system is modeled by a system inductance, a series compensating capacitor and some resistance.

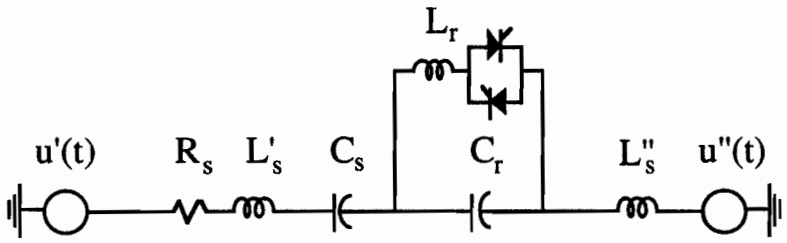

Figure 3.1 Thyristor Controlled Series Capacitor

The switching element of the TCR consists of two oppositely poled thyristors which conduct on alternate half cycles of the supply frequency. The nonlinearity of the circuit only arises from the dependence of the switch on and off times of the thyristors on the system state. Figure 3.2 shows the thyrsitor current and capacitor voltage waveforms.

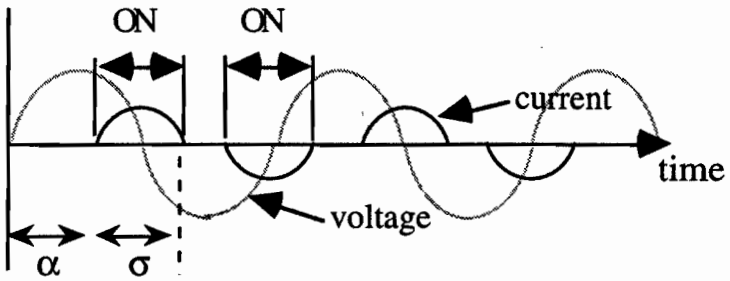

Figure 3.2. Thyristor current and capacitor voltage in TCSC.

During the thyristor conduction or on time, the system state vector x(t) specifies the TCR current, voltage, the line current and the fixed series capacitor voltage:

$$x(t) = \begin{bmatrix} I_r(t) \\ V_r(t) \\ I_s(t) \\ V_s(t) \end{bmatrix} \tag{3-1}$$

The system input u(t)=u'(t)-u''(t) is the net source voltage which is assumed to be periodic with period T and the system dynamics are described by the following set of linear differential equations:

$$\dot{x}(t) = Ax(t) + Bu(t) \tag{3-2}$$

where

$$A = \begin{bmatrix} 0 & 1/L_r & 0 & 0 \\ -1/C_r & 0 & 1/C_r & 0 \\ 0 & -1/L_s & -R_s/L_s & -1/L_s \\ 0 & 0 & 1/C_s & 0 \end{bmatrix} \text{ and } B = \begin{bmatrix} 0 \\ 0 \\ 1/L_s \\ 0 \end{bmatrix} \tag{3-3}$$

During the off time of each thyristor, the circuit state is constrained to lie in the plane $I_r=0$ of zero thyristor current. In this mode, the system state vector y(t) specifies the TCR voltage, the line current and the fixed series capacitor voltage:

$$y(t) = \begin{bmatrix} V_r(t) \\ I_s(t) \\ V_s(t) \end{bmatrix} \tag{3-4}$$

and the system dynamics are given by the linear system

$$\dot{y}(t) = PAP^t y(t) + PBu(t) \tag{3-5}$$

where P is the projection matrix

$$P = \begin{bmatrix} 0 & 1 & 0 & 0 \\ 0 & 0 & 1 & 0 \\ 0 & 0 & 0 & 1 \end{bmatrix} \tag{3-6}$$

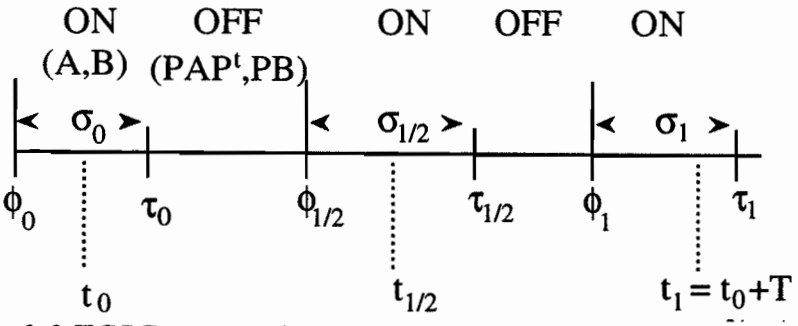

Figure 3.3 TCSC system dynamics

Figure 3.3 describes the system dynamics as the system state evolves over a period T from time t_0 to time t_1. A thyristor starts conducting at time ϕ_0. This mode as described by (3-2) ends when the thyristor current goes through zero at time $\phi_0+\sigma_0=\tau_0$. The non-conducting mode as described by (3-5) follows the conducting mode and continues until the next firing pulse is applied at time $\phi_{1/2}$ where the subscript 1/2 refers to the half cycle. The firing at time $\phi_{1/2}$ starts a similar on-off cycle which lasts until the next period starts at time ϕ_1.

The state at the switch on time ϕ_0 is denoted either by the vector $y(\phi_0)$ or by the vector $x(\phi_0)$. These representations of the state at the switch on time are related by

$$x(\phi_0)=P^t\, y(\phi_0) \tag{3-7}$$

Equation (3-7) expresses the fact that the state in x coordinates at a switch on is computed from the y coordinates by adding a first component which has value zero. The state at the switch off time τ_0 is similarly denoted either by $x(\tau_0)$ or $y(\tau_0)$ and these are related by

$$y(\tau_0)=P\, x(\tau_0) \tag{3-8}$$

The matrix P in equation (3-8) may be thought of as projecting the vector x onto the hyperplane of zero thyristor current.

3.2.1. Synchronization

The thyristor turn on times at $\phi_{1/2}$ and ϕ_1 depend on the firing scheme and the closed loop control. We study the open loop system when operated with one of the four common firing schemes. These are equidistant firing, constant sigma controller and synchronization on the TCSC voltage or the TCSC line current.

(a) In equidistant firing the thyristor turn on pulses are supplied periodically and the system is controlled by varying the phase of the firing pulses, ϕ. Since the relationship between ϕ and the TCR firing angle α depends on the line impedance, a negative feed back loop modifying ϕ is usually used to ensure a requested α. In this section, we restrict our analysis to an equidistant firing with no feed back control i.e., the thyristor turn on times are computed using a requested phase delay ϕ_{req} as follows:

$$\phi_{1/2} = \frac{T}{2} + \phi_{req} \tag{3-9}$$

$$\phi_1 = T + \phi_{req} \tag{3-10}$$

(b) The constant sigma controller determines the next turn on time based on the requested conduction time, σ_{req} and the previous turn on and turn off times as follows:

$$\phi_{1/2} = \frac{\phi_0 + \tau_0 + 2\pi - \sigma_{req}}{2} \tag{3-11}$$

$$\phi_1 = \frac{\phi_{1/2} + \tau_{1/2} + 2\pi - \sigma_{req}}{2} \tag{3-12}$$

(c) The voltage synchronization detects the zero crossings of the voltage across the TCR to compute the thyristor turn on times. This method assumes there are two zero crossing of voltage per cycle which occur when the thyristors are conducting. In other words, if τ_{v0} and $\tau_{v1/2}$ denote the zero crossing of the voltage during the conduction times σ_0 and $\sigma_{1/2}$ respectively, the turn on times $\phi_{1/2}$ and ϕ_1 are computed using a requested delay angle α_{reqv} as follows:

$$\phi_{1/2} = \alpha_{reqv} + \tau_{v0} \tag{3-13}$$

$$\phi_1 = \alpha_{reqv} + \tau_{v1/2} \tag{3-14}$$

(d) Since the line current is fairly stiff (due to the large line inductance), it is reasonable to synchronize the firing times $\phi_{1/2}$ and ϕ_1 to the zero crossing of the line current. In this case, if we let τ_{c0} and $\tau_{c1/2}$ denote the zero crossing of the line current during the nonconducting times of thyristors, $\phi_{1/2}$ and ϕ_1 may be computed using a requested delay angle α_{reqc} as follows:

$$\phi_{1/2} = \alpha_{reqc} + \tau_{c0} \tag{3-15}$$

$$\phi_1 = \alpha_{reqc} + \tau_{c1/2} \tag{3-16}$$

3.3 Harmonic Admittance Methods

Consider the steady state operation of a thyristor controlled reactor. If the operation is periodic, Fourier techniques can be used to calculate the steady state including harmonics. By expressing the TCR voltage and current as a Fourier series, a TCR harmonic admittance matrix can be constructed.

Consider the single phase TCR shown in Figure 3.4. The thyristors are gated once each half cycle allowing control of the current in the reactor and thus allowing control of the reactive current drawn by the circuit. If it is assumed that the thyristors are ideal the on/off states of each thyristor can be expressed using a switching function, H(ωt).

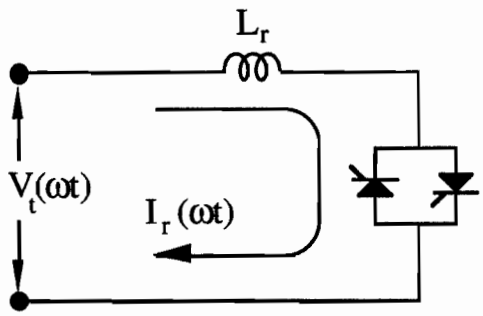

Figure 3.4 Thyristor controlled reactor

The switching function, H(ωt), shown in Figure 3.5 has a value of one whenever a thyristor is on and zero when the thyristors are off. Since a thyristor turns off when its current goes through zero, the conduction time σ depends on the turn on time ϕ, the terminal voltage $V_t(\omega t)$ and the TCR reactance, L_r. Therefore the switching function is dependent on the terminal voltage through the turn on/off time of the thyristors.

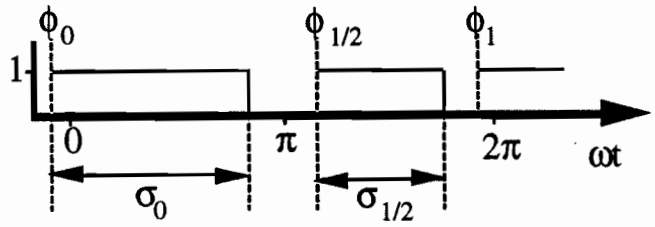

Figure 3.5 The switching function, H(ωt)

Since there are two commutation processes per cycle, one starting at time ϕ_0 and ending at time $\phi_0+\sigma_0$ and the other starting at time $\phi_{1/2}$ and ending at $\phi_{1/2}+\sigma_{1/2}$, there are also two constraint equations which describe the dependence between the terminal voltage and the switching times. Integrating the terminal voltage and keeping in mind that the TCR current is zero both at the turn on and the turn off times, the two constraint equations are:

$$0 = \frac{1}{\omega L_r} \int_{\phi_i}^{\phi_i+\sigma_i} V_t(\omega t)d\omega t \qquad i=0,1/2 \qquad (3\text{-}17)$$

where the subscript i denotes the commutation process starting from the time ϕ_i and ending at time $\phi_i+\sigma_i$. Since the integration is with respect to ωt, the effective reactance is ωL_r. The reactor current, $I_r(wt)$, can be found by integrating the voltage across the reactor $V_r(\omega t)$. Representing $V_r(\omega t)$ by the terminal voltage, $V_t(\omega t)$, multiplied by the TCR switching function $H(\omega t)$, we get:

$$I_r(\omega t) = \frac{1}{\omega L_r} \int H(\omega t)V_t(\omega t)d\omega t \qquad (3\text{-}18)$$

Equation (3-18) shows the time domain relationship among the terminal voltage, reactor current and the switching function. The constraint equations in (3-17) show how the switching function is dependent on the terminal voltage through the thyristor switching times σ and ϕ.

Assuming periodicity, $H(\omega t)$ can be represented by its complex Fourier series:

$$H(\omega t) = \sum_{n=-\infty}^{\infty} h_n(\sigma_0,\phi_0,\sigma_{1/2},\phi_{1/2})\, e^{jn\omega t} \qquad (3\text{-}19)$$

where

$$h_0 = \frac{1}{2\pi}\,(\sigma_0 + \sigma_{1/2}) \tag{3-20}$$

$$h_n = \frac{j}{2n\pi}\left[e^{jn\phi_0}\left(e^{-jn\sigma_0} - 1\right) + e^{jn\phi_{1/2}}\left(e^{-jn\sigma_{1/2}} - 1\right)\right] \tag{3-21}$$

Similarly, representing $V_t(\omega t)$ and $V_r(\omega t)$ by their complex Fourier series:

$$V_t(\omega t) = \sum_{m=-\infty}^{\infty} v_{tm}\, e^{jm\omega t} \tag{3-22}$$

$$V_r(\omega t) = \sum_{k=-\infty}^{\infty} v_{rk}\, e^{jk\omega t} \tag{3-23}$$

where v_{tm} is the mth, and v_{rk} is the kth Fourier component of the terminal voltage and the voltage across the reactor. Note that for steady state operation, equal volt-seconds is always maintained across the reactor L_r so that the DC component of $V_r(\omega t)$ is equal to zero.

Integrating V_r in (3-23) and dividing it by the ωL_r,we obtain:

$$I_r(\omega\tau) = \sum_{k=-\infty}^{\infty} I_{rk} e^{jk\omega t} = I_{dc} + \sum_{\substack{k=-\infty \\ k\neq 0}}^{\infty} \frac{V_{rk}}{jk\omega L_r} e^{jk\omega t} \tag{3-24}$$

From the above, the harmonic currents at each frequency are:

$$I_{rk} = \frac{V_{rk}}{jk\omega L_r} \qquad k\neq 0 \tag{3-25}$$

$$I_{r0} = I_{dc} \tag{3-26}$$

The TCR current is zero during the following two time intervals which represent the nonconducting times of the TCR (see Figure 3-5).

$$\phi_0 + \sigma_0 \leq \omega t_0 \leq \phi_{1/2} \tag{3-27}$$

$$\phi_{1/2} + \sigma_{1/2} \leq \omega t_0 \leq \phi_1 \tag{3-28}$$

Substituting ωt_0 in (3-24) and using that $I_r(\omega t_0) = 0$ solving for the I_{dc} yields:

$$I_{dc} = -\sum_{\substack{k=-\infty \\ k\neq 0}}^{\infty} \frac{V_{rk}}{jk\omega L_r} e^{jk\omega t_0} \tag{3-29}$$

Note that the two time intervals (3-27) and (3-28) reduce to two single points, ϕ_0 and $\phi_{1/2}$, when the TCR is fully on. Therefore, there are at least two different but equivalent ways of representing I_{dc}. Letting $\omega t_0 = \phi_{1/2}$ we get:

$$I_r(\omega t) = \sum_{\substack{k=-\infty \\ k\neq 0}}^{\infty} \frac{V_{rk}}{jk\omega L_r} e^{jk\omega t} - \sum_{\substack{k=-\infty \\ k\neq 0}}^{\infty} \frac{V_{rk}}{jk\omega L_r} e^{jk\phi_{1/2}} \tag{3-30}$$

The following relationship between the Fourier components of the reactor current and the reactor voltage can be obtained from (3-30):

$$\begin{bmatrix} \cdot \\ \cdot \\ I_{r-1} \\ I_{r0} \\ I_{r+1} \\ \cdot \\ \cdot \end{bmatrix} = \begin{bmatrix} \cdot & \cdot & \cdot & \cdot & \cdot & \cdot & \cdot \\ \cdot & \cdot & \cdot & \cdot & \cdot & \cdot & \cdot \\ \cdot & \cdot & \frac{1}{-j\omega L_r} & 0 & 0 & \cdot & \cdot \\ \cdot & \cdot & \frac{e^{-j\phi_1}}{-j\omega L_r} & 0 & \frac{e^{j\phi_1}}{j\omega L_r} & \cdot & \cdot \\ \cdot & \cdot & 0 & 0 & \frac{1}{j\omega L_r} & \cdot & \cdot \\ \cdot & \cdot & \cdot & \cdot & \cdot & \cdot & \cdot \\ \cdot & \cdot & \cdot & \cdot & \cdot & \cdot & \cdot \end{bmatrix} \begin{bmatrix} \cdot \\ \cdot \\ V_{r-1} \\ 0 \\ V_{r+1} \\ \cdot \\ \cdot \end{bmatrix} \tag{3-31}$$

Rewriting (3-31) in short matrix form we obtain:

$$\mathbf{I}_r = \mathbf{Y}_r \mathbf{V}_r$$

$V_r(\omega t)$ is the terminal voltage, $V_t(\omega t)$, multiplied by the TCR switching function $H(\omega t)$:

$$V_r(\omega t) = V_t(\omega t)\, H(\omega t) \tag{3-32}$$

$V_r(\omega t)$ can be thought of as an infinite vector of harmonic voltages, one for each harmonic frequency. Equation (3-32) can be expressed in matrix form as shown in (3-33). It is made up of an infinite dimensional switching function matrix **H**, multiplied by the terminal voltage vector.

$$\begin{bmatrix} \cdot \\ \cdot \\ v_{r-3} \\ v_{r-2} \\ v_{r-1} \\ \cdot \\ \cdot \end{bmatrix} = \begin{bmatrix} \cdot & \cdot & \cdot & \cdot & \cdot & \cdot & \cdot \\ \cdot & \cdot & \cdot & \cdot & \cdot & \cdot & \cdot \\ \cdot & \cdot & h_0 & h_{-1} & h_{-2} & \cdot & \cdot \\ \cdot & \cdot & h_1 & h_0 & h_{-1} & \cdot & \cdot \\ \cdot & \cdot & h_2 & h_1 & h_0 & \cdot & \cdot \\ \cdot & \cdot & \cdot & \cdot & \cdot & \cdot & \cdot \\ \cdot & \cdot & \cdot & \cdot & \cdot & \cdot & \cdot \end{bmatrix} \begin{bmatrix} \cdot \\ \cdot \\ v_{t-3} \\ v_{t-2} \\ v_{t-1} \\ \cdot \\ \cdot \end{bmatrix} \tag{3-33}$$

where h_n is a function of the switching times σ_0, ϕ_0, $\sigma_{1/2}$ and $\phi_{1/2}$, defined in (3-20) and (3-21). The above matrix equation illustrates the coupling between the harmonics which is an important characteristic of all switching circuits. A single frequency of the terminal voltage will produce a whole spectrum of voltage across the reactor. Also, all harmonics of the terminal voltage contribute to a single harmonic voltage across the reactor. Rewriting (3-33) in concise matrix form yields:

$$\mathbf{V}_r = \mathbf{H}(\sigma_0,\phi_0,\sigma_{1/2},\phi_{1/2})\, \mathbf{V}_t \tag{3-34}$$

where $\mathbf{V}_r$ and $\mathbf{V}_t$ are vectors of voltages harmonics across the reactor and across the TCR. **H** is the switching function matrix as defined in (3-19). The harmonics of the TCR current $\mathbf{I}_r$ are given by:

$$\mathbf{I}_r = \mathbf{Y}_r \mathbf{V}_r \tag{3-35}$$

where $\mathbf{I}_r$ is the vector of TCR current harmonics and $\mathbf{Y}_{tcr}$ denotes the admittance of the reactor. Combining (3-34) and (3-35) yields:

$$\mathbf{I}_r = \mathbf{Y}_r\, \mathbf{H}(\sigma_0,\phi_0,\sigma_{1/2},\phi_{1/2})\, \mathbf{V}_t = \mathbf{Y}_{tcr}(\sigma_0,\phi_0,\sigma_{1/2},\phi_{1/2})\, \mathbf{V}_t \qquad (3\text{-}36)$$

Switching matrices are full matrices resulting in a full matrix $\mathbf{Y}_{tcr}$. The off diagonal elements in these matrices indicate the important cross couplings between the different harmonics.

3.1.1 System solution

The harmonic admittance methods can used to compute harmonics in the static VAR and the advanced series compensator examples. Both circuits may be represented by a harmonic Thevenin equivalent as seen from the bus connecting the TCR to the external system as shown in Figure 3.5. Without the TCR connected, the resulting linear system has a harmonic Z_{th} matrix.

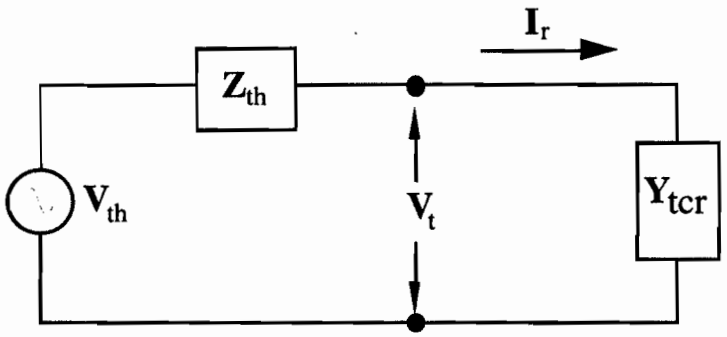

Figure 3.6. The reduced equivalent system

The equivalent system impedance is the diagonal element of the $\mathbf{Z}_{th}$ matrix corresponding to the TCR bus. In the equivalent system shown the voltage across the terminals is:

$$\mathbf{V}_t = \mathbf{V}_{th} - \mathbf{Z}_{th}\, \mathbf{I}_r \qquad (3\text{-}37)$$

Using $\mathbf{I}_r$ given in equation (3-36) allows an expression for $\mathbf{V}_t$ to be written. ($\mathbf{I}$ is the identity matrix)

$$\mathbf{V}_{th} = \left[\mathbf{I} + \mathbf{Z}_{th}\mathbf{Y}_{tcr}\left(\sigma_0, \phi_0, \sigma_{1/2}, \phi_{1/2}\right)\right]\mathbf{V}_t \qquad (3\text{-}38)$$

The zero thyristor current at the switching times ($\phi_0+\sigma_0$) and ($\phi_{1/2}+\sigma_{1/2}$) define two relationships between the times σ_0, ϕ_0, $\sigma_{1/2}$ and $\phi_{1/2}$ and the terminal voltage harmonics. These are:

$$0 = v_{t0}\sigma_i + \sum_{m=-\infty}^{\infty} \frac{v_{tm}}{jm}\left[e^{-jm(\phi_i+\sigma_i)} - e^{-jm\phi_i}\right] \qquad \text{for } i=0,1/2 \qquad (3\text{-}39)$$

where v_{t0} is the DC component of the terminal voltage.

Firing strategies express the two additional relationships between the four switching times and the power system harmonics. See section 3.2. For example, two such firing strategies are equidistant firing, equation (3-9), and constant sigma controller, equations (3-11) and (3-12).

An equidistant firing scheme ensures that the firing pulses are equally spaced twice per cycle. In other words the following relationship between ϕ_0 and $\phi_{1/2}$ represent the equidistant strategy:

$$\phi_{1/2} - \phi_0 = \pi \qquad (3\text{-}40)$$

We can solve the equations (3-38), (3-39) and (3-40) simultaneously for a fixed value of firing phase ϕ_0. For the Newton's solution method, let $\sigma_0=\sigma_{1/2}=2(\pi-\phi_0)$ and solve the linear matrix equation (3-38) for $\mathbf{V_t}$ for the initial guess.

The operation of the constant sigma controller is explained more fully in the Chapter 2 and is summarized here. This method uses a requested conduction value, σ_{req}. The constant sigma controller enforces the following two relationships between the two conduction times σ_0 and $\sigma_{1/2}$ and the two non conduction times ($\phi_0 - \phi_{1/2} - \sigma_{1/2}$) and ($2\pi + \phi_0 - \phi_{1/2} - \sigma_{1/2}$):

$$2\pi - \sigma_{req} = \sigma_0 + 2\,(\phi_{1/2} - \phi_0 - \sigma_0) \qquad (3\text{-}41)$$

$$2\pi - \sigma_{req} = \sigma_{1/2} + 2\,(2\pi + \phi_0 - \phi_{1/2} - \sigma_{1/2}) \qquad (3\text{-}42)$$

Rewriting the above equations yields the following two relationships between the thyristor switching times.

$$\sigma_{req} = \frac{\sigma_0 + \sigma_{1/2}}{2} \tag{3-43}$$

$$\phi_{1/2} - \phi_0 = \pi + \frac{\sigma_0 - \sigma_{req}}{2} \tag{3-44}$$

The control parameter σ_{req} takes a value from 0 to π where σ_{req} is a given control point. Equations (3-38) and (3-39) together with (3-43) and (3-44) give us a complete set of equations to solve for the periodic solutions of the system under the constant sigma controller. Note that if the periodic solution is half wave symmetric we have $\sigma_0=\sigma_{1/2}=\sigma_{req}$ otherwise, σ_{req} represents the average of the two conduction lengths. The suggested solution algorithm is to use the Newton's method as was done earlier for the equidistant firing controller. For initial guess, one may solve (3-22) for $\mathbf{V}_t$ by choosing $\sigma_0=\sigma_{1/2}=\sigma_{req}$, $\phi_{1/2}=\phi_0+\pi$ and

$$\phi_0 = \pi - \frac{\sigma_{req}}{2} \tag{3-45}$$

Computation with the infinite harmonic system vectors and matrices are made by assuming the higher harmonic terms can be neglected. From the details in the appendix, it is seen that the elements in the switching matrix **H**, which defines $\mathbf{Y}_{tcr}$ fall off as 1/n. The harmonics in power systems will generally do the same. This allows the higher harmonics to be ignored. The vectors and matrices can therefore be truncated at a harmonic number above the harmonics of interest.

3.4 Dynamics

Analysis of small signal dynamics assumes a particular steady state and studies the behavior of the transients which occur when the system is slightly perturbed from the steady state. That is, the stability of the steady state is analyzed. Since thyristor switching circuits are nonlinear, the small signal dynamics will depend on the steady state chosen.

The steady state is assumed to be periodic with period T. In particular, the steady state wave forms, sources and switching patterns are assumed to be periodic with period T. The Poincare map is a standard tool from dynamical systems theory to study the dynamics of periodic systems [Guckenheimer1986, Thompson1987]. The main idea of this approach is to sample the system states once per cycle and define the Poincare map as the map which advances the system states by one

cycle. If the system state at time t_0 is denoted by $x(t_0)$, then the Poincare map f maps the state at time t_0 to the state at time $T+ t_0$:

$$f\,[x(t_0)] = x(t_0+ T) \tag{3-46}$$

If $x(t_0)$ is the steady state value of the state at time t_0, then $f[x(t_0)] = x(t_0+ T) = x(t_0)$ and the map f has a fixed point at $x(t_0)$. Fixed points of the Poincare map f correspond to steady states of the system. If the state $x(t_0)$ is perturbed from its steady state value, there will be a transient. Samples of this transient once a cycle can be obtained by applying the Poincare map successively to the perturbed state $x(t_0)$. That is, the samples are $x(t_0)$, $f(x(t_0))$, $f(f(x(t_0)))$, $f(f(f(x(t_0))))$, ... The stability of the transient could be deduced from these samples. However, it is better to use stability theory of discrete time systems here. The samples obtained by succesively applying f are a discrete time system whose stability can be assessed by the eigenvalues of the Jacobian of f evaluated at the steady state. The rule for discrete time systems is that if all the eigenvalues of the Jacobian of f lie inside the unit circle of the complex plane, then the steady state is asymptotically stable. Thus the stability of the steady state can be deduced from the Jacobian of the Poincare map. The Poincare map analysis is equivalent to the sampled data approach [Verghese1986] and Floquet stability theory [Hale1963] The Poincare map and the stability analysis is illustrated in more detail below for the Kayenta system.

The first problem is to compute a Poincare map taking into account the switching of the TCSC. Recall that the switching element of the TCSC consists of two back to back thyristors in series with a reactor which conduct on alternate half cycles of the supply frequency. This element is usually called a Thyristor Controlled Reactor (TCR). The switching of the TCSC can be described through state equations which change their dimension with the operation of the thyristors. For the Kayenta system there are four states during thyristor conduction or on state. These states are the current in the TCR, voltage across the TCSC, line current and the voltage across the fixed capacitor. When both thyristors are off the system reduces to three states by dropping the TCR current as described in section 3.2.

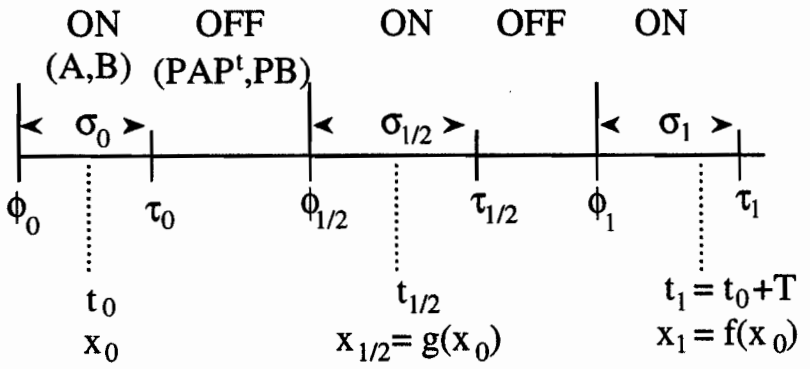

Figure 3.7 TCSC system dynamics over one period.

Figure 3.7 describes the system dynamics as the system state, x_0, evolves over a period T. The conduction starts at times ϕ_0, $\phi_{1/2}$, ϕ_1 which are defined by the control system and the method used to synchronize the firing points to the system states. The turn off times τ_0, $\tau_{1/2}$, τ_1 are defined as the points in time where the current through the thyristors becomes zero. Each of these transitions points are dependent on the system states and signal a change of the dimension of the state equations.

Given a time interval $[s_1,s_2]$, it is convenient to write $f(.,s_1,s_2)$ for the map which advances the state at s_1 to the state at s_2. For example, a Poincare map which advances the state by one period T starting at time t_0 may be written $f(x,t_0,t_0+T)$. For convenience, we adopt the notation that when the thyristor is on during all of the time interval $[s_1,s_2]$, we write $f(x,s_1,s_2)$ as $f_{on}(x,s_1,s_2)$. Similarly, if the thyristor is off during $[s_1,s_2]$, we write $f(y,s_1,s_2)$ as $f_{off}(y,s_1,s_2)$. f_{on} or f_{off} can be computed by integrating the linear system (3-2) or (3-5) over the corresponding time intervals.

The Poincare map $f(x_0)$ can be computed by integrating the appropriate state equations as defined by these transition points. Knowing the starting states x_0 the states at the next sampling point are defined by $f(x_0)$. We construct in stages an expression for the Poincare map $f(x(t_0),t_0,t_0+T)$ in terms of $f_{on}(x,s_1,s_2)$ and $f_{off}(y,s_1,s_2)$ and the coordinate changes (3-47) and (3-48).

$$x(\phi_0)=P^t\, y(\phi_0) \tag{3-47}$$

$$y(\tau_0)=P\, x(\tau_0) \tag{3-48}$$

For convenience, we recall equations (3-2) and (3-5) describing the dynamics of the on and off systems:

$$\dot{x}(t) = Ax(t) + Bu(t) \tag{3-49}$$

$$\dot{y}(t) = PAP^t y(t) + PBu(t) \tag{3-50}$$

At the start of the sampled time t_0, the state is expressed as $x_0=x(t_0)$. The state $x(\tau_0)$ is obtained by integrating the on system, (3-49) , with initial state x_0 from time t_0 to τ_0:

$$x(\tau_0) = f_{on}(x_0, t_0, \tau_0) = e^{A(\tau_0 - t_0)}\left(x_0 + \int_0^{\tau_0 - t_0} e^{-A\alpha} Bu(\alpha + t_0)d\alpha\right) \tag{3-52}$$

The switch off time τ_0 is determined by constraining the thyristor current to zero:

$$0 = cx(\tau_0) = I_r(\tau_0) \tag{3-53}$$

where c=(1,0,0,0). The coordinate change at the switch off (3-48) and integration of the off linear system described by (3-50) yields

$$y(\phi_{1/2})=f_{off}(Px(\tau_0),\tau_0,\phi_{1/2}) \tag{3-52}$$

Similarly, the coordinate change at the thyristor turn on time (3- 47) and integrating the on linear system described by (3-49) yields

$$x(t_{1/2})=f_{on}(P^t\, y(\phi_{1/2}),\phi_{1/2},t_{1/2}) \tag{3-54}$$

A half cycle map (see figure 3.5) is given by combining (3-51), (3-53) and (3-54):

$$g(x_0,t_0,t_{1/2})=f_{on}(P^t\, f_{off}(P\, f_{on}(x_0,t_0,\tau_0),\tau_0,\phi_{1/2}),\phi_{1/2},t_{1/2}) \tag{3-55}$$

The Poincare map may now be written by composing two successive half cycle maps and then neglecting the gory details of the time arguments:

$$f(x_0,t_0,t_0+T) \;= f_{on}\, P^t f_{off}\, P\, f_{on}\, P^t f_{off}\, P\, f_{on}\, x(t_0) \tag{3-56}$$

3.4.1 Jacobian

The stability of the TCSC can now be computed from the Jacobian of the Poincare map evaluated at the steady state or fixed point. We assume that gradient of the thyristor current as it turns off is negative so that the Poincare map is differentiable [Dobson1995b]. Care must be taken to include the dependence of the transition points on the states of the system.

$$\text{Jacobian} = Df(x_0) \tag{3-57}$$

The eigenvalues of this Jacobian provide information on the small signal dynamics of the system. In particular it can be shown that a steady state point, x_0 is exponentially stable if the eigenvalues of the Jacobian evaluated at this point lie inside the unit circle.

The interpretation of these eigenvalues is equivalent to the z-plane formulation of sampled data. The expected relationships between s-plane and the z-plane poles still apply. For example consider a complex pole of the form;

$$s = -\alpha \pm j\omega \tag{3-58}$$

This pole maps to the z-plane as

$$z = e^{-\alpha T} e^{-j\omega T} \tag{3-59}$$

where T is the period of the sampling. The magnitude $|z| = e^{-\alpha T}$ defines the damping. For example a pole at zero in the center of the unit circle implies 100% attenuation or $\alpha =$ – . A pole on the unit circle implies no attenuation or $\alpha = 0$. Any poles outside the unit circle imply an unstable system. The polar angle ωT defines the frequency of oscillation about the sampling frequency. As the polar angle changes from zero to 360° the modulation frequency increases from zero to the sampling frequency of 60 Hz.

To find the Jacobian an important simplification can be made [Dobson1995b]. If we let $[s_1, s_2]$ be a fixed time interval including a thyristor turn off at time τ and no other switchings. For convenience, let x_1 express the state at time s_1. Define $H(x_1,\tau)$ as:

$$H(x_1,\tau) = f_{off}(P\, f_{on}(x_1,s_1,\tau),\tau,s_2) \tag{3-60}$$

$$= e^{PAP^t(s_2-\tau)}Pe^{A(\tau-s_1)}[x_1 + \int_{s_1}^{\tau} e^{A(s_1-\alpha)}Bu(\alpha)d\alpha] + \int_{\tau}^{s_2} e^{PAP^t(s_2-\alpha)}PBu(\alpha)d\alpha \qquad (3\text{-}61)$$

Note that H expresses $y(s_2)$ as a function of x_1 and the switch off time τ. τ is a function of x_1 which is determined by the constraint of zero thyristor current at time τ. The map $f(x_1,s_1,s_2)$ which advances the state x_1 to the state $y(s_2)$ is equal to:

$$f(x_1,s_1,s_2) = H(x_1,\tau(x_1))$$

The chain rule gives:

$$Df(x_1,s_1,s_2) = \frac{\partial H}{\partial x_1} + \frac{\partial H}{\partial \tau}D\tau \qquad (3\text{-}62)$$

$$Jacobian = Df(x_0)$$

where the row vector $D\tau$ is the gradient of the switch off time τ with respect to x_1. The partial of H with respect to τ is the first order variation of H due to a variation in the switch off time τ. Differentiating H with respect to the thyristor turn off time τ yields:

$$\frac{\partial H}{\partial \tau} = e^{PAP^t(s_2-\tau)}PAc^tce^{A(\tau-s_1)}[x_1 + \int_{s_1}^{\tau} e^{A(s_1-\alpha)}Bu(\alpha)d\alpha] \qquad (3\text{-}63)$$

where we have used the identity

$$c^tc = I - P^tP$$

Note that the two terms associated with τ in the limits of the two integrals of (3-61) cancel. Rewriting this equation yields:

$$\frac{\partial H}{\partial \tau} = e^{PAP^t(s_2-\tau)}PAc^tcx(\tau) \qquad (3\text{-}64)$$

which is equal to zero according to the constraint of zero thyristor current at time τ, (3-52). Hence we obtain the following surprising and simple result:

$$Df(x_1, s_1, s_2) = \frac{\partial H}{\partial x_1} = e^{PAP^t(s_2-\tau)} P e^{A(\tau-s_1)} \tag{3-65}$$

Result (3-65) implies that the thyristor turn off time may be regarded as constant when deriving the Jacobian.

Despite the simplification, it is sometimes necessary to compute $D\tau$. The equation which determines the thyristor turn off time τ is the first positive root of:

$$0 = cx(\tau) = ce^{A(\tau-s_1)}[x_1 + \int_{s_1}^{\tau} e^{A(s_1-\alpha)} Bu(\alpha) d\alpha] \tag{3-66}$$

where c=(1,0,0,0). Differentiation with respect to s_1 and solving for $D\tau$ yields:

$$D\tau = \frac{-ce^{A(\tau-s_1)}}{c(Ax(\tau) + Bu(\tau))} = \frac{-ce^{A(\tau-s_1)}}{c\dot{x}(\tau-)} \tag{3-67}$$

$c\dot{x}(\tau-)$ (the limit of $c\dot{x}(t)$ as t approaches τ from below) is the gradient of the thyristor current as it turns off at τ.

When the TCSC is in steady state with a periodic trajectory of period T, the Poincare map has a corresponding fixed point. That is,

$$f(x(t_0), t_0, t_0+T) = x(t_0) \tag{3-68}$$

The stability of a periodic orbit is the same as the stability of the corresponding fixed point of the Poincare map [Guckenheimer1986,Thompson1987]. That is, the stability of the periodic orbit can be computed from the Jacobian of the Poincare map evaluated at the fixed point. In particular, the periodic orbit is exponentially stable if the eigenvalues of the Jacobian lie inside the unit circle. Since the thyristor turn off time and the Poincare map are discontinuous at a switching time

bifurcation, we assume when computing the Jacobian in this section that the system is not exactly at a switching time bifurcation. To compute the Jacobian of the Poincare map define the function H_0 as:

$$H_0(x_0,\tau_0,\phi_{1/2}) = f_{on}(P^t f_{off}(P f_{on}(x_0,t_0,\tau_0),\tau_0,\phi_{1/2}),\phi_{1/2},t_{1/2}) \tag{3-69}$$

Note that H_0 expresses $x(t_{1/2})$ as a function of x_0, the turn off time τ_0 and the turn on time $\phi_{1/2}$. τ_0 is a function of x_0 which is determined by the constraint of zero thyristor current at time τ_0. The turn on time $\phi_{1/2}$ may or may not be a function of x_0 depending on the firing strategy. Then the half cycle map $f(x_0,t_0,t_{1/2})$ is equal to:

$$f(x_0,t_0,t_{1/2}) = H_0(x_0,\tau_0(x_0),\phi_{1/2}(x_0)) \tag{3-70}$$

Using the chain rule, the Jacobian of the half cycle map is:

$$Df(x_0,t_0,t_{1/2}) = \frac{\partial H_0}{\partial x_0} + \frac{\partial H_0}{\partial \tau_0} D\tau_0 + \frac{\partial H_0}{\partial \phi_{1/2}} D\phi_{1/2} \tag{3-71}$$

which reduces to:

$$Df(x_0,t_0,t_{1/2}) = \frac{\partial H_0}{\partial x_0} + \frac{\partial H_0}{\partial \phi_{1/2}} D\phi_{1/2} \tag{3-72}$$

using the simplification discussed earlier. Differentiating H_0 with respect to x_0 and $\phi_{1/2}$ yields:

$$\frac{\partial H_0}{\partial x_0} = e^{(t_{1/2}-\phi_{1/2})} P^t e^{(\phi_{1/2}-\tau_0)} P e^{(\tau_0-t_0)} \tag{3-73}$$

$$\frac{\partial H_0}{\partial \phi_{1/2}} = -e^{(t_{1/2}-\phi_{1/2})} c^t c\dot{x}(\phi_{1/2}+) \tag{3-74}$$

where $c\dot{x}(\phi_{1/2}+)$ is the gradient of the TCR current as it turns on at $\phi_{1/2}$. In (3-72), the row vector $D\phi_{1/2}$ is the gradient of the turn on time $\phi_{1/2}$ with respect to x_0. This term depends on the firing scheme as follows:

a) In an equidistant firing, $\phi_{1/2}=(T/2)+\phi_{req}$ as given in (3-9). Hence $D\phi_{1/2}=0$. This is the simplest firing scheme; the turn on time does not depend on the system state.

b) In the constant sigma controller, $\phi_{1/2}=(\phi_0+\tau_0+2\pi-\sigma_{req})/2$ as given in (3-11). ϕ_0 and τ_0 are the previous turn on and turn off times. Both are dependent on x_0. Differentiation yields:

$$D\phi_{1/2}=\frac{D\phi_0+D\tau_0}{2} \tag{3-75}$$

where $D\phi_0$ and $D\tau_0$ represent the gradient of the turn on time ϕ_0 and turn off time τ_0 with respect to x_0. By analogy with (3-67), $D\tau_0$ and $D\phi_0$ are equal to:

$$D\tau_0=\frac{-ce^{A(\tau_0-t_0)}}{c\dot{x}(\tau_0-)} \tag{3-76}$$

$$D\phi_0=\frac{-ce^{A(\phi_0-t_0)}}{c\dot{x}(\phi_0+)} \tag{3-77}$$

where c=(1,0,0,0), and the terms in the denominator denote the gradients of the TCR current as it turns on at ϕ_0 and turns off at τ_0.

c) Using (3-13), $\phi_{1/2}=\alpha_{reqv}+\tau_{v0}$ when the firing is synchronized with respect to the zero crossing of the TCSC voltage. τ_{v0} represents the time at which the voltage across the TCR crosses zero when the TCR is conducting. τ_{v0} depends on x_0. Differentiation yields:

$$D\phi_{1/2}=D\tau_{v0}=\frac{-me^{A(\tau_{v0}-t_0)}}{m\dot{x}(\tau_{v0})} \tag{3-78}$$

where m=(0,1,0,0) and the term in the denominator is the gradient of the voltage across the TCR current at the zero crossing time τ_{v0}.

d) Using (3-15), $\phi_{1/2} = \alpha_{reqc} + \tau_{c0}$ if the firing is synchronized with respect to the zero crossing of the line current where τ_{c0} denotes the time at which the line current crosses zero when the TCR is off. τ_{c0} depends on x_0. Differentiation yields:

$$D\phi_{1/2} = D\tau_{c0} = \frac{-n[e^{PAP^t(\tau_{c0}-\tau_0)}Pe^{A(\tau_0-t_0)}]}{n\dot{y}(\tau_{c0})} \qquad (3\text{-}79)$$

where n=(0,1,0) and the denominator is the gradient of line current at the zero crossing time τ_{c0}. Note that the numerator is obtained using the simplification which allows the switch off time τ_0 be regarded as a constant when deriving this expression.

Similarly, to compute the Jacobian of the second half cycle map, define $H_{1/2}(x_{1/2},\tau_{1/2},\phi_1)$ as:

$$H_{1/2}(x_{1/2},\tau_{1/2},\phi_1) = f_{on}(P^t f_{off}(P f_{on}(x_{1/2},t_{1/2},\tau_{1/2}),\tau_{1/2},\phi_1),\phi_1,t_1) \qquad (3\text{-}80)$$

Note that $H_{1/2}$ expresses $x(t_1)$ as a function of $x_{1/2}$, the turn off time $\tau_{1/2}$ and the turn on time ϕ_1. $\tau_{1/2}$ is a function of $x_{1/2}$ which is determined by the constraint of zero thyristor current at time $\tau_{1/2}$. The turn on time ϕ_1 may or may not depend on $x_{1/2}$ depending on the firing strategy. Then the second half cycle map $f(x_{1/2}, t_{1/2}, t_1)$ is equal to:

$$f(x_{1/2},t_{1/2},t_1) = H_{1/2}(x_{1/2},\tau_{1/2}(x_{1/2}),\phi_1(x_{1/2})) \qquad (3\text{-}81)$$

Using the chain rule and the simplification, the $Df(x_{1/2}, t_{1/2}, t_1)$ is equal to:

$$Df(x_{1/2},t_{1/2},t_1) = \frac{\partial H_{1/2}}{\partial x_{1/2}} + \frac{\partial H_{1/2}}{\partial \phi_1} D\phi_1 \qquad (3\text{-}82)$$

where each term in the right hand side can directly be written from its corresponding term as defined in the equations (3-72) to (3-79) by replacing all the subscripts "1/2" by "1" and the subscripts "0" by "1/2". Next, using the chain rule, the Jacobian of the Poincare map is given by:

$$Df(x_0,t_0,t_1) = Df(x_{1/2},t_{1/2},t_1)\, Df(x_0,t_0,t_{1/2}) \tag{3-83}$$

where $Df(x_{1/2},t_{1/2},t_1)$ and $Df(x_0,t_0,t_{1/2})$ are given by (3-72) and (3-82).

3.4.2 Simplifications for symmetric periodic orbits

It is convenient to take advantage of symmetry when the periodic orbits are half wave symmetric. Half wave symmetry of a periodic orbit means that the system states are equal in magnitude and opposite in sign to the system states half cycle or T/2 later. That is, if $x(t_0)=x_0$ is the system state at the beginning of the period, then:

$$f(x_0,t_0,t_0+T/2) = -x_0 \tag{3-84}$$

In a half wave symmetric periodic orbit, the two conduction times $\sigma_1=\sigma_2=\sigma$ are equal and the firing pulses are sent every half a cycle. The conduction time σ of the conducting thyristor is given by the constraint equation:

$$0=cx(t_0+\sigma) \tag{3-85}$$

The fixed points x_0 corresponding to half wave symmetric periodic orbits can be computed by solving (3-82) and (3-83) simultaneously. In addition, by inspection, the Poincare map Jacobian simplifies to:

$$Df(x_0,t_0,t_0+T) = \left(\frac{\partial H_0}{\partial x_0} + \frac{\partial H_0}{\partial \phi_{1/2}} D\phi_{1/2}\right)^2 \tag{3-87}$$

where the terms in the right hand side are given in the equations (3-67) and (3-73) to (3-78).

4

BIFURCATIONS, HARMONIC DISTORTIONS AND RESONANCE

As FACTS circuits proliferate in transmission systems, there is an increasing need to better understand their impact on power systems. This need for understanding not only includes the impact of TCSC systems on stability, transmission limits and subsynchronous oscillation but also the problem of harmonic interactions. For example, any thyristor based FACTS system will generate harmonics which in turn will interact with the transmission system causing voltage distortions. These distortions can change the operation of the switching circuit. If the system is designed correctly, these harmonic interactions will not cause problems. However, it is necessary to use the harmonic admittance tools discussed in Chapter 3 to correctly compute and understand these harmonic distortions. Moreover, there is evidence that harmonic interactions are capable of causing new types of instabilities in which switching times jump or bifurcate[Jalali1996]. This chapter is based on [Jalali1992a, Jalali1993, Jalali1996, Dobson1995a]

Present techniques for the study of harmonic interactions can be grouped into three categories: time domain simulation, frequency plane analysis and state variable analysis. Time domain simulation is, in many respects, the most mature methodology. The main drawback is that time domain simulation is a quantitative method which provides little understanding of the important interactions. Frequency plane analysis and linear state variable methods provide useful qualitative information but they suffer from the simplification required to achieve a solution. The models used generally oversimplify either the power system or the switching circuit so that most harmonic interactions are neglected.

The classical analysis is often applicable, but can fail for certain circuit parameters and operating conditions. Under these conditions, the TCR current and voltage wave forms can become highly distorted. For example, Bohmann (1989) showed that a single phase SVC circuit can exhibit behavior much like resonance in a linear circuit for certain parameter values. These large harmonic distortions are associated with the natural frequencies of the circuit, from when the reactor is fully on to when it is fully off, spanning an odd harmonic number. The large harmonic distortions can lead to

instabilities associated with either a new earlier TCR current zero, the disappearance of the TCR current zero or a thyristor misfire (section 4.2). These instabilities, called switching time bifurcations [Jalali1996, Dobson1995b], are very different from conventional bifurcations in that they are not detected by eigenvalues of the Jacobian matrix crossing the unit circle. Section 4.3 sketches an approach to exact prediction of resonance points using eigenvalues.

4.1 Switching time Bifurcations

When the harmonic components of the TCR current and voltage become very large, the current and voltage wave forms become highly distorted. These distortions can lead to instabilities as switching times suddenly change or bifurcate as follows:

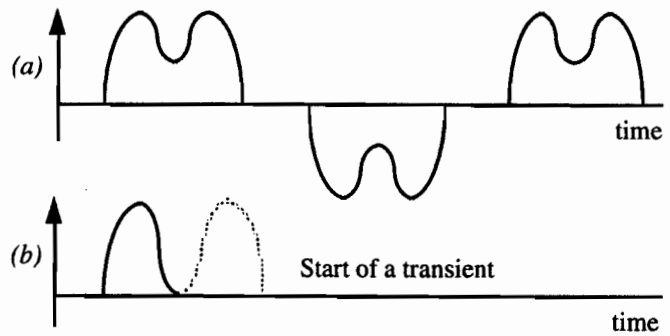

Figure 4.1. A new earlier TCR current zero appears (a) $\sigma > \sigma^*$, (b) $\sigma = \sigma^*$

Figure 4.1 describes one way in which the system can lose stability. Suppose that the harmonic distortion produces a dip in the TCR current as shown in Figure 4.1a. As the conduction time reduces, the dip lowers until, at the critical point σ^*, a new earlier zero of the TCR current is produced (Figures 4.1b). The switching off time of the thyristor has suddenly decreased and the stable operation of the system at the previous periodic orbit has been lost. We call this qualitative change a switching time bifurcation. As soon as the switching time bifurcates, a transient starts.

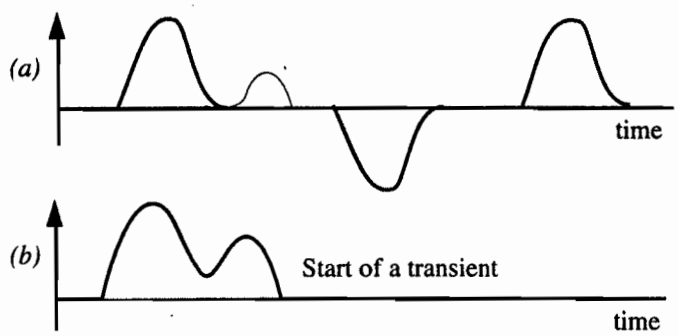

Figure 4.2. Disappearance of two TCR current zeros (a) $\sigma = \sigma^*$, (b) $\sigma > \sigma^*$

Figure 4.2 explains another type of switching time bifurcation in which the system loses stability as a TCR current zero disappears. Figure 4.2a shows a periodic solution for the TCR current with the solid line. The gray line shows the thyristor current that would occur if the thyristor did not switch off for negative current. As the phase delay of the firing pulses slowly decreases, the dip in the dotted line rises until, passing through the critical conduction time σ^*, the current zero disappears and a new, later zero of the TCR current applies (see Figure 4.2b). The switching off time of the thyristor has suddenly increased in a switching time bifurcation and stability has suddenly been lost. Note how the zero of the actual TCR current coalesces with a zero of the fictitious current indicated by the dotted line and disappears. As soon as the switching time bifurcates and system stability is lost, a transient starts.

Figure 4.3 explains the onset of instability due to a thyristor misfire [Jalali1992a, Jalali1993, Rajaraman1993]. The TCR current is denoted by the solid line in the Figure 4.3a and the thyristor starts conducting, as expected, when a firing pulse is applied. The gray lines in Figure 4.3 are used to show the thyristor current that would have obtained if the system were integrated backwards in time with the thyristor on and with the initial TCR current of zero at the firing time. As the firing pulses are moved towards the zero crossings of the TCR voltage, the TCR voltage blocked by the thyristors at the firing time decreases. Assuming thyristors are ideal, the critical point occurs when the turn on firing pulse is sent at the zero crossings of the TCR voltage as shown in the Figure 4.3b. As the voltage at the firing time decreases further, one of the thyristors misfires because the voltage across it is negative when the firing pulse arrives.

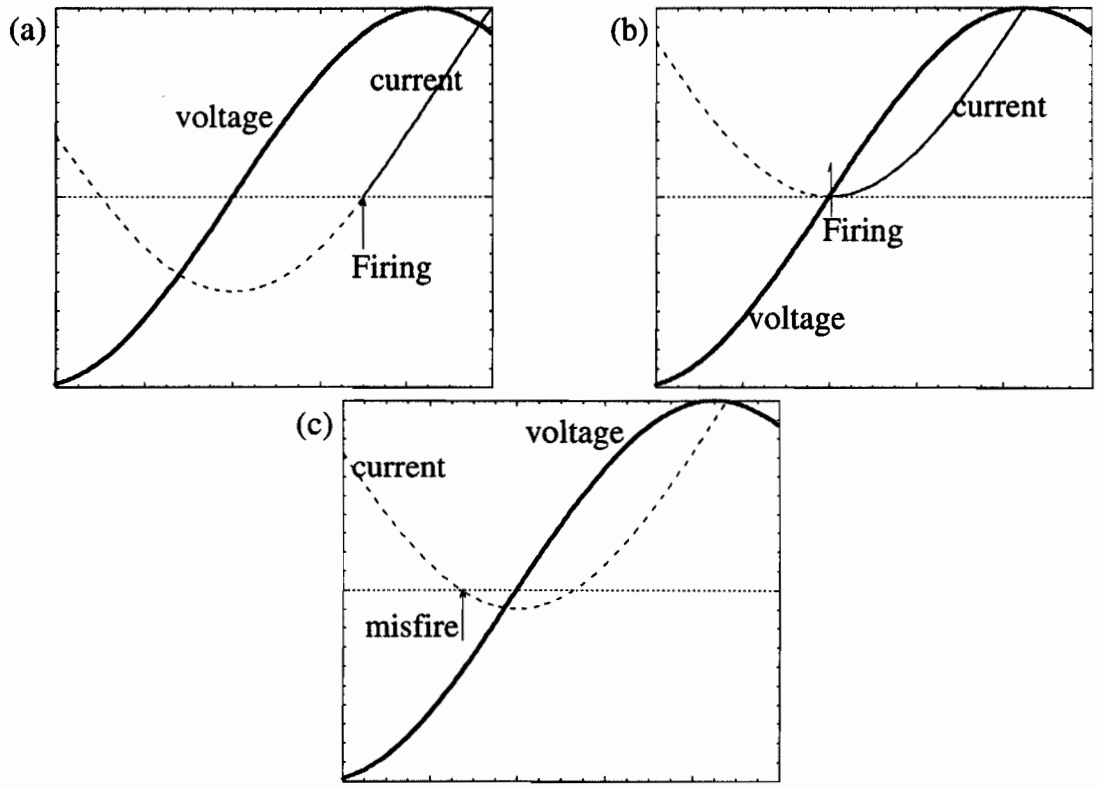

Figure 4.3. Thyristor misfire (a) $\sigma > \sigma^*$, (b) $\sigma = \sigma^*$,(c) $\sigma < \sigma^*$

4.2 Kayenta System

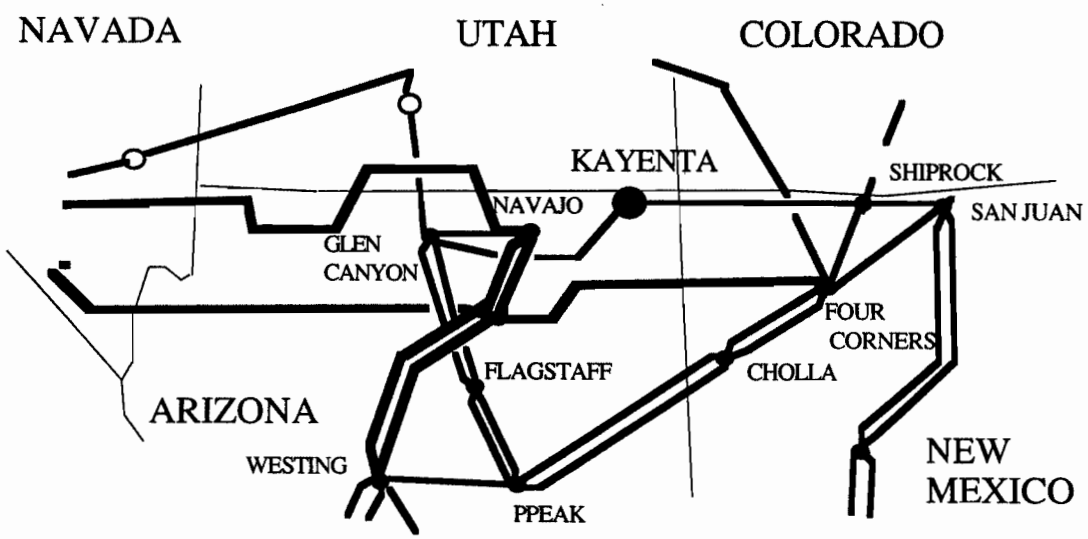

Figure 4.4. System Diagram

The Kayenta Substation on the 190 mile, 230 kV transmission line between Glen Canyon and Shiprock is shown in Figure 4-4.This transmission line was constructed as part of the original Federal 230/345 kV Colorado River Storage Project. With completion in 1964, this line integrated the Colorado River Storage Project loads with new generation at Glen Canyon and Flaming Gorge. The scheduling capability of the Glen Canyon-Shiprock line was approximately 300 MW. In 1968, the four Corners Cholla 345 kV line was completed follow by a 500kV line. The addition of these and other transmission lines out of Four Corners diminished the ability of the Glen Canyon-Shiprock line to carry scheduled power. This ability was regained by the with the addition of a phase shifter to the line in 1977.

Load growth on the interconnected system and restriction on building new lines opened the possibility of operation of the Glen Canyon-Shiprock line closer to its thermal capacity. This resulted in a decision to add 330 Mvar of series capacitor with a 15 Ohm section being controlled using a TCSC. This was placed at the Kayenta Substation and is shown in Figure 4.5.

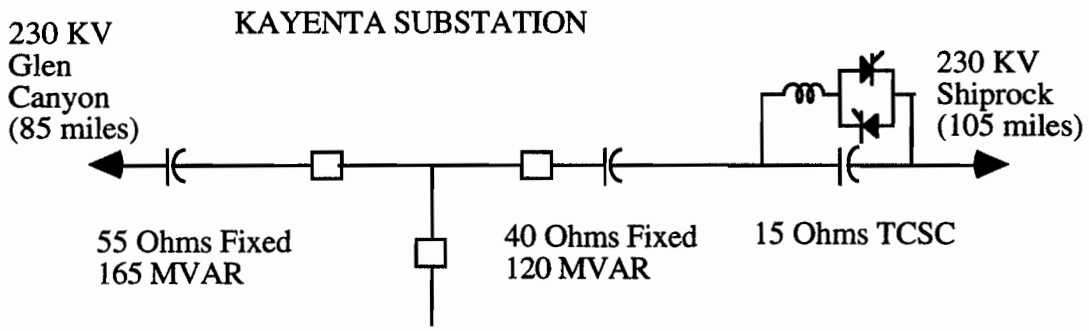

Figure 4.5. Kayenta Substation.

The reduced system is shown in Figure 4.6. This consists of 95 ohms (27.9 μF) fixed and 15 ohms (177 μF) of TCSC. The total system inductance is 153 Ohms with a X/R of 10. In the initial design, the controlled reactor value L_r was fixed at 3.4 mH [xx]. The final system uses a controlled reactor of twice the original value, or 6.8 mH. This change was a response to harmonic instabilities. In this scheme, the system is controlled by varying a requested conduction time σ_p.

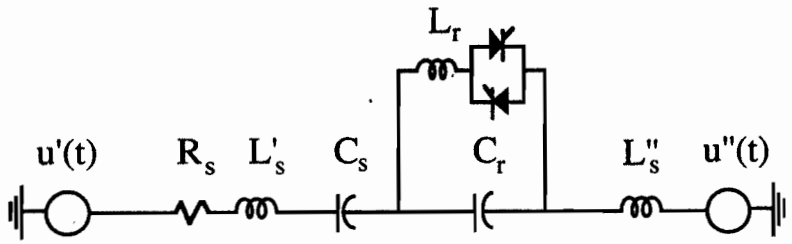

Figure 4.6 The TCSC Model for Kayenta

4.2.1 Classical Steady State Models

There are two approximate approaches to calculating the steady state of a system containing a TCSC. One is the average inductance method and the other is the constant current model. The average inductor model is a simplified but useful method for predicting potential problems with the operation of a TCR. In this model, the TCR is represented as a variable inductance $L_{eq}(\sigma)$ in series with a harmonic voltage source, $V_n(n\omega t,\sigma)$. Both are dependent on the conduction time of the TCR, σ. The variable inductance $L_{eq}(\sigma)$ is defined to be the ratio of the TCR voltage (assumed sinusoidal at the fundamental frequency) to the fundamental component of the TCR current.

$$L_{eq}(\sigma) = L_r \frac{\pi}{\sigma - \sin(\sigma)} \qquad 0 \le \sigma \le \pi \tag{4-1}$$

L_r is the series inductance in the TCR branch. Equation (4-1) defines a minimum value equal to L_r when each thyristor is conducting for half a cycle ($\sigma=\pi$) and a maximum value of infinity when neither thyristor is conducting ($\sigma=0$). This model predicts a potential resonance point for the values of σ for which $L_{eq}(\sigma)$ is tuned at some integer harmonic number with the rest of the system.

The resonant frequency of the Kayenta system can be computed from the above equivalent model by replacing the TCR in Figure 3 with an average inductor model. The resonant frequencies are given by:

$$f_r = \frac{1}{2\pi}\sqrt{A + \sqrt{A^2 - \frac{1}{C_r C_s L_s L_{eq}(\sigma)}}} \tag{4-2}$$

where $A = \frac{1}{2L_sC_s} + \frac{1}{2L_sC_r} + \frac{1}{2L_{eq}(\sigma)C_r}$.

Equation (4-2) implies that the system harmonic resonance frequency depends on the conduction time, σ, of the TCR and the inductive and capacitive components. For example, the circuit can have resonance at the 2nd, 3rd or 4th harmonic for typical values of system impedance and σ. In cases where the harmonic voltage generated by the TCR is at the same frequency, this model predicts that large harmonic voltage and currents will flow.

Figure 4.7 shows the predicted resonance points using the average inductor model as σ varies from zero to 180° for three possible values of L_T, namely 1.7 mH, 3.4 mH and 6.8 mH . This model suggest a basic resonance at the fundamental frequency and at the 2nd, 3rd and/or 4 th.. depending on the value of L_T.

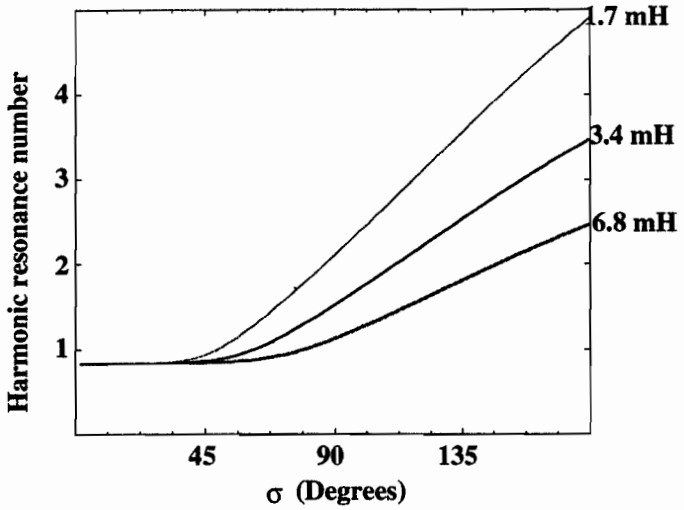

Figure 4 .7 Resonance predictions using the average inductor model

The basic shortcoming of the average inductor model is the assumption that the voltage across the capacitor is an ideal sinusoid at the fundamental frequency. This implies no harmonics and a fixed voltage magnitude. This is an excellent approximation for static VAR compensators which are used to control bus voltage and used with filters to control harmonics. For the TCSC there are major distortions in the voltage including a fundamental resonance which results in error using the average inductance method.

An alternative to the average inductor model is to assume that the current in the transmission line is a constant current source. In this case the thyristor current can be expressed as:

$$I_{SCR} = A\cos(\omega t) - A \cdot \cos(\frac{\sigma}{2})\frac{Cos(\omega_0 t)}{Cos(\kappa\frac{\sigma}{2})}$$

$$A = \frac{\omega_0^2}{\omega_0^2 - \omega^2} \qquad \kappa = \frac{\omega_0}{\omega} \qquad \omega_0 = \frac{1}{\sqrt{LC}}$$

The fundamental resonance point is defined as:

$$Cos(\kappa\frac{\sigma}{2}) = 0 \qquad \kappa\sigma = \pi$$

This gives a different and normally better prediction of the location of the fundamental resonance point than that achieved by the average inductance methods. The predicted points for both methods are given in the table below.

Table 4.1 Sigma Operating Point for Fundamental Resonance

Inductance	1.7 mh	3.4 mh	6.8 mh
Average Inductance	54°	68°	88°
Constant Current	37°	53°	74°

The fundamental impedance of the Kayenta TCSC with a 6.8 mh reactor is shown in Figure 4-8. Note that the impedance changes from capacitive to inductive as sigma increases. In most systems the operating region is confined to the capacitive region. The amount of controlled capacitance ranges from 1 to 3 pu based on the installed value of capacitance. For Kayenta this control range is between 15 and 45 Ohm.

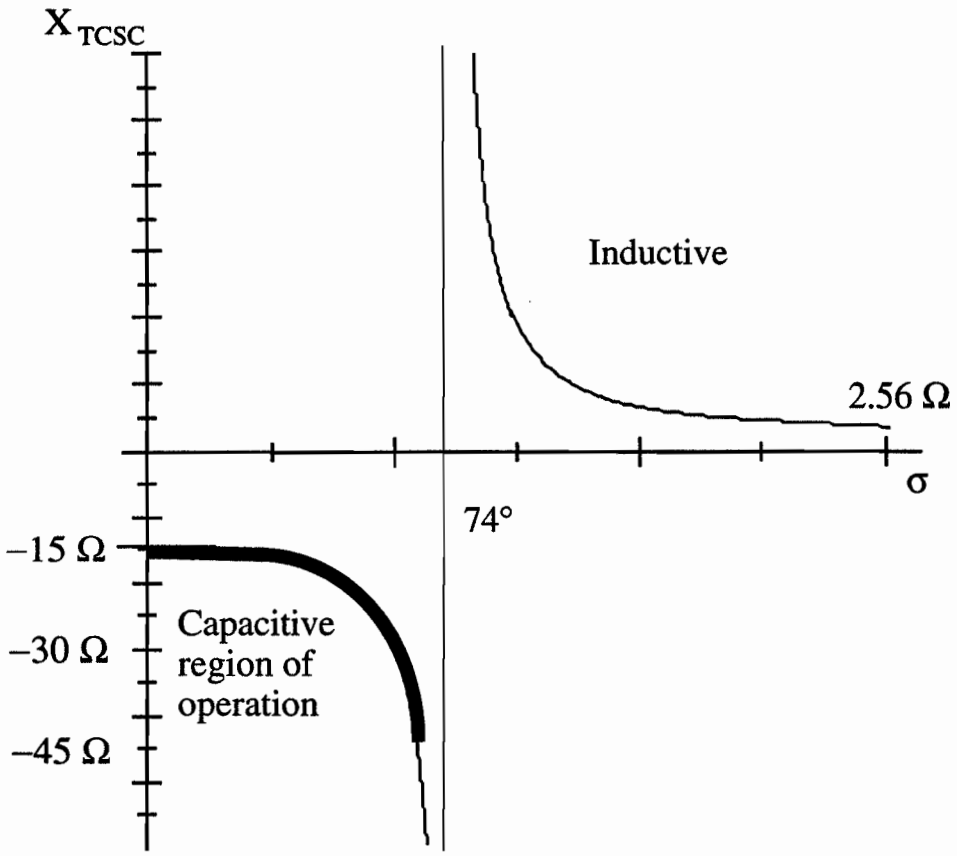

Figure 4.8 Fundamental Impedance of TCSC with 6.8 mh Reactor

4.2.2 Exact Steady State Solutions.

The average inductance model and the constant current approximation are useful in some cases. However, errors can arise from assuming either that voltage or current is harmonic free. In the actual system there will be harmonics in current and voltage which must be included in any steady state calculation. Steady state operation implies a stable periodic solution. In such cases, Fourier techniques are used to calculate the harmonic content. By expressing the voltage and current as a Fourier series, a harmonic admittance matrix for the TCR can be constructed from which the steady state solution for the Kayenta system can be solved.

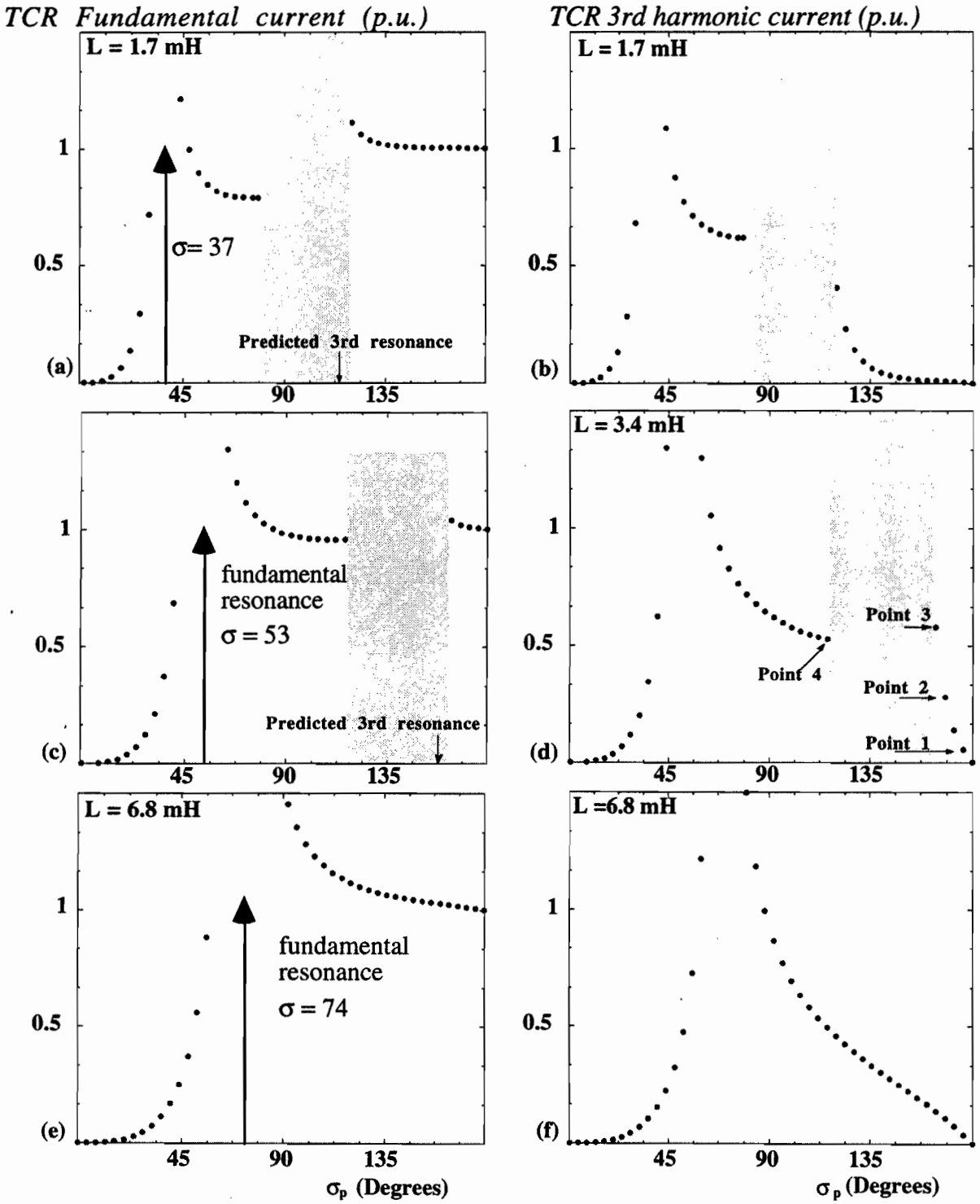

Figure 4.9 (a), (c) and (e) show the fundamental current. (b), (d) and (f) show the third harmonic current in the TCR for possible values of L_r for the Kayenta system.

Figure 4.9 shows the solution to the harmonic matrix equations for the Kayenta system described earlier. Figures (a), (c) and (e) show the fundamental component of the TCR current for three possible values of L_R , namely 1.7 mH, 3.4 mH and 6.8 mH respectively. Similarly, Figures (b), (d) and (f) show the 3rd component of current. These harmonic currents are plotted as a function of the control sigma parameter σ_p. Only solutions which are half wave symmetric are shown in this Figure. All the plots are normalized to the fundamental component of the TCR current at full conduction, σ_p equal to 180 electrical degrees.

The expected fundamental resonance along with the predicted values are shown. In addition to the fundamental resonance, the Kayenta system with the L_R values 1.7 mH or 3.4 mH also shows a region delimited by switching time bifurcations. These region do not have any half wave symmetric periodic solutions as calculated using the harmonic admittance method. Moreover, as σ_p is decreased from 180 degrees towards this region, a rapid 3rd harmonic current builds up as seen. Note that the previously predicted 3rd harmonic resonance points from the average inductor model falls within the shaded regions for both cases.

For L_R value of 6.8 mH the region delimited by switching time bifurcations completely disappears and the system harmonics behave as expected. Two general ways by which the periodic solutions can be lost are described in Section 4.2. This loss is either through disappearance of a current zero or through the creation of a new current zero. In both cases the harmonic interaction and the resulting distortion of the thyristor current is critical. This is demonstrated by time domain simulations of the Kayenta system with L_R value of 3.4 mH.

4.2.3 EMTP simulations, Points 1,2 and 3 (L_R=3.4 mH)

The first group of EMTP study focuses on how the periodic solutions end as we decrease the system parameter σ_p from 180 degrees towards the shaded region for the Kayenta system with the L_R value of 3.4 mH as seen in Figure 4-9(d) For this purpose, three periodic solutions are labeled as "point 1", "point 2" and "point 3" in the Figure 4-9(d). The simulation in the Figure 4.10(a),(b) and (c) show the periodic solutions of the TCR current for the points 1, 2 and 3 respectively. Note that as we move towards the third point, the harmonics generated by the system nonlinearities produce a dip in the TCR. Figure 4.10(c) shows that the dip in the TCR for the third point is almost touching the zero axis.

Figure 4-10(d) shows the transient which occurs when requesting the system to operate in the shaded region of Figure 4-9 which is the region of no solutions. As can be seen the system is initially in

steady state operating close to point three. As the control parameter, σ_p, is decreased by 4 degrees, the dip in the TCR current lowers and a new zero of the TCR current is produced. The switching off time of the thyristor is suddenly decreased and the system stable operation at the previous periodic orbit is lost. Upon this, a transient starts and the controller attempts to find another nearby periodic solution but is not successful.

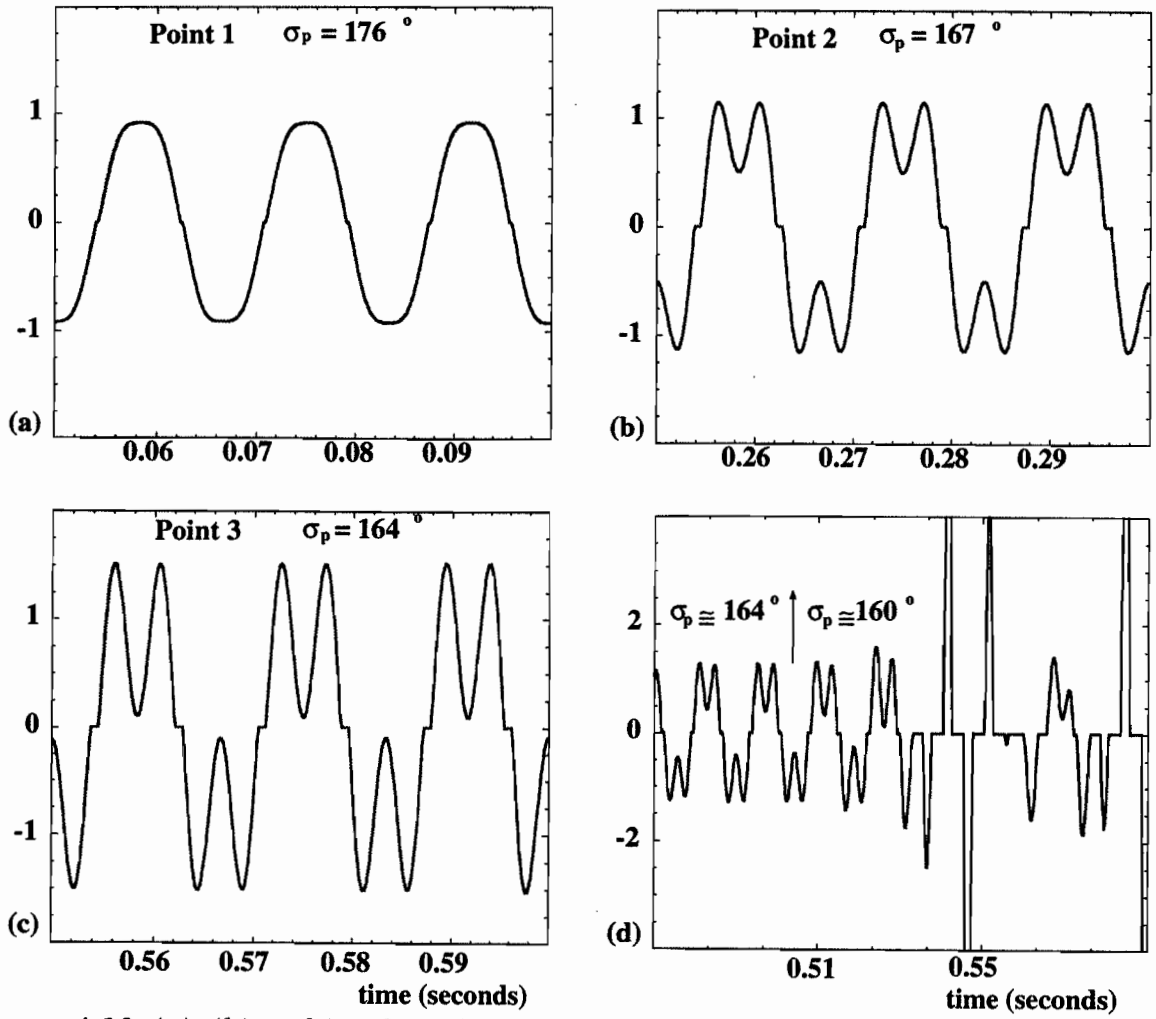

Figure 4.10. (a), (b) and (c) show the TCR current (p.u.) at points 1,2 and 3 (d) transient which occur when requesting the system to operate in the shaded region.

4.2.4 EMTP simulations, Point 4 (L_R=3.4 mH)

This study focuses on how the periodic solutions end as we increase the system parameter σ_p, so as to approach the shaded region for the Kayenta system with the L_R value of 3.4 mH. For this purpose, the periodic solution is labeled as "point 4" in Figure 4.11. This is a combination of

Figures 4.9(c) and (d) showing both the fundamental and third harmonic current around the region of interest.

The EMTP study shows the system in steady state close to point 4 as seen in the Figure 4.12. A transient occurs upon increasing σ_p by 4 degrees. As can be seen, the transient starts when the TCR current misses the first zero. At this point, the switching off time of the thyristor suddenly increases and the system stable operation at the previous periodic orbit is lost and the controller attempts to find another nearby periodic solution . Figure 4.13 shows the system transients starting from the time the periodic solution is lost until a new periodic solution is found, referred here as "point 5". It is clear from the time domain simulations that the new periodic solution is no longer half wave symmetric.

The harmonic components of the point 5 can be calculated using the system harmonic matrix equations and is shown in the Figure 4.11. As can be seen from this plot, the set of periodic orbits which contains point 5 covers only a small region. The periodic solutions in this new region are no longer half wave symmetric, $\sigma_1 \neq \sigma_2$. This also introduces even harmonics into the system.

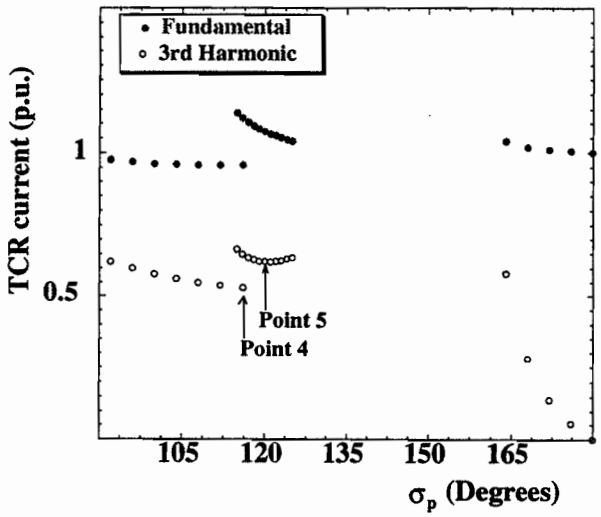

Figure 4.11 Kayenta system , L_R is 3.4 mH

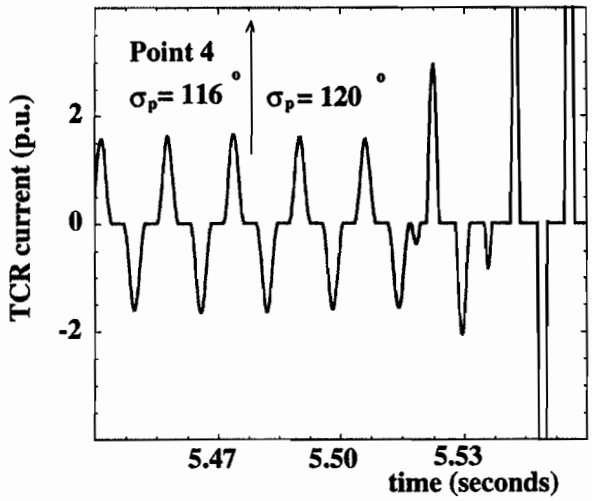

Figure 4.12 Point 4 and $\sigma_p = \sigma_p + 4$ degrees.

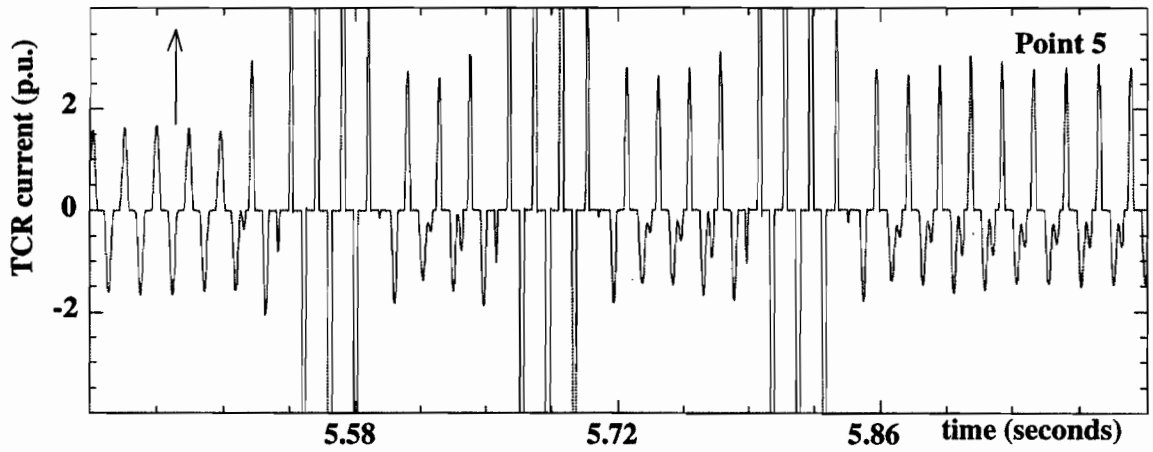

Figure 4.13. Point 5; σ_p steps up from 115 degrees to 120 degrees

4.2.5 Periodic orbits of the Kayenta system with a 0.1 % Ambient second harmonic (L_R=6.8 mH)

Figure 4.14 shows that the average inductor model predicts a 2nd harmonic resonance condition for the Kayenta system for all of the three possible values of L_R if there exits an ambient second harmonics in the power system. In particular, this model predicts that the final design for the Kayenta 230 kV Substation which has an L_R=6.8 mH contains a 2nd harmonic resonance point when sigma is close to 147 degrees. This section investigates this potential problem. For this study, we assume there exists approximately 0.001 p.u. ambient second harmonic voltage across the TCSC module when operating at σ =0°.

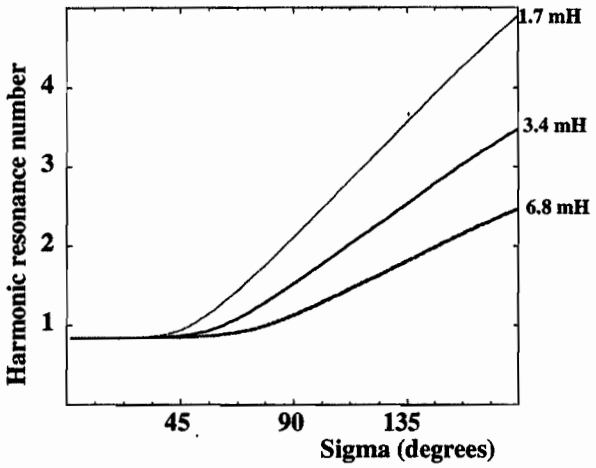

Figure 4.14. Harmonic resonance predictions

Figure 4.15 shows the fundamental and second harmonic component of the TCR current as a function of the control parameter, σ_p which is obtained by solving the system harmonic matrix equations. The periodic solutions break up into two sets of periodic solution between which a no solution region, "shaded gray", is introduced. As can be seen from this Figure, one set of periodic solutions ends at σ_p=142 degrees while the other set ends at σ_p =152 degrees. Note that the previously predicted 2nd harmonic resonance point from the average inductor model, σ_p=147, falls within the shaded regions.

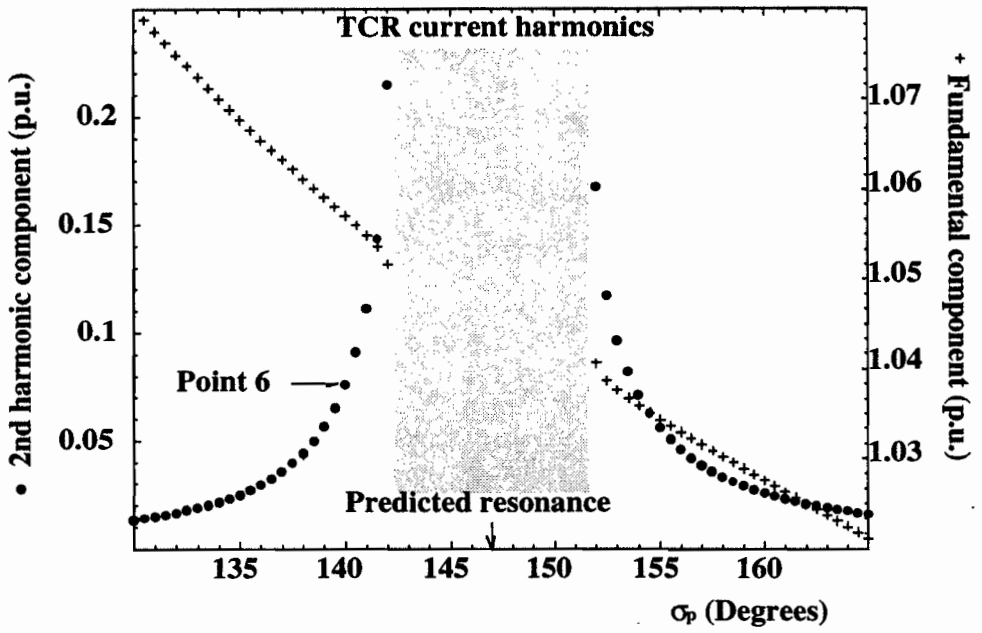

Figure 4.15 The fundamental and the 2nd component of the TCR current

EMTP was used again to study the transients which occurs as the system loses stability when trying to enter the shaded region. In particular, we study the system behavior as we order the system to move from point 6 (cf. Figure 4.15) into the shaded region by increasing the sigma parameter, σ_p by four degrees.

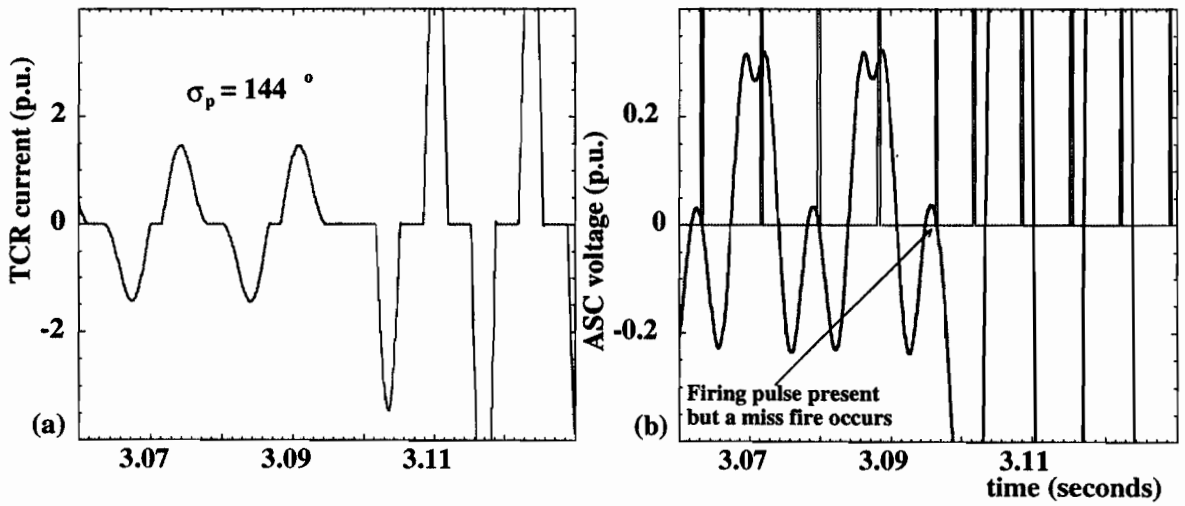

Figure 4.16(a) Transient in the TCR; (b) Firing error due to ambient 2nd.

The system is initially in steady state at point 6 as shown in the right side of Figure 4.16(a). Figure 4.16(a) also shows the transient which occurs upon slowly increasing σ_p. As the system slowly drifts

towards the new value of σ_p, the system gets closer to the shaded region. Once the dynamics of the system hits this boundary, a transient starts upon which the controller attempts to find another periodic solutions nearby.

Figure 4.16(b) shows the voltage across the TCR and the firing pulses sent to the back to back thyristors. As the system drifts towards the shaded region, the 2nd harmonic voltages across the TCR is magnified. This produces an increasing asymmetry in the TCSC voltage waveforms which eventually results in a thyristor misfire (cf. Figure 4.16(b)). This starts a transient upon which the controller attempts to find another nearby periodic solution.

4.3 Resonance

The previous sections have discussed approximate methods of determining circuit resonance points. Exact methods of determining resonance points have been developed for a single phase SVC circuit with equidistant firing in [Dobson1995a, Jalali1993] and this approach is sketched in this section. The resonance is explained by associating it with an eigenvalue of the half wave map H being -1.

When a periodic orbit is halfwave symmetric, the system states at the half cycle are equal in magnitude and opposite in sign to the system states at the beginning of the cycle. If we write y_0 for the system state at the beginning of the cycle, then this may be written in terms of the halfwave map H:

$$H(y_0)= -y_0 \tag{4-3}$$

(H is similar to a Poincare map except that it only advances the state by half a cycle). The thyristor switch off time τ_0 is given by a constraint equation:

$$c(y(\tau_0))=0 \tag{4-4}$$

which expresses the condition that the thyristor current be zero at the thyristor switch off. The state y_0 and the switch off time τ_0 can be computed by solving (4-3) and (4-4) simultaneously. Now suppose that a values of τ_0 consistent with (4-4) is available. We can then compute y_0 by solving (4-3) and examine the size of y_0 to try to detect when a resonance occurs. Equation (4-3) has the form

$$DH\, y_0 + g(\tau_0) = -y_0 \tag{4-5}$$

where DH denotes the Jacobian matrix when the firing is equidistant. Equation (4-5) may be written in full by integrating the system equations and taking into account the coordinate changes at the switching (see Chapter 3). g is a bounded function with terms involving the integration of the input over the period. Rewriting (4-5) as:

$$y_0 = -(I+DH)^{-1}\, g(\tau_0) \qquad (4\text{-}6)$$

shows that y_0 can become unbounded as an eigenvalue of DH approaches -1. Thus the resonance (unbounded y_0) can be associated with an eigenvalue of DH being close to -1. Circuits with resistance will have eigenvalues of DH which will only come close to -1 at resonance. For details see [Dobson1995a].

5.0

DYNAMICS OF TCSC

To address the dynamics of TCSC control systems, the nonlinearity of the thyristor switchings must be taken into account. In particular, the system nonlinearity causes the dynamic response of a TCSC to change as a function of its firing point. This dependence on operating point is discussed in papers describing the design of the Kayenta system [Johnson1991, Christl1992].

$\sigma = 20°$	$s = -14.5. \pm j\ 56.2$
$\sigma = 40°$	$s = -13.5. \pm j\ 48.1$
$\sigma = 50°$	$s = -10.6. \pm j\ 30.2$
$\sigma = 60°$	$s = -11.9. \pm j\ 11.9$

The design of the Kayenta controller was achieved by first finding the open loop response of the line current to changes in the firing point using a detailed EMTP model. The resulting envelope of the line current response enabled the control engineers to find a transfer function which approximated the dynamics of the system around an operating point. This transfer function was of fourth order having two poles on the real axis and a complex pair of poles. The dependence of these complex poles on the operating point is illustrated in Table 1. The operating points specified by s in the first column are the conduction times in electrical degrees for the thyristors in the TCSC. The natural frequencies of oscillation range from 9 Hz to 1.9 Hz.

The control design for Kayenta was achieved by using these transfer functions in a closed loop model allowing the use of standard tools to optimize the control response. This

method is effective but provides little insight into the behavior of the system and requires detailed EMTP simulations to find the necessary transfer functions. This chapter presents a first principles eigenvalue method which can be used for the design of TCSC control systems. The nonlinearities of the thyristor switching are taken into account. The chapter is based on [Jalali1994a, Jalali1993].

5.1 Kayenta TCSC

The Kayenta system presented in Section 4.2 will be used to demonstrate the methods developed for control design. Recall from Section 4.2 that the Kayenta system is a 230 kV, 330 Mvar TCSC project installed in northeastern Arizona. The configuration includes two conventional 165 Mvar series capacitor banks with a nominal reactance of 55 Ohms each. One of these segments is divided into 40 Ohms and 15 Ohms. The 15 Ohms unit is configured as a TCSC. This consists of 15 Ohms of capacitance in parallel with a Thyristor Controlled Reactor (TCR). The reactor is sized at 3.4 mH. The Kayenta system is shown in Figure 5.1.

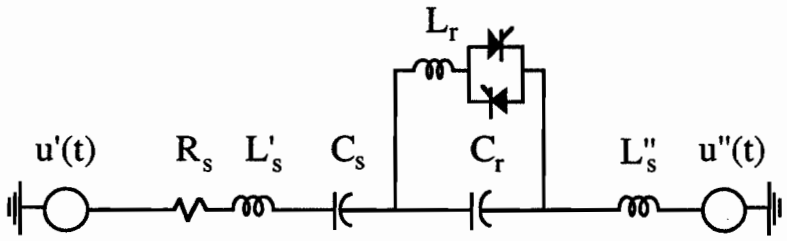

Figure 5-1 Kayenta System

The fundamental impedance of the TCSC is similar to a parallel LC circuit with a variable inductance. With the thyristors off and the conduction time s = 0, the impedance per phase is 15 Ohms. As s is increased the capacitance increases to infinity at the fundamental resonance point at s = 72°. For the TRC full on, s = 180° and the TCSC is inductive at 3.1 Ohms. As s is decreased towards the resonance the inductive value increases to infinity. This behavior is illustrated in Figure 5-2.

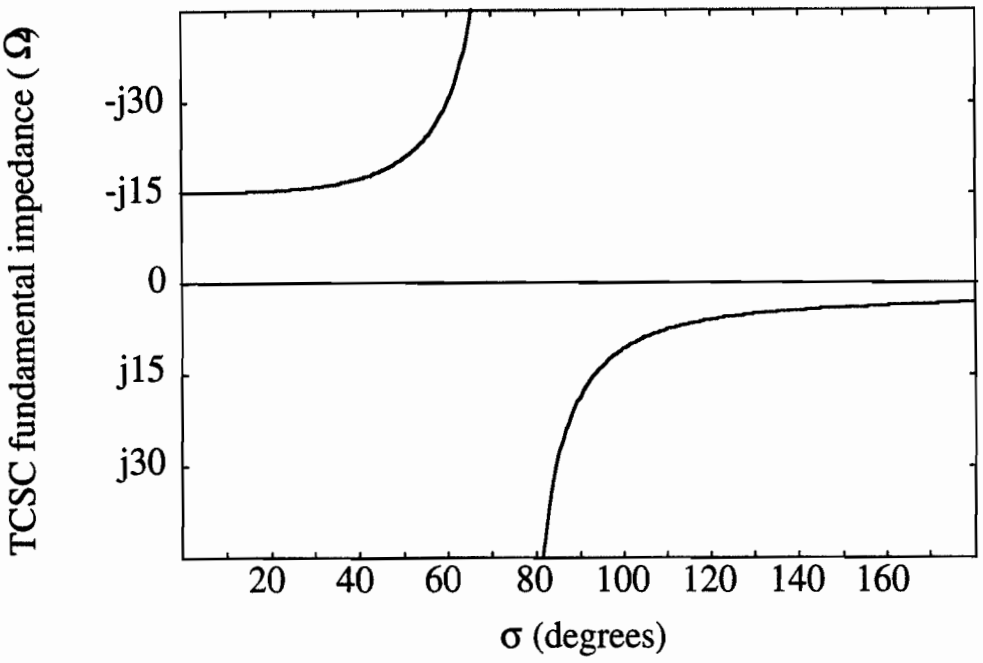

Figure 5-2. TCSC Impedance vs. Sigma

It is assumed that control limits prevent even temporary operation into the area of resonance. It is also assumed that operation will be limited to the capacitive region except for full bypass with s = 180°.

5.2 Dynamics of TCSC

Figure 5-3 describes the system dynamics as the system state, x_0, evolves over a period T. The conduction starts at times f_0, f_1, f_2 which are defined by the control system and the method used to synchronize the firing points to the system states. The turn off times t_0, t_1, t_2 are defined as the points in time where the current through the thyristors becomes zero. Each of these transitions points are dependent on the system states and signal a change of the dimension of the state equations. For the Kayenta system there are four states during thyristor conduction or on state. These states are the current in the TCR, voltage across the TCSC, line current and the voltage across the fixed capacitor. When both thyristors are off the system reduces to three states by dropping the TCR current.

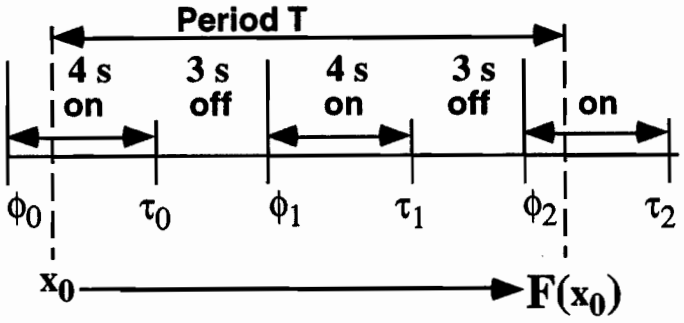

Figure 5-3 System dynamics over one period

The TCSC dynamics are studied using the Poincare map f discussed in section xx which maps an initial state x_0 forward in time by one period. In particular, the eigenvalues of the Jacobian of the Poincare map evaluated at the steady state are used to define the small signal stability of the system. In particular, section xx explains that the steady state is exponentially stable if the eigenvalues of the Jacobian lie inside the unit circle. Section xx also explains that the interpretation of these eigenvalues are equivalent to the z-plane formulation of sampled data.

Open loop response

The first task is to calculate the eigenvalues for the open loop response including loop response synchronization. There are at least three methods to synchronize firing for TCSC systems. One method is to use a voltage controlled oscillator as used in the HVDC systems, another way is to synchronize to the voltage across the TCSC or to the line current. In this chapter we will address the latter two. The voltage controlled oscillator has also been studied but space prohibits its inclusion.

In all examples we will use the Kayenta system described above. The dynamic open loop response for both voltage and current synchronization are shown in Figure 5-4. The solid lines are the envelope of line current using a detailed EMTP model. The dots are derived from the Jacobian. This response agrees with the results given in ref. [xx??]. Figure 5-4 also shows the dependence of the dynamics on the operating point of s and how well the methods discussed in this paper describe this phenomenon.

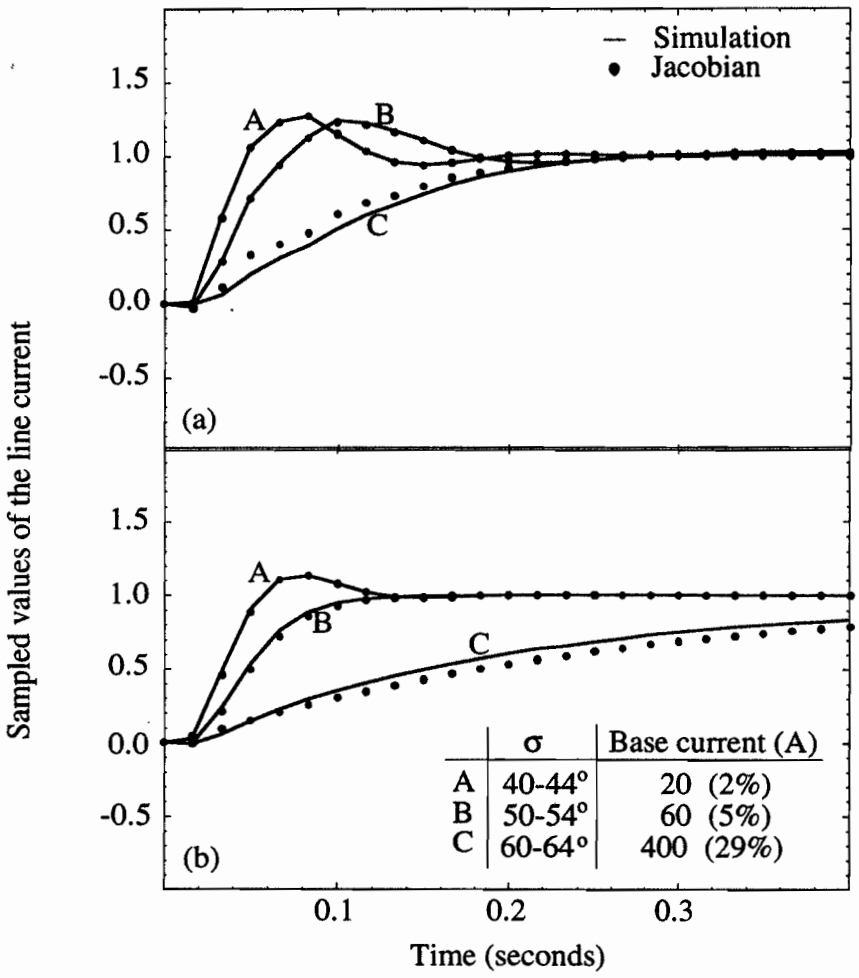

Figure 5-4. Response of line current to 4° step change in σ when synchronizing in the zeros of (a) TCSC voltage (b) line current

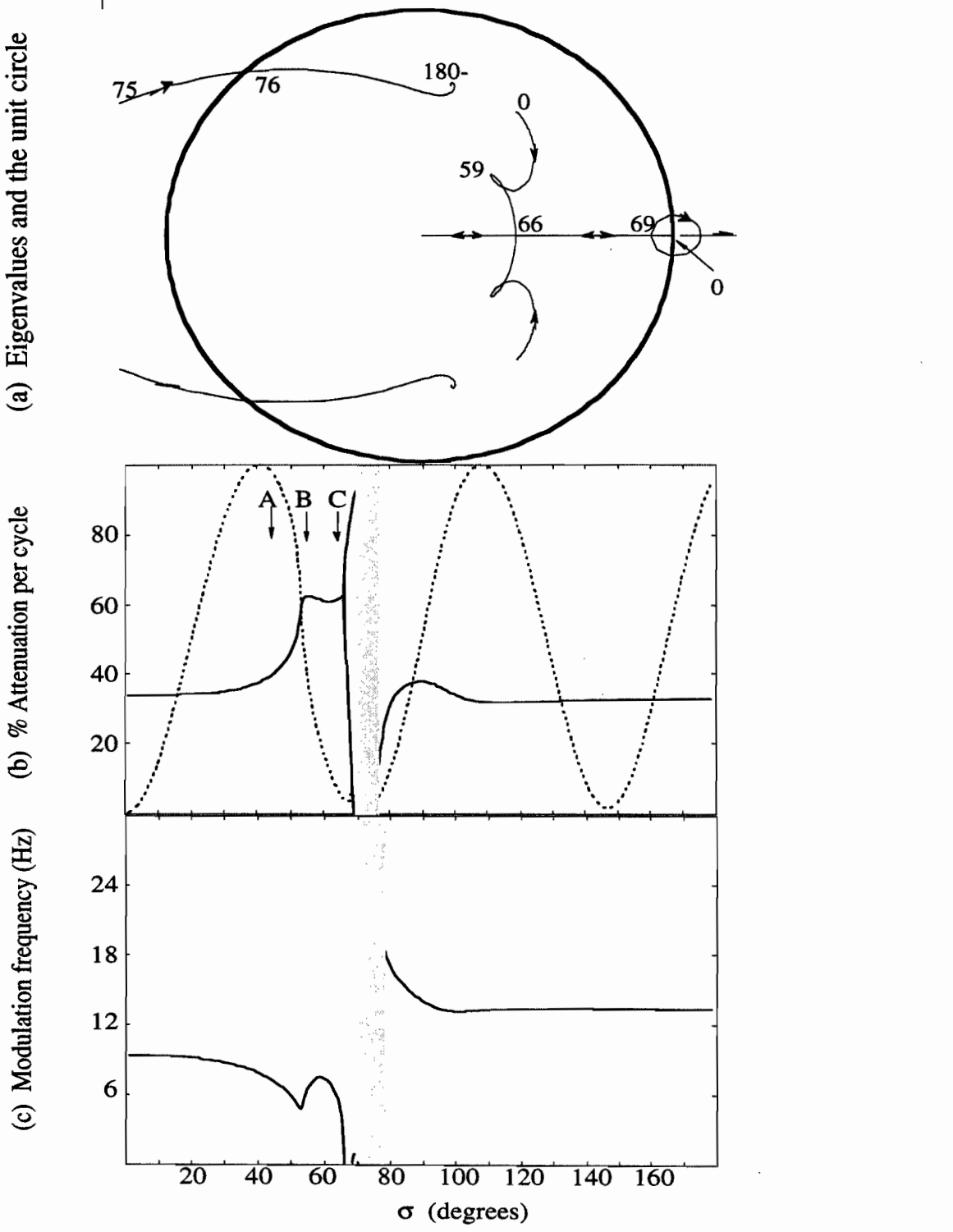

Figure 5-5. Eigenvalues for synchronizing to Voliage zeros. (a) trace of eigenvalues for different values σ (b) Attenuation (c) modulation frequency

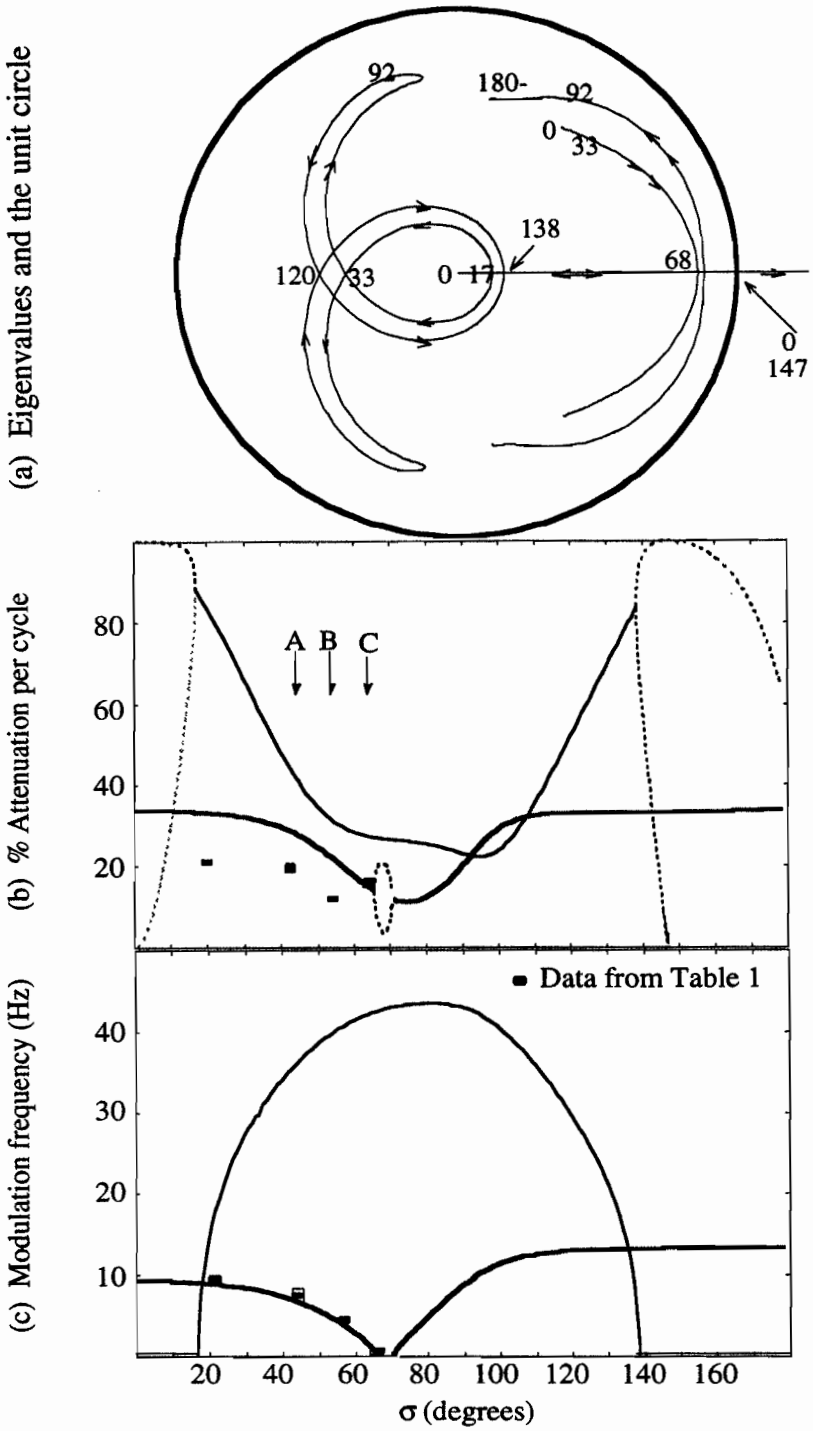

Figure 5-6. Eigenvalues for synchronizing to line current zeros. (a) trace of eigenvalues for different values σ (b) Attenuation (c) modulation frequency

Figure 5-5 shows the details of the calculated eigenvalues when the firing is synchronized to zeros of the voltage across the TCSC. The system has four eigenvalues. For some values of s these eigenvalues form complex pairs while at other values they reside on the real axis. This is best seen in figure 5(b) and(c). In all cases this system is stable. The dynamics approximation shown in Table 1 from [Christl1992] found by fitting a fourth order transfer function are also shown in this figure as crosses. The differences may be do to the fitting methods used or do to the inclusion of filters or other dynamic components in the synchronization methods used in their detailed model .

Figure 5-6 shows the details of the calculated eigenvalues when the firing is synchronized to the zeros of the line current. It is the synchronization method used in the final controls for Kayenta. In general the line current is very stable and less susceptible to ambient harmonics. The eigenvalues show very different behavior when compared to Figure 5-5. For s between 69 and 76 the system is not stable. The control design issue is to insure that the closed loop response removes these instabilities and provides a more uniform response over the range of operating points.

Closed loop control

A basic control issue for TCSC is the dependence of the dynamic response on the operating point of s , see Figure 4. To reduce this variance a feed back control on s is proposed. In this controller the error function is the difference between a requested s_r and a measured value.<s>.The measured value <s> is updated twice per cycle while the requested value can change continuously depending on the action of higher level controllers. The goal is to demonstrate a feedback control on s, which provides a faster and more uniform response to step changes in s using the tools developed in the appendix of this paper.

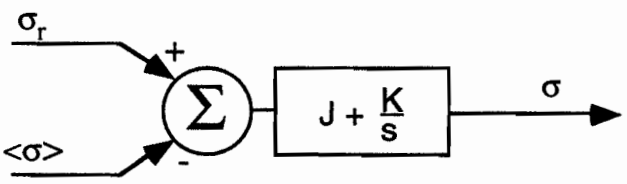

Figure 5-7 Sigma Controller

The controller used is a simple PI controller with a nonlinear gain. The nonlinear gain is defined as $J = A(1 + e^S)$

The basic task is to find the gains for this controller which provide the desired response of the system to step changes in sigma. This objective can be achieved using the techniques described in the appendix of this paper. The open loop map discussed in the last section mapped the states x_0 to the next sampling point. This map must be generalized to include the controller states, y_0. The map for the system including the controller states can be defined as $F(x_0, y_0)$. In addition to the system map there is a map which accounts for the dynamics of the controller which depends on the system and controller states. This map is defines as $f(x_0, y_0)$.

The eigenvalues of this Jacobian describe the dynamic of this closed loop system. Traditional tools, such as root locus can be applied to find the gains to achieve our goal of uniform response. For this example line current synchronization was assumed. The controller gains used are:

$$J = -10e^{-\sqrt{(65-\sigma)/2}}$$

$$K = -23 - 24e^{-\sqrt{(\sigma-65)/2}}$$

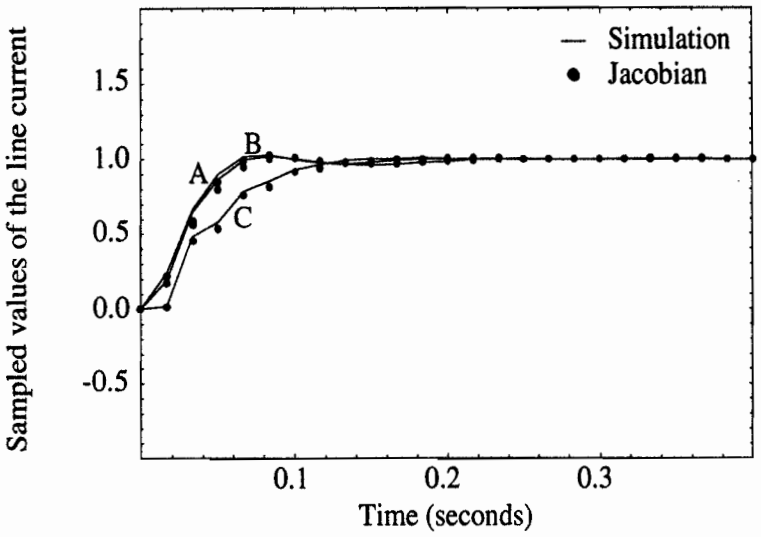

Figure 5-8 System Response

The resulting dynamic response is given in Figure 5-8. This is for the same step changes in sigma as for the open loop case. The solid line are from exact EMTP simulations while the dotted line are a Jacobian approximation. The dynamics are greatly improved when compared to the open loop response shown in Figure 5-4.. The dynamics are almost uniform across the operating points of sigma. The overshoot and undershoot is greatly reduced. The transients come to steady state in half the time required in the open loop cases.

The resulting closed loop eigenvalues are show in Figure 5-9

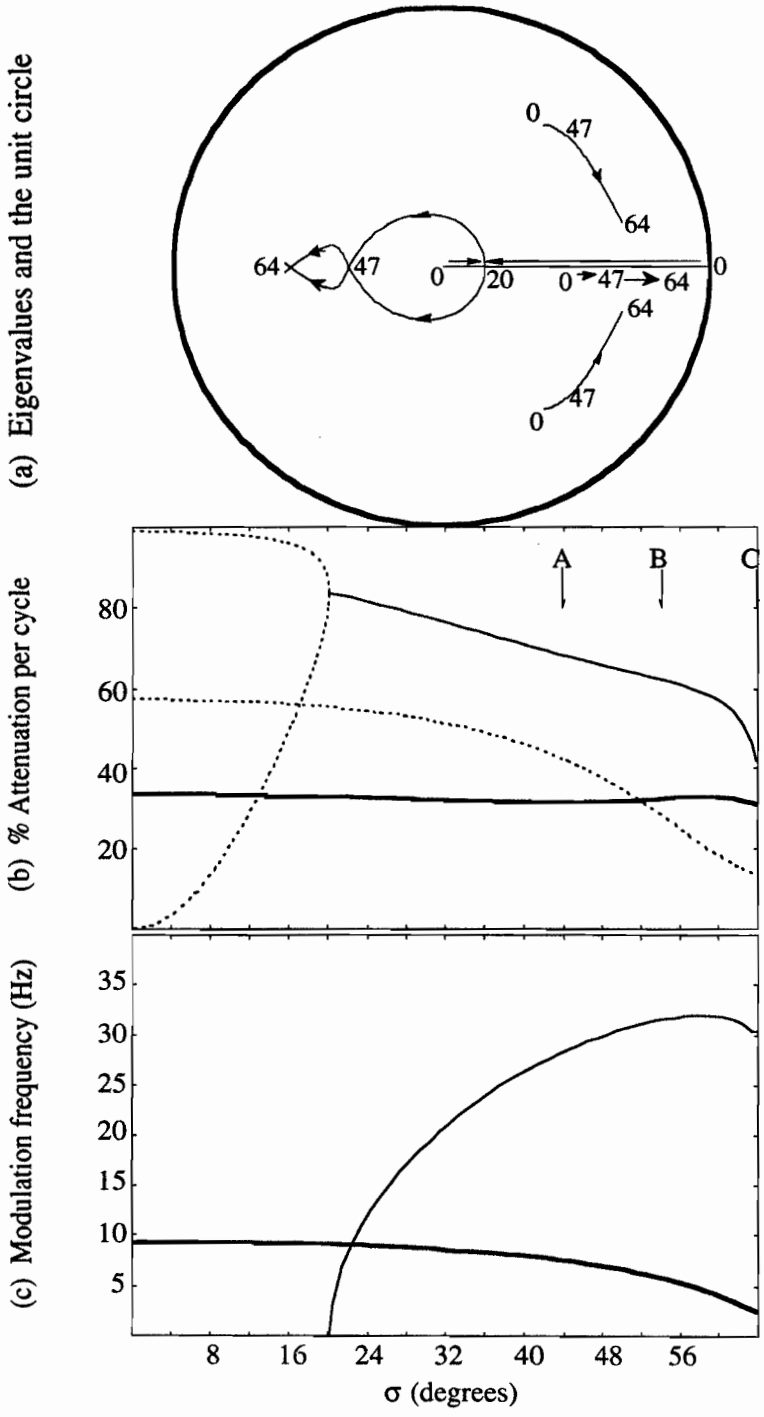

Figure 6-9 Eigenvalues of the closed loop system

6

METHODS OF COMPUTING THE DAMPING OF SUBSYNCHRONOUS OSCILLATIONS DUE TO A THYRISTOR CONTROLLED SERIES CAPACITOR

6.1. Introduction

Subsynchronous resonance and the associated turbine-generator torsional interactions are a major constraint for many series compensated transmission systems. Series capacitor compensation of long transmission lines increases their power transfer, but may inadvertently increase the potential for subsynchronous resonance (SSR). Such torsional interactions are an instability in which large subsynchronous torques can cause extensive damage to turbine-generator shafts. Flexible AC transmission systems such as the Thyristor Controlled Series Capacitor (TCSC) offer the possibility of power flow control and suppression of SSR instabilities through controlled series compensation. This chapter is based on [Rajaraman1995b, Rajaraman1996a, Rajaraman1996b].

Analytical tools for the study of SSR problems without thyristor controlled devices are well established. SSR in power systems with no thyristor switching devices can be accurately analyzed by eigenvalue analysis (e.g. [Anderson1990]), torque per unit velocity methods [Bowler1973, Bowler1976, Hedin1995, Kilgore1976, Canay1982] and time domain simulation. Each of these approaches has strengths and weaknesses. Time domain simulation is accurate, applies to large, detailed system models and can be used to study large signal effects. However, estimating the damping of the various system modes can be difficult, especially when one of the modes is unstable. Complementary to time domain simulation and yielding different insights are the methods of eigenvalue analysis and torque per unit velocity. These methods are confined to small signal stability, but they both yield the modal dampings. Eigenvalue analysis is exact but requires a linearized model of the entire electromechanical system to be developed. The torque per unit velocity method is a good approximation due to Bowler, Hedin, Kilgore and others which only requires steady state simulation of the electrical system.

These approaches are being developed to study SSR problems with thyristor controlled devices, but there are some problems in accurately representing the thyristor switchings. A recent IEEE committee reported [IEEE1992] that one of the shortcomings of eigenvalue analysis was that `Switching devices, e.g., thyristor valves, are represented by approximated linear transfer functions which neglect the possible impact of switching on the system behavior'.

The papers on the inclusion of the TCSC in SSR studies are centered on two field installations, Western Area Power Administration's Kayenta site [Christl1991,Christl1992], and Bonneville Power Administration's Slatt substation [Nyati1994,Larsen1992]. The Kayenta system was analyzed with time domain simulation of a detailed model of the AC system, a machine and TCSC with controls [Christl1992]. This model was used to measure the frequency response of the TCSC. The measured response at a subsynchronous frequency (35 Hz) showed pure capacitive behavior at small TCSC conduction angles and inductive behavior with resistance for conduction angles above 20°. This implies that a 35 Hz subsynchronous instability would be eliminated if the TCSC was operated with conduction angles above 20°.

For the Slatt system, the effect of the TCSC was evaluated by measuring the electrical damping torque as a function of machine rotor speed. Analog and digital simulators modeled the AC system, machine and TCSC with controls. In the analog studies, a transfer function was calculated by modulating the synchronous machine rotor speed with white noise. The results showed that as the conduction interval of the TCSC was increased, the negative electrical damping was significantly reduced at the critical torsional modes [Nyati1994]. In the digital studies [Larsen1992], the TCSC was represented by linear transfer functions obtained from time domain simulations. The time domain simulations were used to compute a steady state operating point for the nonlinear system and to provide the data needed to approximate the linear transfer functions for each operating point. This work also shows the possibility of damping subsynchronous oscillations at suitable operating points.

This chapter presents two methods for computing the eigenvalues and damping of SSR modes when the system includes a switching device. The first method [Rajaraman1995b].is an exact eigenvalue analysis which computes the modal damping via the Poincare map methods of Chapter 3. The second method [Rajaraman1996b].generalizes the torque per unit velocity method to account for switchings. The test case for both methods is the IEEE SSR first benchmark model [IEEE1977] with a TCSC. The results for both methods agree well and are consistent with ElectroMagnetic Transient Program (EMTP) time domain simulations.

6.2. IEEE first benchmark SSR model with TCSC

The first benchmark model was created by the IEEE SSR Task Force [IEEE1977] as a standard test model to facilitate analysis and comparison of calculations of SSR. This test case is described and the challenges it poses to analysis are described.

6.2.1 Description of system

The electrical part of the system is shown in Fig. 6.1(a).

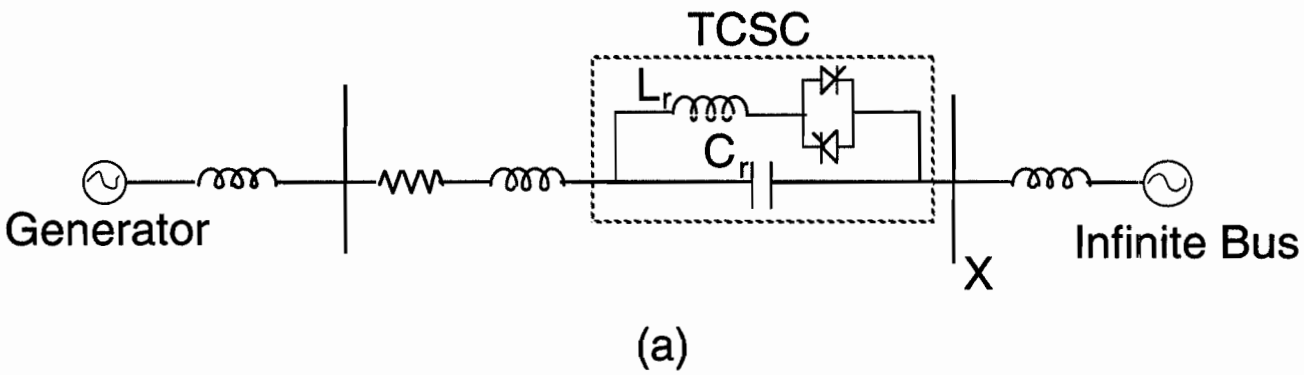

Figure 6.1(a): Electrical part of First Benchmark Model with TCSC

Fig. 6.1(b) represents the mechanical part of the first benchmark model. The turbine-generator shaft is modeled as 6 masses with torsional springs. There are five torsional modes TM1 through TM5 for the mechanical system with respective frequencies 16, 20, 25, 32 and 47 Hz. There is also a rigid body mode TM0 corresponding to power swings of the system. The TM4 mode is highly unstable when the series capacitors compensation level is 29% of the combined transmission and transformer impedances. When the series compensation level is 43%, TM3 is the most unstable mode. For 53% compensation, TM2 is a highly unstable mode.

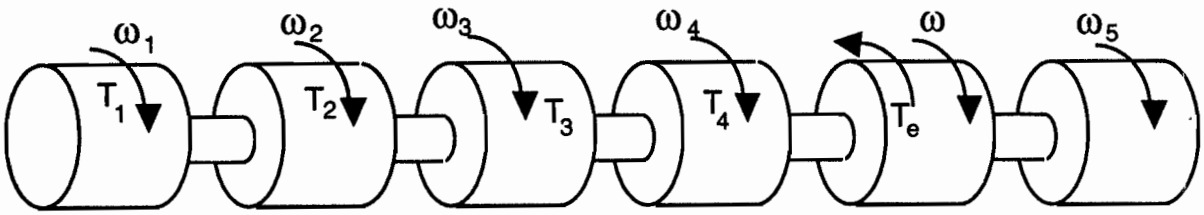

Fig 1(b). Rotor Model for SSR study

Figure 6.1(b): Mechanical part of First Benchmartk Model

Each phase of the TCSC consists of a fixed capacitor with a parallel connected thyristor controlled reactor as shown in Fig. 6.1(a). The switching element is two oppositely poled thyristors which conduct on alternate half cycles of the supply frequency. The reactor is sized so that the resonance between the capacitor and parallel reactor is below the third harmonic [Christl1991]. System parameters are given in Appendix A and [IEEE1977]. The TCSC changes from capacitative to inductive operation at a conduction angle of 68°.

Two firing schemes are used for the TCSC:

- Constant firing angle

- Firing angle synchronized to the zeros of the line current.

Open loop σ control is a good approximation to the constant firing angle for the TCSC if the line current is stiff.

6.2.2. System modeling

The generator is modeled in a standard way [Anderson1990]. The machine windings in the stator and rotor circuits may be represented by seven coils: one each for the stator A, B and C phases; one each for the field, d-axis amortisseur, q-axis field and q-axis amortisseur windings. These seven circuits are coupled to each other through mutual inductances. The use of Park's transformation converts the stator A, B, C frame of reference into Odq frame of reference (or the rotor reference).

The turbine shaft is modeled as a lumped masses connected by linear torsional springs. The mechanical damping is small and is assumed to be zero for SSR studies. Generally, the spring-mass model of the turbine -generator shaft is known with relatively good accuracy [Anderson1990].

As explained in section 3.1, we model the thyristor as an ideal diode with a gate. The thyristor turns on when a firing pulse is applied at the gate, conducts current only in the forward direction, and turns off when the current through the thyristor becomes zero. For simplicity, equal distance thyristor firing pulses or thyristor firing synchronized with the line current are considered here; other synchronizations and controls which may be combined with the equations of this Chapter may be found in Chapter 5 and [Jalali1994a, Rajaraman1996a].

The constant firing angle control is modeled as follows. In phase A, the thyristors are fired at $\tau_{A0}+(\pi-\sigma_{req})/2$, where τ_{A0} is the zero of the line current in phase A at steady state, and σ_{req} is the requested conduction angle of the thyristor. The thyristors in phases B and C are fired in a similar way.

The firing angle synchronized to the zeros of the line current is modeled as follows. The phase A thyristor is fired at $\tau_A+(\pi-\sigma_{req})/2$, where τ_A is the zero of the phase A line current, and σ_{req} is the requested conduction angle of the thyristor. The synchronization scheme for the B and C phases is similar. Note that if the line current is assumed to be relatively stiff for some perturbations around the steady state, then the constant firing angle control is equivalent to the firing angle synchronized to the zeros of the line current.

6.2.4. Challenge to analysis

Both generators and TCSCs are nonlinear and time varying devices; when included together in a system, they further complicate analysis. For example, if the load is balanced, the generator equations simplify with Park's transformation so that an observer on the generator rotor sees a time invariant system. However, if a TCSC is included, the system is instantaneously unbalanced whenever some thyristor are on and others are off, and the observer on the rotor sees the TCSC as a nasty time varying system.

The thyristor controlled reactors of the TCSC are switched in and out of the circuit in a regular pattern and our analysis reflects this by modifying the system equations accordingly at each

switching. The TCSC is nonlinear because the thyristor switch off times depend on the thyristor current and this is accounted for in the analysis.

6.3. Exact eigenvalue analysis

The system is analytically linearized about the steady state [Anderson1977, Anderson1990, Jalali1994a, Steinbuch1992]. The system linearization depends on the steady state periodic operating point and this steady state is computed numerically. The system linearization varies over the supply cycle and is numerically integrated to yield the Jacobian of the Poincaré map. Modal dampings are then computed from the eigenvalues of the Jacobian. These discrete time eigenvalues can then be converted to their continuous time counterparts for convenience as explained in section 3.4.1.

Fig. 6.2 shows a typical sequence of thyristor switchings over a period T. The system starts at a vector x_0 at time ϕ_0 and progresses through the various thyristor switchings until it arrives at the end of the period at $\phi_0 + T$ with states $f(x_0)$. The Poincaré map f takes into account the the dependence of the switching times on the system states.

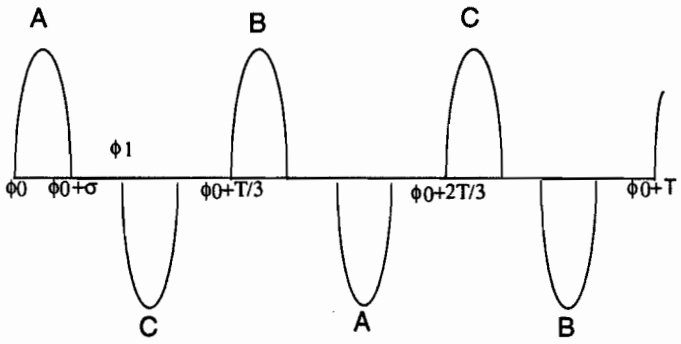

Figure 6.2. Three phase thyristor currents in one period.

Steinbuch and Bosgra [Steinbuch1992] analyze a similar problem in linearizing a synchronous generator supplying a three phase rectifier. Their results are expressed in terms of Floquet theory and may be translated to our terminology by noting that the eigenvalues of the Poincaré map are Floquet multipliers of the steady state periodic operating point.

6.3.1 State space equations

The state space equations for the first SSR benchmark model with the TCSC are described in this section. The system equations can be obtained by a judicious combination of the standard techniques of Anderson [Anderson1977,Anderson1990] to describe the generator dynamics in 0dq axes and Jalali [Jalali1994a,Jalali1993] to describe the TCSC taking proper account of the thyristor switchings including synchronization and controls. All quantities including time are assumed to be in per unit. A more detailed description of how to write and assemble the system equations is given in [Rajaraman1995b]. The description here has the merit of not obscuring the essentials of the derivation with familiar details of the machine equations.

One of the possible modes of operation of the three phase TCSC is when one thyristor conducting alternates with no thyristors conducting ($\sigma < 60°$ as shown in Fig. 6.2). Other modes of operation of the three phase TCSC arise when $\sigma > 60°$. In particular, when $60° < \sigma < 120°$, one thyristor conducting alternates with two thyristors conducting and when $120° < \sigma < 180°$, two thyristors conducting alternates with three thyristors conducting. Here we assume the mode of operation with $\sigma < 60°$; similar equations can be developed for the other modes.

The current through the conducting thyristor is denoted by i_r. The remaining 22 electromechanical system states are collected in a vector y. (y consists of 3 capacitor voltages, 3 line currents, field current, 3 amortisseur currents, 6 shaft angles and 6 shaft velocities.) The electromechanical system inputs are collected in a vector u. (u consists of 2 components of the infinite bus voltage, field voltage and the shaft accelerations due to mechanical torques.)

We first give the electrical system equations when the thyristor in phase A is conducting; the equations are similar when the thyristor in phase B or C is conducting. When the phase A thyristor is conducting, the state vector is $x=(y,i_r)$. [Rajaraman1995b] shows that by using [IEEE1977, Anderson1977, Anderson1990] for the machine equations and circuit laws for the TCSC equations as in chapter 3, the system differential equations when a thyristor is conducting can be written in the form:

$$\dot{x} = A_{on}(t,x)\ x + B_{on}(t,x)\ u(x) \qquad (6\text{-}1)$$

The dependence of the matrices A_{on} and B_{on} on the state x show that the equations are nonlinear. (In particular, the A_{on} matrix depends on the generator rotor angle and angular velocity.) The dependence of the matrices A_{on} and B_{on} on time t shows that equations (6-1) are time varying. Equations (6-1) are time varying even when Park's transformation is used to transform some of the system states because the electrical network is unbalanced when a thyristor is on.

When no thyristors are conducting, the thyristor current i_r is identically zero and the state vector is y. The system differential equations when no thyristors are conducting may be written in the form

$$\dot{y} = A_{off}(t,y)\ y + B_{off}(t,y)\ u(y) \tag{6-2}$$

where

$$A_{off}(t,y) = \boldsymbol{G}\, A_{on}(t,x)\, \boldsymbol{G}^t \tag{6-3}$$

$$B_{off}(t,y) = \boldsymbol{G}\, B_{on}(t,x) \tag{6-4}$$

and the 22×23 matrix $\boldsymbol{G} = (\, I_{22} \;\; 0_{22x1}\,)$ and $\boldsymbol{G}^t$ is the transpose of $\boldsymbol{G}$.

At a thyristor switch on, the states are related by

$$x(s_{on}) = \boldsymbol{G}^t\, y(s_{on}) \tag{6-5}$$

Examination of the form of the matrix $\boldsymbol{G}^t$ shows that the meaning of (6-5) is that the first coordinate of $x(s_{on})$ is zero and the last 22 coordinates of $x(s_{on})$ are the coordinates of $y(s_{on})$.

At a thyristor switch off, the states are related by

$$y(s_{off}) = \boldsymbol{G}\, x(s_{off}) \tag{6-6}$$

That is, the coordinates of $y(s_{off})$ are the last 22 coordinates of $x(s_{off})$.

We now describe the system operation when the combined electro-mechanical system has a steady state periodic solution with period $T = 2\pi / \omega_R$. To facilitate understanding, consider Fig. 6.2.

At ϕ_0 , the phase A thyristor turns on. This mode, as described by (6-1) ends when the thyristor current goes through zero at time $\phi_0 + \sigma$, and the thyristor is switched off. The non conduction mode, described by (6-2), follows the conduction mode and ends when a new firing pulse is applied at ϕ_1 and the phase C thyristor turns on. This starts a new series of similar on and off cycles continuing until time $\phi_0 + T$, when the next period starts.

Equations (6-1) and (6-2) are variable structure, time dependent nonlinear differential equations of the combined electromechanical system. The system includes additional nonlinearity because the time of transition from (6-1) to (6-2) is the thyristor switch off time σ_{off} which depends on the system state.

6.3.2 System linearization and Poincaré map

Section 3.4 explains the Poincare map approach to system stability used here. The small signal stability of the system is computed from the Jacobian J of the Poincaré map evaluated at a sampled steady states x_0 , i.e., $J = Df(x_0)$. The eigenvalues of J are the z-plane poles of the sampled data transfer function of the linearized system. These eigenvalues or poles lie on the z-plane familiar from sampled data systems. The steady state x_0 and the associated periodic steady state is asymptotically stable if the eigenvalues of the Jacobian J lie strictly inside the unit circle. Our eigenvalue results are presented as continuous time s-plane poles $-\alpha + j\beta$ which correspond to the z-plane poles $e^{-\alpha T}\ e^{j\beta T}$. $-\alpha$ specifies the damping and β denotes the frequency of the pole, determined with attention to possible aliasing.

The complexity of the system equations make it impossible to obtain an analytic expression for the Poincaré map. We compute J as follows [Guckenheimer1986, section 1.5]: First linearize the system equations around the steady state solution. Then J is the linear map that advances a perturbation in state at time ϕ_0 , through the linearized system, to $\phi_0 + T$.

We now linearize the thyristor turn on and turn off equations (6-5) and (6-6). Let a thyristor turn on at s_{on} and note that s_{on} is a fixed quantity. Linearizing (6-5) in the case of constant thyristor firing angle yields

$$\Delta x(s_{on}) = \boldsymbol{G}^t \, \Delta y(s_{on}) \tag{6-7}$$

The linearization of the switch on in the case of firing angle synchronized to the line current is described in Appendix B.

If the system is not at a switching time bifurcation [Jalali1993,Jalali1995,Dobson1995], we can linearize (6-6) to get

$$\Delta y(s_{off}) = [\boldsymbol{G}\, \dot{x}_*(s_{off}) \; -\dot{y}_*(s_{off}) \;] \, \Delta s_{off} \; + \boldsymbol{G}\, \Delta x(s_{off})$$

where the subscript star means that the quantity is evaluated along the steady state solution. But the first term vanishes due to (6-3) and (6-4):

$$\boldsymbol{G}\, \dot{x}_*(s_{off}) \; -\dot{y}_*(s_{off}) \; =$$

$$\boldsymbol{G}\, A_* \; x_*(s_{off}) \; - \; \boldsymbol{G}\, B_* u_* \; - \; \boldsymbol{G}\, A_* \;\; \boldsymbol{G}^t \, y_*(s_{off}) \; - \boldsymbol{G}\, B_* u_* \; = 0$$

Hence,

$$\Delta y(s_{off}) = \boldsymbol{G}\, \Delta x(s_{off}) \tag{6-8}$$

This useful simplification is analogous to the simplification in [Dobson1995] and was overlooked in [Steinbuch1992].

Now we assemble the formula for the Poincare map Jacobian J by computing the map that advances a small state perturbation $\Delta\, y(\phi_0)$ from ϕ_0 to $\phi_0 + T$ through the linearized system. Let $\Phi_{on}(t_0,t_1)$ be the state transition matrix of the linearization of (6-1) in the time interval $[t_0, t_1]$. (Then, for example, $\Delta x(t_1) = \Phi_{on}(t_0,t_1) \; \Delta\, x(t_0)$. Similarly, let $\Phi_{off}(t_0,t_1)$ be the state transition matrix of the

linearization of (6-2) respectively in the time interval $[t_0, t_1]$. Consider Fig. 6.2 and divide the interval $[\phi_0, \phi_0 + T]$ into three equal subintervals, $[\phi_0, \phi_0 + T/3]$, $[\phi_0 + T/3, \phi_0 + 2T/3]$, $[\phi_0 + 2T/3, \phi_0 + T]$. The three phase symmetry implies that the map that advances a perturbation through the linearized system in each subinterval must be the same. Thus the map from ϕ_0 to ϕ_1 through the linearized system is

$$J_1 = \Phi_{off}(\phi_0+\sigma,\phi_1)\, G\, \Phi_{on}(\phi_0,\phi_0+\sigma)\, G^t$$

Similarly, the map advancing a perturbation at ϕ_1 to $\phi_0 + T/3$ is

$$J_2 = \Phi_{off}(\phi_1+\sigma,\phi_0+T/3)\, G\, \Phi_{on}(\phi_1,\phi_1+\sigma)\, G^t$$

Then the map advancing a perturbation in the first subinterval from ϕ_0 to $\phi_0 + T/3$ is $J_2 J_1$. The system states have a three phase symmetry, i.e, the system states in phase B (phase C) lag (lead) the corresponding phase A system states by T/3 units of time. Therefore the map that advances a perturbation through the linearized system in each subinterval $[\phi_0 + T/3, \phi_0 + 2T/3]$, $[\phi_0 + 2T/3, \phi_0 + T]$ must be the same and the Jacobian

$$J = (J_2\ J_1)^3 \qquad (6\text{-}9)$$

6.3.3 Computational issues

The modeling of the benchmark system has been done in MATLAB [MathWorks1993]. The system has 23 states when a thyristor is conducting, and 22 states when all thyristors are off. Newton's algorithm is used to find the periodic steady state solution by solving $f(x(\phi_0)) = x(\phi_0)$ where f is the Poincare map. An approximate steady state solution to initialize the Newton method is found by approximating the thyristor controlled switched capacitor as an average impedance [Christl1991,Christl1992] and by using the techniques of [Anderson1977]. For an relative error tolerance of 10^{-6}, this method converges in under five iterations.

The Poincaré map is evaluated by solving the stiff, time varying, nonlinear differential equations (6-1), (6-2) using the implicit trapezoidal rule [Conte1980]. The implicit trapezoidal rule is considered an accurate and computationally convenient method for solving stiff differential equations. The backward Euler method is used for the first few time steps after each switching to avoid numerical oscillations [Lasseter1988].

To compute the Jacobian, the state transition matrices Φ_{off} and Φ_{on} of the linearization of (6-1), (6-2) are found by numerical integration. That is, the fundamental solutions of these linearizations are computed. As for the steady state case, a combination of the backward Euler method (to avoid numerical oscillations) and the implicit trapezoidal rule (for more accuracy) is used.

6.3.4. Exact Eigenvalue Results

This section shows the results of applying eigenvalue analysis to compute the damping of torsional modes as the thyristor conduction time σ varies from 0° to 48°. The case $\sigma = 0°$ corresponds to blocking the thyristors. At $\sigma = 0°$, the TCSC effective reactance X_c is $X_{c0} = -j\ 0.20$ p.u..

Fig. 6.3 shows the damping of the modes TM0 through TM5 when the series compensation is 29%. (Negative damping of a mode implies instability of that mode.) The electrical modes are always well damped and are not shown. The mode TM4 has severe negative damping of $-0.45\ s^{-1}$ when σ=0, but its damping increases as σ increases. The damping of modes TM1, TM2, and TM3 slightly decreases when σ is initially increased. The mode TM5 has small damping that is unaffected by σ and its graph lies under the zero damping line of Fig. 6.3. All the torsional modes TM1--TM5 become positively damped for σ>35° ($X_c = 1.1\ X_{c0}$). The frequencies of the torsional modes TM1—TM5 are approximately constant, remaining within 0.5 Hz of their natural frequencies as σ is varied while the TM0 mode has frequency less than 1.4 Hz. The TM0 mode becomes unstable near σ= 47°.

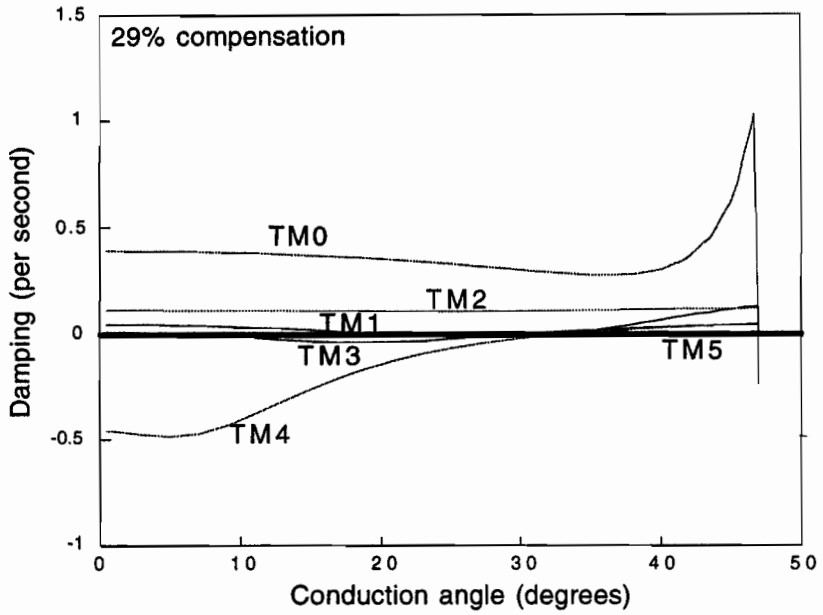

Figure 6.3. Modal Dampings

When σ is between 35° and 47° (X_c between 1.1 X_{c0} and 1.4 X_{c0}), the results show positive damping for all modes and hence small signal stability for the system. Contrast this with Fig. 6.4 which shows the damping of the torsional modes TM1 through TM5 as a function of σ by approximating the thyristor controlled switched capacitor by an average impedance (see section 3.1). The average model predicts insignificant impact of thyristor switchings on the damping for $\sigma \leq$ 30° and shows that the mode TM2 is slightly worsened when $\sigma \geq 30°$.

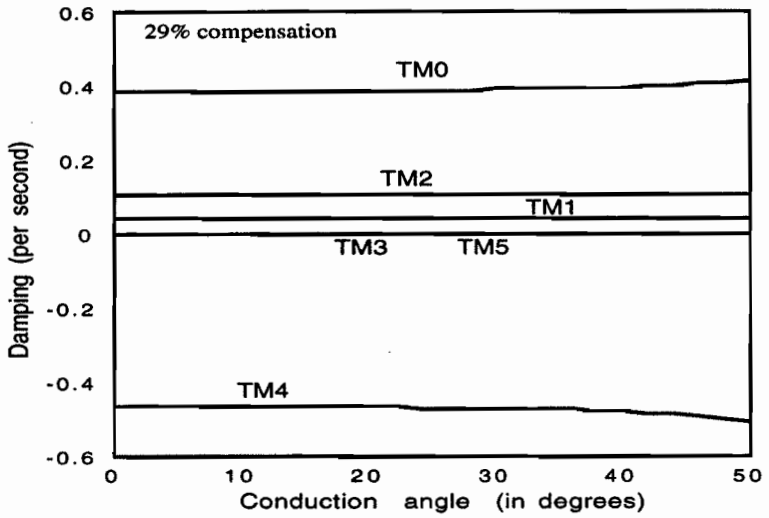

Figure 6.4. Modal Dampings for average impedance model

Figures 6.5 and 6.6 show the modal dampings for 43%, 53% line compensation respectively. Note that the most unstable modes at $\sigma = 0$ stabilize as the conduction angle is increased. The stability of the TM0 mode however decreases. Fig. 6.7 shows the modal dampings for the case of the thyristor firings synchronized to the zeros of the line current.

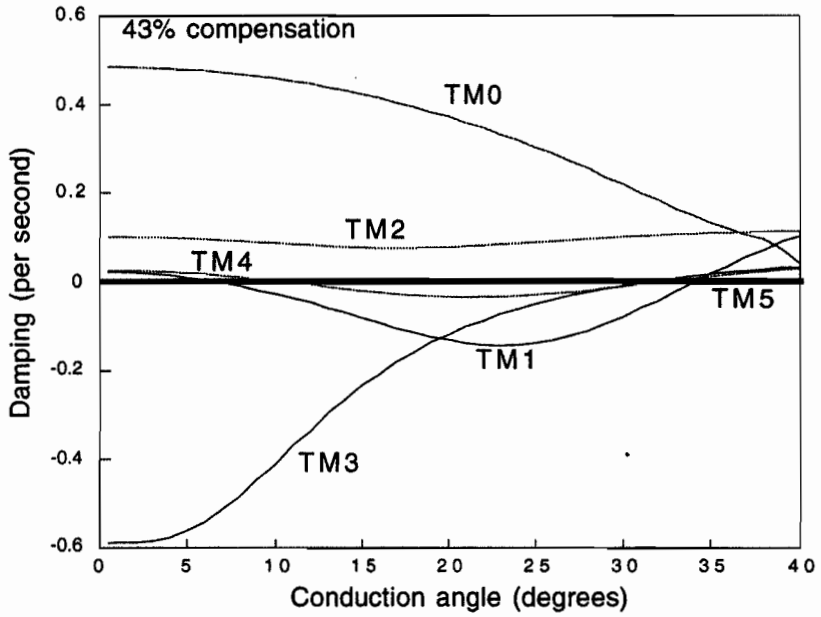

Figure 6.5. Modal Dampings

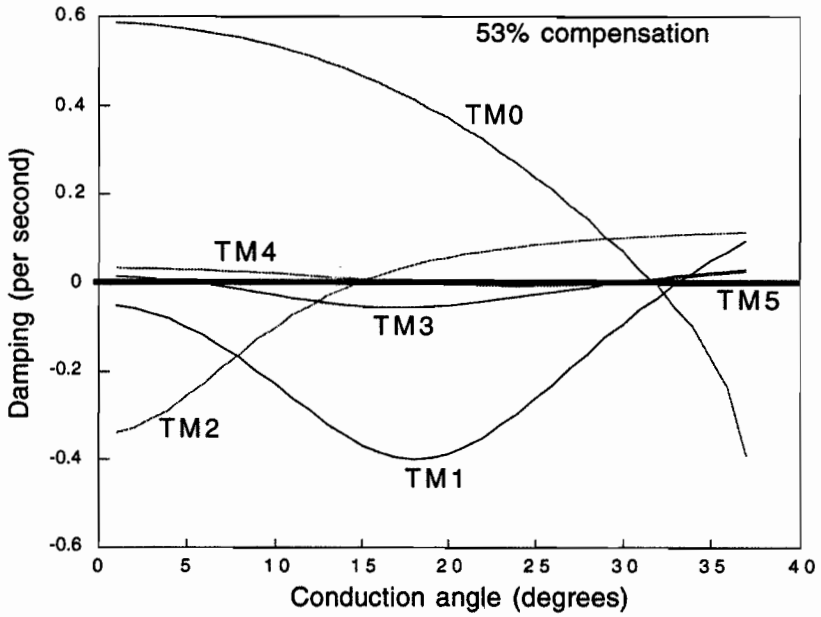

Figure 6.6. Modal Dampings

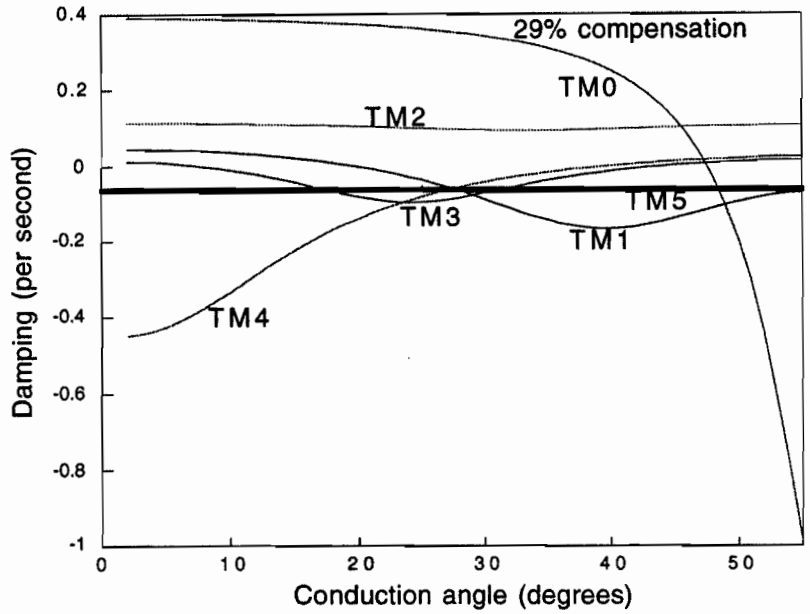

Figure 6.7. Modal Dampings for thyristor firing synchronized to line current

For each value of σ, the solution time for computing the modal dampings steady state and finding theJacobian is roughly six minutes on an HPRISC machine using a general math package [MathWorks1993].

6.3.5. EMTP Results

The EMTP is used to simulate the test system to support the eigenvalue results. A detailed machine model, thyristor models with firing synchronized to the line current zeros and an open loop σ controller are used. Three cases are considered.

Case 1 illustrates the TCSC damping SSR oscillations when operated at a constant firing angle. The thyristors are blocked at time 0 and a simultaneous three-phase line to ground bus fault is simulated at point X of Fig. 6.1a at approximately 117 ms and cleared after $4\frac{1}{2}$ cycles. (The fault is modeled as

parallel impedances of 14.8 and j 0.04 pu.) The fault at each of the phases is cleared at the first current zero of the phase after 192 ms. At 2 s, the thyristors are commanded to operate with $\sigma = 40°$. Fig. 6.8 shows a representative torsional response of the shaft. All torques are expressed in per unit deviation from steady state (the base torque 2.367×10^6 Nm is that required to deliver the generator rated mechanical power at synchronous speed). During the first 2 seconds the oscillations associated with the TM4 mode grow. while the TM0 mode is damped. After 2 seconds, the oscillations are damped out by the TCSC operating at $\sigma = 40°$. The shaft torque of Fig. 6.8 damps with a time constant of approximately 30 s, i.e., modal damping approximately equal to 0.033 s^{-1} which compares with the computed damping of 0.04 s^{-1} (in Fig. 6.3) for the dominant TM4 mode.

Case 2 shows the system instability predicted by the eigenvalue results in Fig. 6.3 when σ is changed from 40° to 10°. Initially, the TCSC operates in steady state at 40°. At 1 s, a change in σ to 10° is commanded by ramping σ down from 40° to 10° in 750 ms. The shaft torsional response of Fig. 6.9 shows the initial TM0 mode decaying and the TM4 mode increasing. The shaft torque of Fig. 6.9 increases with modal damping approximately equal to –0.35 s^{-1} which compares with the computed damping of -0.41 s^{-1} (in Fig. 3) for the dominant TM4 mode. The positive and negative modal dampings as σ varies in cases 1 and 2 are evident in the EMTP results and are consistent with the behavior predicted by the eigenvalue analysis in Fig. 6.3.

Case 3 shows the system instability predicted by the eigenvalue results in Fig. 6.3 when σ is changed from 40° to 54°. Initially, the TCSC operates in steady state of σ=40°, and a change in σ to 54° is commanded at 1 s by ramping σ up from 40° to 54° in 750 ms. Fig. 6.10 shows the increasing oscillations associated with the low frequency TM0 mode. There is only qualitative agreement between the eigenvalue results and the EMTP when the TM0 mode is unstable. We attribute this to the fact that the equal distance firing assumed for the eigenvalue results is a poor approximation to the synchronization scheme used in the EMTP results when the TM0 mode is unstable (the zeros of line current have significant variations when the TM0 mode is unstable). There are indications in the literature suggesting that this instability can be solved by suitable firing angle controls [Larsen1992].

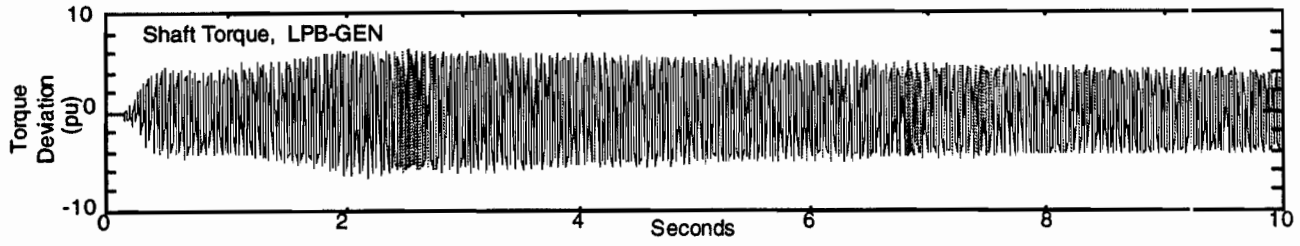

Figure 6.8. Response curve for Case 1 (σ = 0^0 -> 40^0)

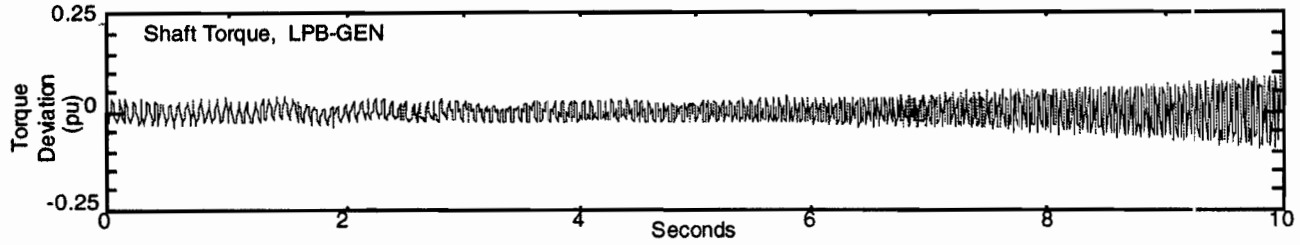

Figure 6.9. Response curve for Case 2 (σ = 40^0 -> 10^0)

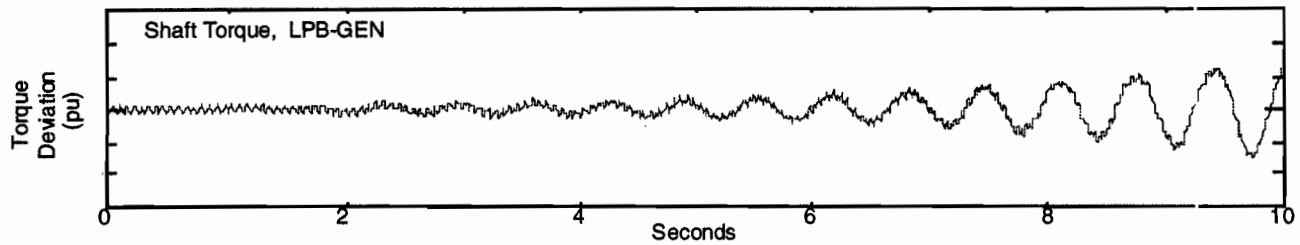

Figure 6.10. Response curve for Case 3 (σ = 40^0 -> 54^0)

6.4. Generalized torque per unit velocity method

This section presents two torque per unit velocity methods:

1) A torque per unit velocity method for estimating the damping of SSR modes in general multimachine power systems with thyristor switching devices.

3) A new torque per unit velocity method for estimating the damping and frequency of the swing mode.

In addition, a generalization to treat the case of multiple torsional modes having the same natural frequency in a multimachine system is presented in Appendix C.

The section focuses on presenting and illustrating these torque per unit velocity methods. (see [Rajaraman1996b] for more detail). The methods are rigorously derived in [Rajaraman1996a, Rajaraman1995c] using an eigenvalue perturbation technique.

Frequency domain analysis of SSR in systems containing thyristors has been attempted for the Kayenta system in [Christl1992] and for the Slatt substation in [Larsen1992, Nyati1994]. In the Kayenta system, the frequency response of a TCSC was measured using time domain simulation. For the Slatt system, the effect of the TCSC was evaluated by representing the TCSC by a linear transfer function obtained from simulations. A frequency domain analysis of the TCSC was also carried out in [Hedin1973]. These studies measured the response of the TCSC only at the frequency of the input and other frequency components involved in the response were not discussed.

6.4.1 SSR analysis without switching devices

This section reviews the torque per unit velocity method for balanced power systems with no switching devices. When the power system operates under symmetrical and balanced three phase conditions, Park's transformation of the electrical system can be used to obtain system equations whose coefficients do not vary with time. Linearizing these equations yields a time invariant linear system.

The basic idea of the torque per unit velocity method is to trace the effect of a small sinusoidal mechanical disturbance of a generator rotor through the electrical network and determine the electromagnetic torque which acts either regeneratively (negative damping) or degeneratively (positive damping) on the initial displacement.

Suppose that we wish to estimate the damping of the ith mechanical mode. Then the frequency of the sinusoidal mechanical disturbance is chosen to be the natural frequency ω_i of the ith mode. ω_i is evaluated as $\omega_i = \sqrt{K_i/M_i}$ where M_i and K_i are the modal inertia and spring constant of mode i. A SSR torsional mode has $\omega_i \neq 0$ and a power swing mode has $\omega_i = 0$.

ΔT_i is the modal torque; it is the torque fed back to the ith mode. The modal inertias M_i are large so that the electromagnetic acceleration $\Delta T_i / M_i$ is small (typically two orders of magnitude smaller

than other terms in the elctromagnetic torque equation). The smallness of $\Delta T_i / M_i$ also causes the SSR modal frequency to remain very close to the rotor natural frequency.

Suppose that the small disturbance of the rotor is represented by an input of $e^{j\omega_i t}$ to the linearized electrical system. Then the electromagnetic torque response to this input has the form

$$\Delta T = \Delta T\ (j\omega_i)\ e^{j\omega_i t} \qquad (6\text{-}10)$$

The phasor $\Delta T\ (j\omega_i)$ is a constant and the electromagnetic torque response ΔT has the same frequency as the input because the linearized electrical system is time invariant. $\Delta T_i(j\omega_i)$ can be used to estimate the closed loop modal damping γ_i with the formula

$$\gamma_i = \text{Real}\left\{\frac{\Delta T_i(j\omega_i)}{2\, j\, \omega_i\, M_i}\right\} \qquad (6\text{-}11)$$

The method works by cleverly exploiting the weak coupling from the electrical to the mechanical system. [Bowler1976] gave formula (6-11) for the case of a single machine power system without switching devices (in the notation of [Bowler1976], $\Delta T_i(j\omega_i) = Q_{ii}^2\ \Delta T_e(j\omega_i)$).

6.4.2. SSR analysis with switching devices

This section explains how thyristor switching devices cause the system linearization to be time varying and the response of the electrical system to subsynchronous rotor oscillations to be complicated. Whenever some thyristors are conducting and other thyristors are off, the 3 phase network is instantaneously unbalanced and this causes the system to be periodically time varying even when Park's transformation is used. Unbalanced electrical networks without switching devices have been proposed for SSR mitigation [Edris1990] and these also lead to a periodically time varying system. When these systems are linearized about their periodic steady state a linear periodically time varying system results. That is, the coefficients of the linear system vary periodically with time at some frequency ω_0. For example, ω_0 is typically $120\,\pi$ rad/s for 3 phase

power systems with TCSC. The effect of the time varying linear system is that the steady state torque response to small rotor input $e^{j\omega t}$ has the general form (see [D'Angelo1970]):

$$\Delta T_i = \Delta T_i(j\omega_i)\ e^{j\omega_i t} + g_{other} \qquad (6\text{-}12)$$

where the term $\Delta T_i(j\omega_i)\ e^{j\omega_i t}$ is the response at frequency ω and g_{other} contains the remaining frequency components of the response. While $\Delta T_i(j\omega_i)$ can be thought of as the fundamental frequency part of the response, the term g_{other} is quite complicated; for example, if ω_0 and ω are not in an integer ratio, g_{other} is not even periodic in t !

6.4.3 Assumptions about system

This section describes the assumptions about the electrical system and the equations of the generator shafts. We consider a general multimachine power system which contains thyristor switching devices and their controls. The system is assumed to be operating at a periodic steady state (typically with a 60 Hz frequency) and to be linearizable about the periodic steady state.

The electrical parts of the system and its controls are modeled in a standard way [Anderson1990] (see section 6.3.1 also). Full account must be taken of the thyristor switchings and their controls. For example, the thyristors which are off are effectively removed from the circuit and the thyristors switch off when their current becomes zero. (See Chapter 5, Appendix B and [Rajaraman1996a, Jalali1994a] for modeling the electrical system with detailed representation of thyristor switchings and controls.)

We assume that a simulation of the electrical system and controls is available. In particular, this simulation must be able to determine the steady state torque response of any generator to a sinusoidal displacement of any generator rotor about the steady state operating condition. Then the steady state torque response to the complex signal $e^{j\omega_i t}$ can be evaluated as

$$\text{response to } \cos\omega_i t + j\ (\text{response to } \sin(\omega_i t))$$

Since the power system with switching devices is time varying, the response to $\cos(\omega_i t)$ is not simply the response to $\sin(\omega_i t)$ delayed by one quarter of a period. That is, for time varying systems, the responses to $\cos(\omega_i t)$ and $\sin(\omega_i t)$ must be determined individually.

The mechanical turbine-generator rotors of all the generators are modeled as lumped masses connected by lossless linear torsional springs . The natural mechanical dampings of the shafts are small and are assumed to be zero (if the natural dampings are available, we add them to the dampings due to the electromechanical interaction to get total damping).

6.4.4. Modal damping formulas for SSR modes

This section presents and explains formulas for estimating the damping of SSR modes in general multi-machine power systems with thyristor switching devices. We compute the damping of the torsional SSR mode i whose subsynchronous frequency ω_i is distinct (well separated) from other modal frequencies. (The case of multiple modes with the same or almost the same frequency is treated in Appendix C.)

Recall from equation (6-12) that the modal torque has the form

$$\Delta T_i = \Delta T_i(j\omega_i)\ e^{j\omega_i t} + g_{other} \qquad (6\text{-}12)$$

where $\Delta T_i(j\omega_i)$ is the response of ΔT_i at frequency ω_i and g_{other} contains the other frequency components. According to [Rajaraman1995c], $\Delta T_i(j\omega_i)$ can be used to estimate the closed loop modal damping γ_i with the formula:

$$\gamma_i = \text{Real}\left\{\frac{\Delta T_i(j\omega_i)}{2\,j\,\omega_i\,M_i}\right\} \qquad (6\text{-}13)$$

Formula (6-13) is accurate to first order in the small quantity $\Delta T_i / M_i$ [Rajaraman1995c, Rajaraman1996b]. To this accuracy, the other frequency components g_{other} do not appear in formula (6-13) and have no effect on the damping estimate. It is straightforward to obtain $\Delta T_i(j\omega_i)$ from the signal ΔT_i by multiplying ΔT_i by $e^{-j\omega_i t}$ and taking the average of the resulting signal over one period. Fig. 6.11 gives a schematic interpretation of (6-13).

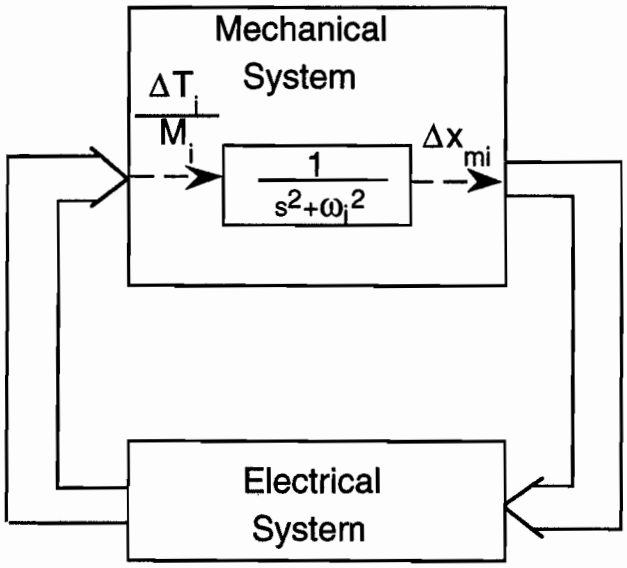

Figure 6.11. Electromechanical System Interaction

6.4.5. Damping formulas for the swing mode

This section presents special formulas and iterative methods to estimate the damping of a swing mode. To avoid the complications of multiple swing modes, only the single generator case is treated. Formula (6-13) for SSR modes does not apply to the swing mode. Instead the swing modal eigenvalue γ is estimated by

$$\gamma = \sqrt{-\Delta T_i (j\,0)/M_i} \qquad (6\text{-}14)$$

where ΔT_i (j 0) is the zero frequency or constant part of the modal torque response to an input $\Delta x_{mi} = e^{j0t} = 1$ [Rajaraman1995c, Rajaraman1996b]. ΔT_i (j0) /M_i is a real number. Moreover, for typical power systems, ΔT_i (j0) is positive and $\gamma = \sqrt{-\Delta T_i (j\,0)/M_i}$ is purely imaginary. Thus we estimate the closed loop frequency of swing mode as $\beta = \sqrt{\Delta T_i (j\,0)/M_i}$ and the closed loop damping of the swing mode as zero. β is typically in the range 1–2 Hz.

To better estimate both the damping and frequency of the swing mode, we use an iterative technique [Rajaraman1995c, Rajaraman1996b]. Let $\Delta T_i = \Delta T_i (j\,\beta)\, e^{j\beta t} + g_{other}$ be the response to the input $\Delta x_{mi} = e^{j\beta t}$. Let the estimate of the closed loop modal eigenvalue after k iterations be $\gamma[k] = \alpha[k] + j\beta[k]$. Start with the open loop eigenvalue estimate $\gamma[0] = 0$ and compute the k^{th} closed loop eigenvalue estimate as:

$$\gamma[k+1] = \sqrt{-\Delta T_i (j\,\beta[k])/ M_i} \qquad (6\text{-}15)$$

($T_i (j\,\beta[k])$ is used in the right hand side of (6-15) because for practical power systems α is much smaller than β so that $\Delta T_i (j\,\gamma[k])$ is well approximated by $\Delta T_i (j\,\beta[k])$.)

We have found the iteration to converge to a good estimate of the swing mode damping in about three iterations.

6.4.6. Results

The electrical torque response $\Delta T (j\omega_1)$ used in the formulas of Sections 6.4.4 and 6.4.5 can be computed by using a simulator. (System simulation is usually required for other purposes anyway such as checking large signal performance.) The electrical part of the system used to compute the steady state electrical torque response is typically stable with well damped modes. Therefore it is straightforward to compute the steady state torque response from simulation. This advantage applies even when the entire electromechanical system is unstable. Alternatively, if the linearized system equations are available in explicit form, harmonic admittance methods (see [Jalali1993,

Jalali1994b]) can be used to compute $\Delta T(j\omega_i)$ on the periodically varying linearized system. The method is simpler than exact eigenanalysis of the entire electromechanical system because it only requires the response of the electrical system and the mechanical system need not be represented in computing this response.

We now give an example of estimating damping of torsional modes and the power swing mode for the IEEE SSR first benchmark model [IEEE1977] with a TCSC as the thyristor conduction angle σ varies. The results are compared with the exact eigenvalue analysis of Section 6.3.

The thyristor switch on times in Fig. 6.12, 6.13 and 6.14 are determined by the equal distance firing synchronization method, and the switch on times in Fig. 6.15 are synchronized to the zeros of the line current. The case $\sigma = 0°$ corresponds to blocking the thyristors. Detailed system description and parameter values are provided in [IEEE1977, Rajaraman1995b].

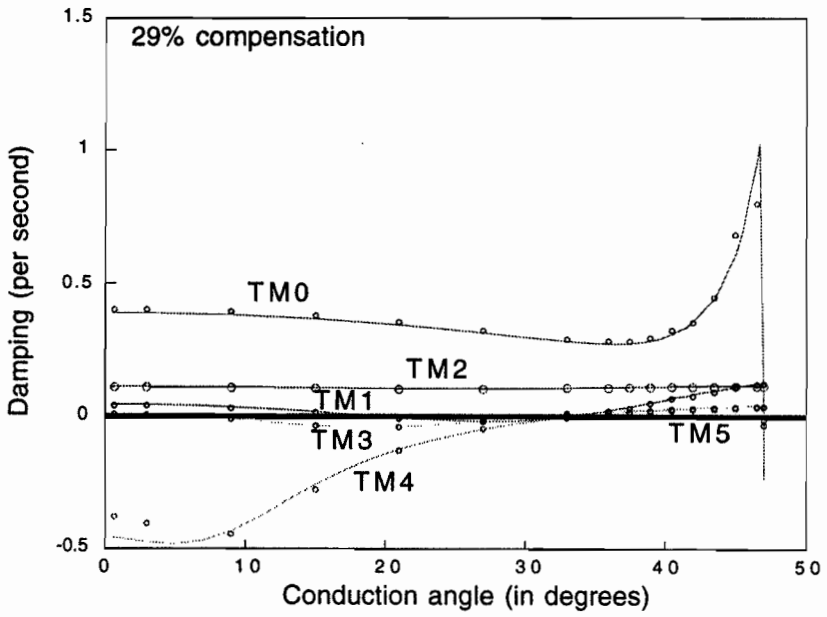

Figure 6.12. Estimated Modal Dampings

Fig. 6.12 shows the net damping of the modes TM0 through TM4 when the series compensation is 29%. (The mode TM5 damping is zero throughout and obscured by the horizontal axis of Fig.

6.12.) Negative modal damping implies modal instability. The circles are the estimates of this paper and the solid lines are obtained by exact eigenanalysis using the methods of section 6.3. (The net modal damping was obtained by adding the natural modal damping to the modal damping due to SSR.) The results demonstrate the close reproduction of the results of exact eigenanalysis with torque per unit velocity methods. The larger errors in the SSR and swing modes occur far from zero damping and these modes are estimated accurately when their damping is small. This is to be expected because the method works by perturbing about the small natural mechanical damping.

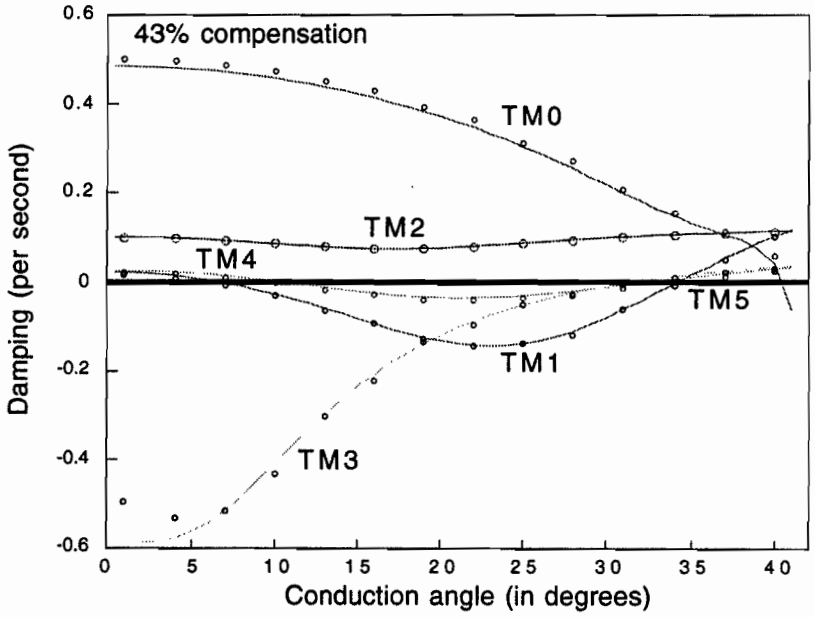

Figure 6.13. Estimated Modal Dampings

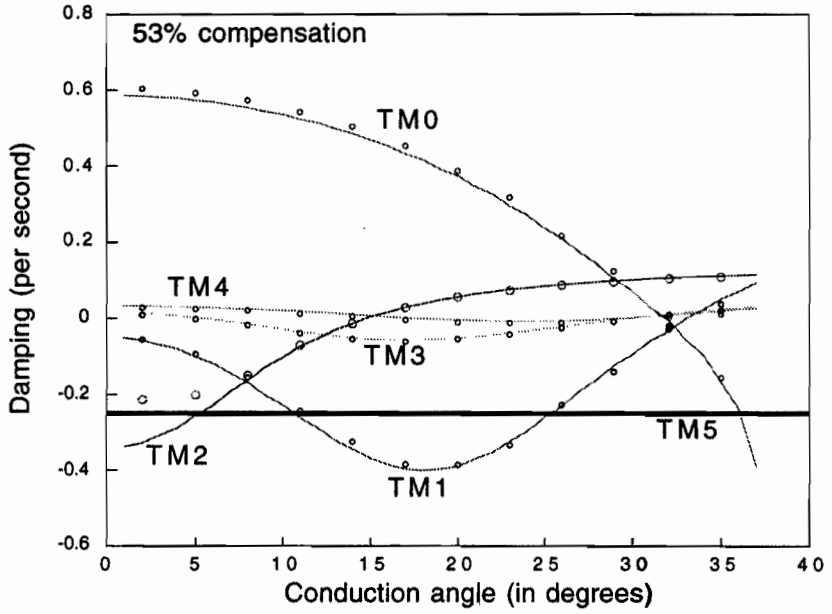

Figure 6.14. Estimated Modal Dampings

Figs. 6.13 and 6.14 show the estimated net damping of the torsional and swing modes for 43%, 53% line compensation respectively for the equidistant firing scheme. Fig. 6.15 shows the estimated net damping of the modes for 29% line compensation for the case when the thyristor current is synchronized to the zeros of the line current. The close match between the estimated and exact results is evident.

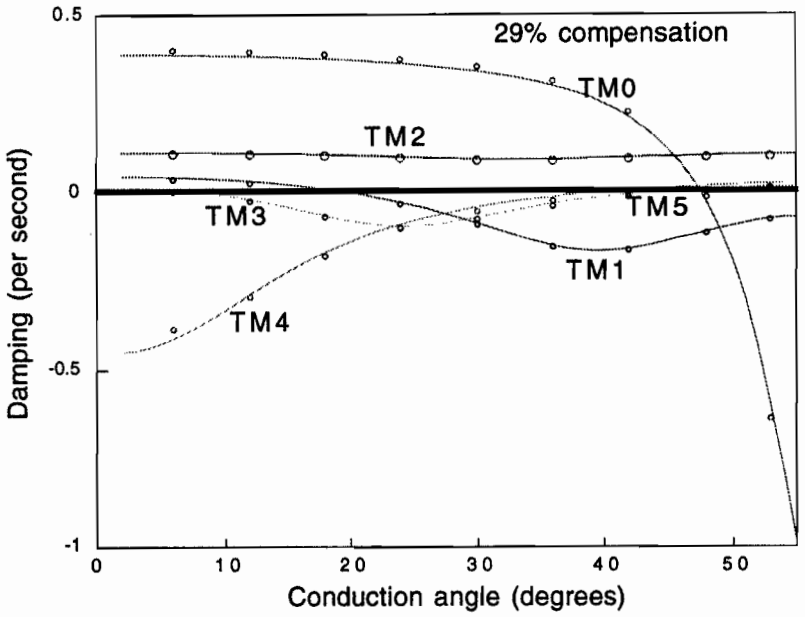

Figure 6.15. Estimated Modal Dampings for thyristor firing synchronized to line current

These results were obtained by time domain simulation using MATLAB [Mathworks1993]. Formula (6-13) was used for the damping estimation of the torsional modes and three iterations of (6-15) were used for the power swing mode. For each value of σ, the time for computing modal dampings was roughly ten minutes on an HPRISC machine.

6.5. Conclusions

We show how to extend the eigenvalue analysis commonly used to study SSR to circuits containing thyristors. In particular, we present eigenvalue analysis for the IEEE first benchmark SSR model with a TCSC. The analysis takes account of time variations and nonlinearities due to the generator and the thyristor switchings. Illustrative eigenvalue results are supported by EMTP simulations.

The eigenvalue results for the first benchmark model show that the thyristor switchings can have a significant effect on system stability and that the effect varies with the firing angle. For simplicity,

the firing angle was assumed constant. A study devoted to applying the methods developed in this chapter would additionally represent synchronization effects as described in Appendix B and other synchronization and control effects by augmenting the equations with those of Chapter 5 or [Jalali1994a]. Our eigenvalue results are consistent with the damping effect associated with thyristors turning off described in [Jalali1993, Dobson1995a, Dobson1995b, Rajaraman1995a] . Other damping effects involving thyristors are described in [Hingorani1980, Hedin1980]. The results do show possibility of sufficient damping to suppress SSR when the thyristors are operated at a constant firing angle. This could be termed `passive' damping since the firing angle is not actively controlled as it is in several schemes for modulating the thyristor firings to damp SSR [Hingorani1980, Hedin1980].

Eigenanalysis via the Poincare map is a rigorous and accurate method to compute the damping of SSR modes with a TCSC. When applied to larger power systems, there is effort in programming and handling the system equations as well as the numerical burden of integrating the linearized equations along a steady state solution. While exact eigenanalysis applies to any general case, at some size or complexity, it will become too burdensome. In particular, the matrix differential equations which are numerically integrated to compute the Poincare map Jacobian have size which is the square of the number of states. We would expect the computations to be feasible for small power systems, say with up to 3 generators and 2 TCSC devices, but would expect the method to be burdensome for larger power systems. However, the torque per unit velocity method does not require formulation and manipulation of the system equations but only a simulation of the system to be available. Such a simulation is often needed for other purposes such as large signal studies anyway. Thus we recommend using the exact eigenvalue methods for small power systems and the generalized torque per unit velocity methods for larger power systems. The exact eigenvalue method can serve as a benchmark for validating approximate methods such as the torque per unit velocity method.

This chapter stated simple formulas for estimating the damping of SSR and power swing modes when the power system includes thyristor switching devices. In the electrical part of these systems, a small sinusoidal perturbation of a machine rotor at a modal frequency leads to a complicated electrical torque response with many frequency components. However, we show that the damping may be estimated from the component of the electrical torque response at the modal frequency. The formulas extend to the case of multiple torsional modes having the same natural frequency. The formulas are rigorously derived in [Rajaraman1996a,Rajaraman1995c]. Thus the the torque per unit velocity method can be extended to systems with thyristor switchings. We also give a new and

simple method to compute the damping of the power swing mode and to improve the estimates by an iteration.

The torque per unit velocity method formulas require the steady state electrical torque response of the electrical system to sinusoidal machine rotor perturbations to be computed and this can be done by time domain simulation or harmonic admittance methods. The method is simpler than exact eigenanalysis of the entire electromechanical system and testing on the IEEE SSR first benchmark model with a TCSC shows excellent agreement with exact eigenanalysis.

6.6 Appendices

Appendix A. System parameters

For a full description of the parameters see [Rajaraman1995b].

L_0	L_d	L_{AD}	L_F	L_D	L_q	L_{AQ}	L_G	L_Q
0.135	1.79	1.66	1.722	1.665	1.71	1.58	1.906	1.675

r_0	r_F	r_D	r_G	r_Q
100	0.53/ 377	1.54 / 377	5.3/ 377	3.1/ 377

$r_a = r_b = r_c = 0,\ C_r = 1/0.2,\ L_r = \frac{1}{7C_r},\ \omega_R = 1$

$\boldsymbol{L}$ has elements 1.0533 on the diagonal and 0.3533 off the diagonal. $\boldsymbol{R}$ has elements 0.18 on the diagonal and 0.16 off the diagonal.

Mechanical dampings (in 1/sec) for the modes TM1--TM5 [IEEE1977] are:

TM1	TM2	TM3	TM4	TM5

0.05	0.11	0.028	0.028	0

(The modal damping for TM5 was not given in [IEEE1977] and is taken to be zero.)

The generator operating conditions are power output = 0.9, power factor = 0.9, and the generator terminal voltage = 1.0.

Appendix B: Linearization of thyristor turn on synchronized to line current

This appendix outlines how to compute the Jacobian when the TCSC firing is synchronized to the zeros of the line current. Details are found in [Rajaraman1996a]. To obtain the Jacobian, (6-1), (6-2), (6-5) and (6-6) have to be linearized. The linearization of (6-1), (6-2) and (6-6) is similar to that of the constant firing delay case. The linearizarion of (6-5) is more complicated. We describe the linearization for the case when the thyristor in phase A turns on; other cases are handled similarly.

The synchronization equation is:

$$s_{on} = \tau_A + (\pi - \sigma_{req})/2 \qquad (6\text{-}16)$$

Linearizing (6-16), we get

$$\Delta s_{on} = \Delta \tau_A \qquad (6\text{-}17)$$

The line current in phase A satisfies:

$$c_1(\tau_A)\, y(\tau_A) = 0 \qquad (6\text{-}18)$$

where $c_1(t)$ depends on the inverse Park transformation and picks off the phase A line current from the odq frame of reference. Linearizing (6-18), we obtain:

$$\Delta s_{on} = \Delta \tau_A = \frac{-c_1(\tau_A)}{\dot{c}_1 y(\tau_A) + c_1(\tau_A)\,\dot{y}} \Delta\, y(\tau_A) \qquad (6\text{-}19)$$

Define h so that (6-19) can be conveniently written as:

$$\Delta s_{on} = h(\tau_A)\, \Delta y(\tau_A) \tag{6-20}$$

Repeating (6-5) for convenience:

$$x(s_{on}) = G^t\, y(s_{on}) \tag{6-5}$$

Linearizing, we obtain:

$$\Delta x(s_{on}) = (G^t\, y_*(s_{on}) - x_*(s_{on})\,)\, \Delta s_{on} + G^t\, \Delta y(s_{on})$$

$$= (G^t\, y_*(s_{on}) - x_*(s_{on})\,)\, h(\tau_A)\, \Delta y(\tau_A) + G^t\, \Delta y(s_{on})$$

If the map from $\Delta y(\tau_A)$ to $\Delta y(s_{on})$ is known, then the linearization for the system equations would be similar in form to that for the equidistant firing case and the Jacobian can be obtained using the methods of Section 6.3.2. However, note that $\Delta x(s_{on})$ depends on a state $\Delta y(\tau_A)$ that occurs before s_{on}. Similarly, $\Delta y(\tau_A)$ would depend on a state that occurs before τ_A and so on. This means a direct expression for map from $\Delta y(\tau_A)$ to $\Delta y(s_{on})$ is difficult to obtain.

Therefore, we suggest the following iterative method to compute the Jacobian. First note that the linearized system is periodic in T and hence the map H from $\Delta y(\tau_A)$ to $\Delta y(s_{on})$ is also the map from $\Delta y(\tau_A+T)$ to $\Delta y(s_{on}+T)$. Assume an initial guess for $H(\tau_A,s_{on})$, and compute the approximate Jacobian and the map $H(\tau_A+T,s_{on}+T)$ using the methods in Section 6.3.2. Set $H(\tau_A,s_{on})$ to the estimated $H(\tau_A+T,s_{on}+T)$ and repeat the process to obtain improved estimates of the Jacobian and $H(\tau_A+T,s_{on}+T)$. The iteration is stopped if the normed difference of successive estimates of the Jacobian is less than some tolerance.

For the benchmark model described in this chapter, excellent results were obtained using an initial guess of $H(\tau_A,s_{on})$ to be the zero matrix. Using an error tolerance of 10^{-5}, the Jacobian was obtained in less than six iterations.

Appendix C: Multiple modes with the same frequency

We now compute the dampings of two or more torsional modes having the same natural frequency. This case can occur when a natural frequency of one generator turbine system coincides with a natural frequency of another generator turbine system. We assume that the first two torsional modes have the same nonzero natural frequency so that $\omega_1 = \omega_2$; the analysis for more than two such modes is similar. Now there are two independent modes having natural frequency ω_1 ; in general, the first two oscillators will participate in both modes. This implies that the output of both oscillators must be taken into account in determining the damping of these SSR modes.

Let $\Delta T_{ik}(j\omega_k)$ be the response of ΔT_i at frequency ω_i due to the k^{th} oscillator input $x_{mk} = e^{j\omega_k t}$. (As before, the frequency components not at frequency ω_k can be neglected.) Define the matrix

$$B = \frac{1}{2j}\begin{pmatrix} \Delta T_{11}(j\omega_1)/(M_1\omega_1) & \Delta T_{12}(j\omega_2)/(M_1\omega_1) \\ \Delta T_{21}(j\omega_1)/(M_2\omega_2) & \Delta T_{22}(j\omega_2)/(M_2\omega_2) \end{pmatrix}$$

Then [Rajaraman1995c] proves that the damping estimates of the first two torsional modes are the real parts of the eigenvalues of B. (If $w_1 \neq w_2$ and the frequency separation $w_1 - w_2$ is more than the bandwidth of each oscillator's response, then the off diagonal terms of B are zero and the multiple mode case reduces to two instances of formula (6-13). However, if $w_1 \neq w_2$, but w_1 is close to w_2, then the practical computation of B can yield nonzero off diagonal terms and the multiple mode method applies.) The computation for k torsional modes with the same frequency is similar except that B becomes a $k \times k$ matrix.

REFERENCES

P.M.Anderson, A.A.Fouad (1977), Power system control and stability-vol. 1, Iowa State Univ. Press, IA.

P.M. Anderson, B.L. Agrawal, J.E. Van Ness (1990), Subsynchronous resonance in power systems, IEEE Press, NY.

L Angquist, G. Ingestrom, H. Othman, "Synchronous Voltage Reversal (SVR) Scheme- A New Control Method for Thyristor Controlled Series Capacitors," Proceedings: FACTS Conference 3, Baltimore, Maryland, October 1994.

L.J. Bohmann, R.H. Lasseter (1989), Harmonic interactions in thyristor controlled reactor circuits, IEEE Trans. Power Delivery, vol. 4, no. 3, pp. 1919-1926, July.

C.E.J. Bowler, D.N. Ewart, C. Concordia (1973), Self excited torsional frequency oscillations with series capacitors, IEEE Trans. Power Apparatus and Systems, vol. PAS-92, pp. 1689-1695.

C.E.J. Bowler Understanding subsynchronous resonance (1976), IEEE Power %Engineering Society Winter Meeting and Tesla Symposium.

I.M. Canay (1982), A novel Approach to the Torsional Interaction and Electrical Damping of the Synchronous Machine, Parts I and II, IEEE Trans., Vol. PAS-101, No. 10, pp. 3630-3644.

N. Christl et al. (1991), Power system studies and modeling for the Kayenta 230KV substation advanced series compensation. IEE Intl. Conference on thyristor and variable static equipment for AC and DC transmission, London.

N. Christl, R. Hedin, P.E. Krause, S.M. McKenna, K. Sadek, P. Lützelberger, A.H. Montoya, D. Torgerson (1992), Advanced series compensation (ASC) with thyristor controlled impedance. Cigré 14/37/38-05, Paris, Aug.-Sept.

C. Concordia, R.B. Bodine, G. Kron (1943), Self-excited oscillations of capacitor-compensated long distance transmission systems, AIEE Transactions, vol. 62, pp. 41-44.

S.D. Conte, C. de Boor C. (1980), Elementary numerical analysis; an algorithmic approach, third edition, McGraw-Hill, NY.

H. D'Angelo (1970), Linear time-varying systems: analysis and synthesis, Boston, MA.

I. Dobson, S.G. Jalali, R. Rajaraman (1995a), Damping and resonance in a high power switching circuit, in Systems and Control Theory for Power Systems (eds. J.H. Chow, P.V. Kokotovic, R.J. Thomas), IMA volume 64 in mathematics and its applications, Springer Verlag, pp. 137-156.

I. Dobson (1995b), Stability of ideal thyristor and diode switching circuits, IEEE Transactions on Circuits and Systems, Part 1, vol. 29, no. 9, September, pp. 517-529.

A.A. Edris (1990), Series compensation schemes reducing the potential of subsynchronous resonance, IEEE Trans. Power Systems, PWRS-5, no.1, pp. 219-226.

EPRI Development Coordination Group (1989), EMTP Workbook III.

J.F. Gronquist, W.A. Sethares, R.H. Lasseter, "Power Swing Damping Control Strategies for FACTS Devices Based Upon Locally Measurable Information",

J. Guckenheimer, P. Holmes, (1986) Nonlinear oscillations, dynamical systems and bifurcations of vector fields, Springer-Verlag, NY.

R.H. Hedin, R.C. Dancy, K.B. Stump (1973), An analysis of the subsynchronous interaction of synchronous machines and transmission networks, Proceedings of the American Power Conference, vol. 35, pp. 1113-1119.

R.A. Hedin et al. (1995), SSR characteristics of alternative types of series compensation schemes, IEEE Trans. Power Systems, vol. 10, no. 2, May, pp. 845-852.

J.K. Hale (1963), Oscillations in nonlinear systems, McGraw Hill, NY.

R.A. Hedin, K.B. Stump, N.G. Hingorani (1980), A new scheme for subsynchronous resonance damping of torsional oscillations and transient torque--Part II, IEEE PES Summer Meeting, Minn., MN.

R.A. Hedin et al (1995), SSR characteristics of alternative types of series compensation schemes, IEEE Trans. Power Systems, vol. 10, no. 2, May, pp. 845-852.

N.G. Hingorani (1980), A new scheme for subsynchronous resonance damping of torsional oscillations and transient torque -- Part I. IEEE PES Summer Meeting, Minneapolis, MN.

IEEE Committee Report (1977), First benchmark model for computer simulation of subsynchronous resonance, IEEE Trans. on Power Apparatus and Systems, vol. PAS-96, no. 5, Sept., pp. 1565-1572.

IEEE Committee Report (1985), Terms, definitions, and symbols for subsynchronous resonance oscillations. IEEE Trans. on Power Apparatus and Systems, vol. PAS-104, June 1985, pp. 1326-1334.

IEEE Committee Report (1992), Reader's guide to subsynchronous resonance. IEEE Trans. on Power Systems, vol. 7, no. 1, Feb., pp. 150-157.

S.G. Jalali, R.H. Lasseter (1991), Harmonic interaction of power systems with static switching circuits", Power Electronics Specialists Conference, June, MIT MA, pp. 330-337.

S.G.Jalali, R.H.Lasseter (1992a), Harmonic instabilities in advanced series compensators, EPRI FACTS Conference II, Boston MA, May 1992, in Electric Power Research Institute report TR-101784.

S.G. Jalali, I. Dobson, I., R.H. Lasseter (1992b), Instabilities due to bifurcation of switching times in a thyristor controlled reactor, Power Electronics Specialists Conference, Toledo, Spain, July, pp. 546-552.

S.G. Jalali (1993), Harmonics and instabilities in thyristor based switching circuits, Ph.D. Thesis, April 1993, University of Wisconsin at Madison.

S.G. Jalali, R.H. Lasseter, I. Dobson (1994a), Dynamic response of a thyristor controlled switched capacitor, IEEE Trans. on Power Delivery, vol. 9, no 3, July, pp. 1609-1615.

S.G. Jalali, R.H. Lasseter (1994b), A study of nonlinear harmonic interaction between a single phase line-commutated converter and a power system, IEEE Trans. on Power Delivery, vol. 9, no. 3, July, pp. 1616-1624.

S.G. Jalali, I. Dobson, R.H. Lasseter, G. Venkataramanan (1996), Switching time bifurcations in a thyristor controlled reactor, to appear in IEEE Transactions on Circuits and Systems, Part 1, scheduled March 1996.

R. Johnson, P. Krause, A. Montoya, N. Christl, R. Hedin (1991), Power systems studies and modeling for the Kayenta 230 kV substation advanced series compensator, IEE Fifth Intl. Conf. on AC and DC Power Transmission, Sept., London, UK.

G. Juette, P. Luetzelberger, A. Schultz, S. McKenna, D. Torgerson, "Advanced Series Compensation (ASC) Main Circuit and Related Components," Proceedings:FACTS Conference 2, Boston, Massachusetts, December 1992, EPRI TR-101784, pp.3.4-1 to 3.4-13.

L.A. Kilgore, E.R. Taylor, L.C. Elliott (1971), The prediction and control of self-excited oscillations due to series capacitors in power systems, IEEE Transactions on Power Apparatus and Systems, vol. PAS 90, no. 3, pp. 1305-1311, May/June.

L.A. Kilgore D.G. Ramey M.C. Hall (1976), Simplified transmission and generation system analysis procedures for subsynchronous problems. IEEE Power Engineering Society Winter Meeting and Tesla Symposium.

P. Kundur (1994) Power system control and stability, McGraw Hill, New York.

E. Larsen, C. Bowler, B. Damsky, S. Nilsson (1992), "Benefits of thyristor controlled series compensation." Cigré Paper 14/37/38-04, Paris.

E. Larsen, K. Clark (1993), "Thyristor Controlled Series Capacitor Vernier Control System," US Patent, 5,202,583, April 13, 1993.

R.H. Lasseter, F.L. Alvarado, J.J. Sanchez(1983), "Testing of Trapezoidal Integration with Damping for the Solution of Power Transient Problems", IEEE PAS, pp. 3783- 3790, December 1983.

Lasseter, R.H.(1992a),"Interaction of Power Systems with Thyristor Controlled Reactors and Other FACTS Devices," Invited paper, Proceedings: FACTS Conference I-The Future in High-Voltage Transmission, March 1992, EPRI TR-100504, Section 2.4 pp.1-16.

Lasseter, R.H. and S. Jalali(1992b), "Harmonic Instabilities in Advanced Series Compensators," Keynote paper, Proceedings: FACTS Conference II, December 1992, EPRI TR-101784, Section 1.4 pp.1-16.

The MathWorks, Inc. (1993), MATLAB User's Guide, Natick, MA, 1993.

S. Nyati et al. (1994), Effectiveness of thyristor controlled series capacitor in enhancing power system dynamics: an analog simulator study, IEEE Trans. on Power Delivery, vol. 9, no. 2, April, pp. 1018-1027.

R. Rajaraman, I. Dobson, S.G. Jalali (1993) Nonlinear dynamics and switching time bifurcations of a thyristor controlled reactor, IEEE International Symposium on Circuits and Systems, Chicago, IL, May, pp. 2180-2183.

R. Rajaraman, I. Dobson (1995a), Damping and incremental energy in thyristor switching circuits, IEEE International Symposium on Circuits and Systems, Seattle, Washington, May, pp.~291-294.

R. Rajaraman, I. Dobson, R.H. Lasseter, Y. Shern (1995b), Computing the damping of subsynchronous oscillations due to a thyristor controlled series capacitor, 95SM403-6PWRD, IEEE PES Summer meeting, Portland, Oregon, July.

R. Rajaraman, I. Dobson (1995c), Justification of torque per unit velocity methods of analyzing subsynchronous resonance and a swing mode in power systems, report ECE-95-9, July, Electrical and Computer Engineering Department, University of Wisconsin, Madison, WI 53706.

R. Rajaraman (1996a), Damping of subsynchronous resonance and nonlinear dynamics in thyristor switching circuits, PhD Thesis, University of Wisconsin-Madison.

R. Rajaraman, I. Dobson (1996b) Damping estimates of subsynchronous and power swing oscillations in power systems with thyristor switching devices, paper 96WM255-0-PWRS, IEEE PES Winter meeting, Baltimore, MD, January .

M. Steinbuch, O.H. Bosgra (1992), Dynamic modeling of a generator/rectifier system, IEEE Trans. on Power Electronics, vol. 7, no. 1, Jan., pp. 212-223.

J.M.T. Thompson, H.B. Stewart (1987), Nonlinear Dynamics and chaos: geometrical methods for scientists and engineers, John Wiley, London, 1986, reprinted 1987.

J. Urbenek, R. Piwko, D. McDonal, N. Artinez, "Thyristor-Controlled Series Compensation-Equipment Design for the Slatt 500KV Installation," Proceedings:FACTS Conference 2, Boston, Massachusetts, December 1992, EPRI TR-101784, pp.3.1-1 to 3.1-19.

G.C. Verghese, M.E. Elbuluk, J.G. Kassakian (1986), A general approach to sampled-data modeling for power electronic circuits, IEEE Trans. Power Electronics, vol. 1, no. 2, April, pp. 76-89.